Feedforward Tracking Control of Nonminimum Phase and Uncertain Linear Systems using Filtered Basis Functions – with Application to 3D Printing

by

Keval S. Ramani

A dissertation submitted in partial fulfillment
of the requirements for the degree of
Doctor of Philosophy
(Mechanical Engineering)
in the University of Michigan
2020

Doctoral Committee:

Associate Professor Chinedum E. Okwudire, Co-Chair
Professor A. Galip Ulsoy, Co-Chair
Associate Professor Kira Barton
Professor James Freudenberg

Keval S. Ramani

ksramani@umich.edu

ORCID iD: 0000-0002-1113-3613

DEDICATION

This dissertation is dedicated to my parents and my sister

ACKNOWLEDGEMENTS

My journey towards a doctoral degree has been a significant part of my life. This journey has been shaped with the support of many individuals and I would like to take this opportunity to express my sincere gratitude towards them.

First, I would like to thank my advisors Profs. Chinedum Okwudire and Galip Ulsoy for their guidance and support. I still remember meeting Prof. Okwudire in September 2013 in his office seeking an opportunity to work with him and I would like to thank him for giving me that opportunity. Over the last six years, I have learnt a lot from him about research, teaching, mentoring and life. His passion and tenacity towards his work, has always inspired me to give my best towards my research. Prof. Ulsoy has been guiding me since 2015 and during these four years, I have learnt a lot from him. On numerous occasions, his feedback has helped enhance my research. Both Profs. Okwudire and Ulsoy have helped me understand myself as a researcher and person, and I would like to thank them for it. I would like to thank my committee members Profs. Kira Barton and James Freudenberg for consenting to be on my dissertation committee. Their guidance and feedback have been valuable to me and is greatly appreciated.

I would like to thank all my past and present colleagues at the Smart and Sustainable Automation Research Lab for their intellectual support and friendship. I would like to especially thank Drs. Molong Duan and Deokkyun Yoon for their valuable feedback and support towards my research. I would like to thank the National Science Foundation (NSF) for financially supporting this research. I would like to take this opportunity to thank family and friends in Michigan as well as in India, for their support and encouragement. Last but not the least, I would like to thank my parents and my sister, for their support throughout this journey.

TABLE OF CONTENTS

LIST OF TABLES

LIST OF FIGURES

LIST OF APPENDICES

ABSTRACT

Tracking control is a fundamental problem in a wide range of fields such as manufacturing, robotics, automotive and aerospace. The objective of tracking control is to force the output trajectory of the controlled system to follow a desired trajectory as closely as possible. Feedforward control plays a crucial role in many industrial applications, as an alternative or complement to feedback control. One example is in the rapidly growing domain of 3D printing where feedforward is often entirely responsible for motion control. Perfect tracking control can be achieved using model inversion-based feedforward control. However, perfect tracking control cannot be realized if the system has: (i) nonminimum phase (NMP) zeros and (ii) model uncertainty.

This dissertation presents and studies the filtered basis functions (FBF) approach as an excellent alternative to existing techniques for tracking control of discrete-time linear systems with NMP zeros and/or model uncertainty. The FBF approach expresses the control input to the plant as a linear combination of user-defined basis functions. The basis functions are forward filtered through the plant dynamics and the coefficients are obtained such that the tracking error is minimized. Compared to other tracking control approaches in the literature, the FBF approach is observed to be very versatile and consistent – it is applicable to all discrete-time linear systems and its tracking accuracy does not vary significantly depending on plant dynamics. It also possesses a degree of freedom not available to other tracking controllers – i.e., the choice of basis functions.

The FBF approach is shown to almost always result in a time varying controller, even when the plant dynamics is time invariant. The conditions for uniqueness and existence of a solution to the FBF controller design problem are derived. To analyze the FBF controller, the Frobenius norm of the lifted system representation (LSR) of dynamics is proposed as a metric. The proposed metric is shown to be effective in characterizing the tracking performance of the FBF controller relative to those of other tracking controllers. It is shown that the metric for FBF's tracking error dynamics

is independent of the type of basis functions and plant dynamics, while those of other tracking controllers are dependent on plant dynamics, in agreement with observations.

Even though the (nominal) tracking accuracy of the FBF approach does not vary significantly with the type of basis functions, its control effort and robustness to model uncertainty heavily depend on the type of basis functions used. There is a wide variety of basis functions that can be used with the FBF approach but there is no work to date on how to select the best set of basis functions. Using the Frobenius norm metric applied to controller dynamics, an optimal set of basis functions that minimize the control effort without sacrificing tracking accuracy is proposed. Similarly, an optimal set of basis functions that maximizes robustness in the presence of plant uncertainty, without sacrificing nominal tracking accuracy and with constraints on the required control effort is proposed. The proposed optimal basis functions are shown in simulations and experiments on a 3D printer to, in some cases, yield orders of magnitude improvement in control efficiency and robustness compared to popular basis functions like B-splines and discrete cosine transforms. Besides the choice of basis functions, it is observed that a significant factor affecting the robustness of the FBF approach is the nominal model used for filtering the basis functions. For selection of the optimal nominal model, this dissertation formulates a robust filter using lifted domain optimization. The filter is selected such that a Frobenius norm metric dependent on the known uncertainty is minimized. The combination of optimal choice of nominal model and basis function is shown in simulations and experiments on a 3D printer to significantly improve the robustness of the FBF approach as compared to popular basis functions.

Chapter 1

Introduction and Literature Review

This doctoral dissertation proposes and studies the filtered basis functions (FBF) approach for tracking control of discrete-time linear systems with nonminimum phase (NMP) zeros and/or model uncertainty, and its application to 3D printing. Section 1.1 provides background and motivation for the study, Section 1.2 reviews the literature on tracking control of systems with NMP zeros and/or model uncertainty and Section 1.3 discusses the contributions of the dissertation and outlines the contents of the dissertation.

1.1 Background and Motivation

Tracking control is a fundamental problem in a wide range of application domains, including manufacturing [1–3], robotics [4–6], automotive [7–9] and aerospace [10–12] (see Figure 1.1). The objective of tracking control is to force the output of the controlled system to follow a desired trajectory. Tracking control can be achieved using feedforward and/or feedback approaches. Feedforward (FF) control uses *a priori* knowledge about a given system and its disturbances to influence the system's behavior in a pre-defined way. However, unlike feedback (FB) control, it does not adjust the control variable in response to how the system actually reacts. In other words, FF control is proactive while FB control is reactive. Feedforward approaches are very important to tracking control applications, where they are often used to complement feedback approaches. Perfect tracking control (PTC) can be achieved using feedforward control by inverting a model of the plant (i.e., pole-zero cancellation) [13]. However, such model-inversion based FF methods cannot be realized in practice. Two prominent challenges faced by model-inversion based FF methods include presence of NMP zeros (i.e., unstable zeros) and uncertainty in the plant model [14]. This dissertation focuses on addressing these two challenges and is motivated by several applications where feedforward is the only or primary recourse for tracking control, e.g., due to technological, practical or economic infeasibility of sensing. Examples include the over $300

billion semiconductor industry [15] and the rapidly growing $7 billion additive manufacturing industry [16].

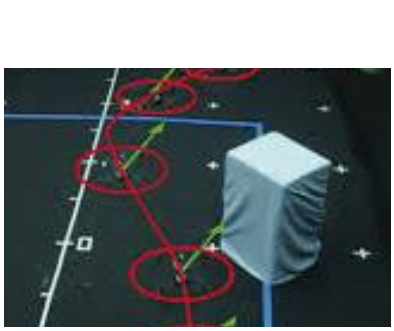

(a)

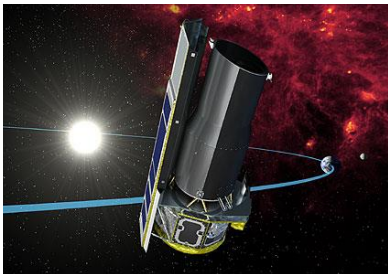

(b)

(c)

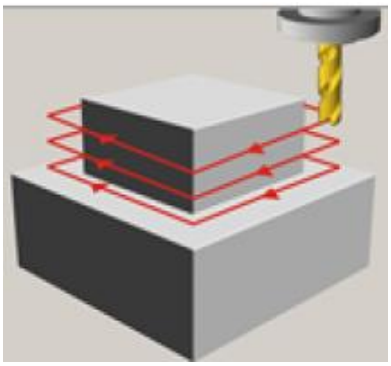

(d)

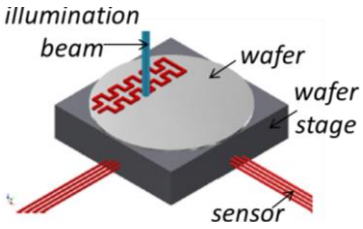

(e)

(f)

Figure 1.1 Examples of tracking control (a) quadcopter (b) space telescope (c) car (d) milling (e) wafer scanning (f) 3D printing

A wafer stage, shown in Figure 1.1(e), is a device used to deliver ultra-precise motion needed for the photolithography process in integrated circuit manufacturing [17]. Wafer stages must achieve sub-nanometer servo errors in tracking motion trajectories with velocities of up to 1 m/s and 10 g acceleration [18]. Over 99% of the control effort required for generating the desired motion is contributed by FF control [15], because wafer stages are specially designed to minimize uncertainties and unknown disturbances. In a typical wafer stage, model-based inversion FF is achieved by inverting a rigid body model of the stage of mass (i.e., control input (i.e., force) =

mass × desired acceleration) [18]. However, as the desired acceleration increases, there is a push to reduce the mass so that the required control input is not excessive. An unintended result of reducing the mass is that the stiffness of the stage reduces, thus invalidating the rigid body assumption used for model-inversion based FF. This has given rise to so-called 'beyond rigid body (BRB)' FF control which considers the flexible modes of the stage in model-inversion based FF control of wafer stages [18]. A major concern that arises with the inclusion of flexibilities in model-inversion based FF control is the presence of NMP zeros [18], which are almost certain to occur when sensors and actuators are non-collocated [19], as in wafer stages. Moreover, model uncertainties increase as high frequency vibration modes are introduced into model-inversion based FF. These issues are further complicated by the fact that the structural dynamics varies from location to location on the wafer stage, hence a position (and time) varying model is required for model-inversion based FF control [18].

To keep their weight and costs low, commercial desktop 3D printers (see Figure 1.2(a)) incorporate timing belts and lightweight components, which introduce structural flexibilities into their dynamics. Hence, manufactured parts suffer from surface waviness and registration errors caused by excess vibration (see Figure 1.2(b)), especially when high-acceleration motions are commanded [20], similar to wafer stages described above. Moreover, most 3D printers are driven in open loop by stepper motors. Hence, they cannot sense and counteract motion-induced vibration via feedback control. Feedforward methods like limited preview filtered B-splines (LPFBS) approach [20], a method based on the FBF approach discussed in this dissertation, can mitigate these vibrations by modifying the motion commands sent to the 3D printer and improves accuracy of the parts, without incurring any additional costs from feedback sensors. Up to 77% lower RMS surface roughness of a printed block (see Figure 1.3) and significant reductions in printing time (see Table 1.1) are obtained using the LPFBS approach as compared to the baseline case (no vibration compensation). This example shows the significant impact feedforward control and especially FBF can make in the motion control of 3D printers. Much like wafer stages, NMP zeros and model uncertainties (see Figure 1.4) are significant issues in control of 3D printer and need to be dealt with. Hence, this dissertation focuses on control of systems with NMP zeros and model uncertainties.

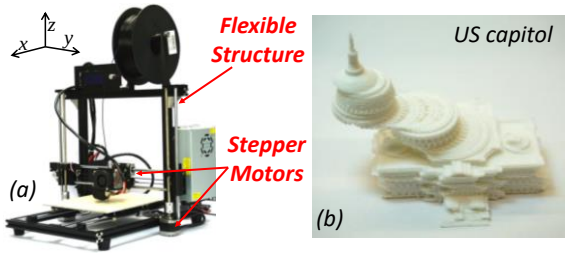

Figure 1.2 (a) Desktop 3D printer; (b) Scrapped 3D printed part due to excessive vibration of printer [20]

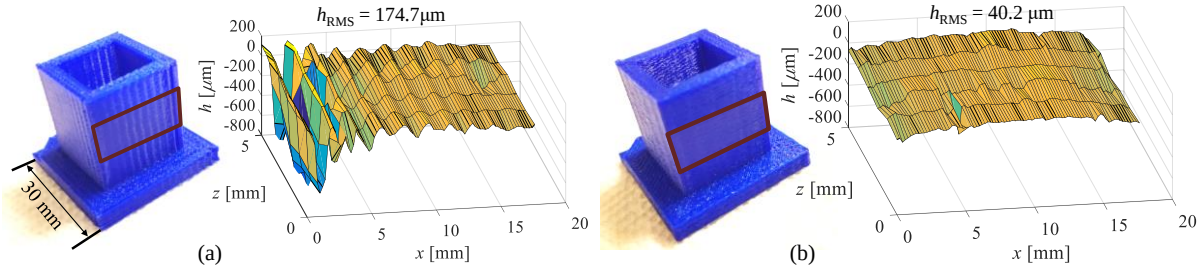

Figure 1.3 Comparison of photographs and measured surface profiles (h) of the highlighted surfaces of blocks printed using (a) baseline approach (no vibration compensation) and (b) LPFBS method [20]

Table 1.1 3D printed models of US Capitol using different acceleration limits (which influences total printing time). Comparison of LPFBS with no vibration compensation case [20]

Acc. limit	1 m/s^2	3 m/s^2	5 m/s^2	7 m/s^2	10 m/s^2
Printing time	3:59 h	2:42 h	2:22 h	2:12 h	2:06 h
Baseline					
LPFBS					

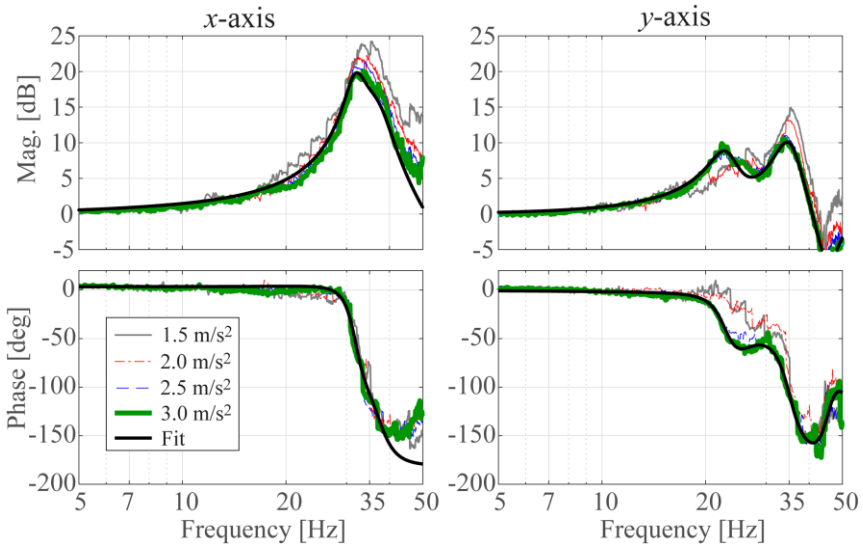

Figure 1.4 Frequency response functions of the 3D printer for various magnitudes of excitation input (acceleration) [20]

1.2 Literature Review

As discussed in Section 1.1, PTC can ideally be achieved through pole-zero cancellation, but in practice NMP zeros and model uncertainties are the two major factors limiting performance of model-inversion based FF control [14]. Section 1.2.1 reviews literature on feedforward tracking control of NMP systems and Section 1.2.2 reviews literature on feedforward tracking control of systems with model uncertainties.

1.2.1 Feedforward Tracking Control of NMP Systems

When applied to systems with NMP zeros, PTC gives rise to highly oscillatory or unstable control trajectories which are unacceptable. NMP zeros are quite prevalent in practice. For example, they occur in systems with fast sampling rates [21], as well as in systems with non-collocated placement of sensors and actuators [19]. Hence a lot of research has been done on developing methods for tracking control of systems with NMP zeros. Based on excellent review articles like [18,22–24], available approaches can be classified into two broad categories: approximate model inversion, e.g., [13,25–33] and direct model inversion with bounded control trajectories, e.g., [34–43].

The most-straightforward way of implementing approximate inversion is to cancel all poles and cancellable zeros while ignoring the NMP and poorly damped zeros (hereinafter referred to as uncancellable zeros). This technique is called stable pole-zero cancelling or nonminimum phase zero ignore (NPZ-ignore) [29,31], and it results in a controlled system that exhibits magnitude and phase errors between its desired and output trajectories. Zero magnitude error tracking control (ZMETC) [24,29,30] focuses on cancelling magnitude errors across all frequencies at the expense of phase errors, whereas zero phase error tracking control (ZPETC) [13] focuses on cancelling phase errors across all frequencies at the expense of magnitude errors. Depending on the system and the performance specifications, NPZ-ignore, ZMETC and ZPETC may not yield satisfactory tracking performance due to the approximations involved. For instance, using case studies, Butterworth et al. [29,44] showed that the performance of NPZ-ignore, ZMETC and ZPETC is highly dependent on the location of the NMP zero in the z-plane; they particularly noted significant differences when tracking systems with left-hand-plane (LHP) and right-hand-plane (RHP) NMP zeros (see Figure 1.5).

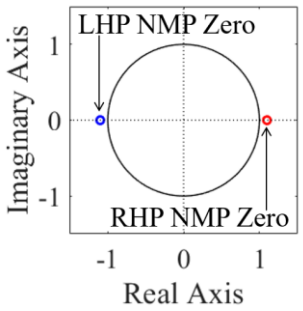

Figure 1.5 Left-hand-plane (LHP) and right-hand-plane (RHP) NMP zeros

Various methods have been suggested to improve the tracking performance of the aforementioned approximate inversion methods [26–28,32,33]. The most notable is extended bandwidth zero phase error tracking control (EBZPETC) [26], which is based on the power series expansion of ZPETC. The tracking performance of EBZPETC gets progressively better compared to ZPETC as more terms are added to the power series, provided that the series is convergent [28]. The problem is that the series is not convergent for RHP NMP zeros, in which case the performance of EBZPETC becomes worse compared to that of ZPETC [28]. As an improvement to EBZPETC, the truncated series (TS) approximation method [25] uses the power series of the inverse of the

uncancellable dynamics to improve the tracking accuracy of the system. The TS method results in a convergent series for uncancellable zeros on the right and left half z-plane. However, it fails completely (i.e., is undefined) when the uncancellable zeros lie on the unit circle. Moreover, as the uncancellable zeros approach the unit circle, the number of terms required to achieve an acceptable level of tracking accuracy increases drastically. Another approximate inversion approach is H_∞ model matching [24,30]. This method finds a controller such that the worst-case frequency domain gain deviation between the actual and desired overall dynamics is minimal. One benefit of H_∞ model matching is it can readily account for model uncertainties. However, it is computationally complex [24], and its performance is highly dependent on user-defined weighting filters – which must be properly chosen based on NMP zero locations.

Direct inversion techniques [34–38] can achieve perfect tracking with infinite preview (i.e., knowledge of future desired trajectories) or pre-actuation (i.e., actuation applied before a time interval without affecting the output during the time interval). The dynamics of the inverse of the plant is decomposed into stable and unstable portions. The solution to the stable portion is obtained from past information, whereas, the solution to the unstable portion is calculated based on future information of desired trajectory and, hence, infinite preview is required. However, infinite preview or pre-actuation is infeasible. Therefore, methods with finite preview or pre-actuation have been developed to achieve approximate tracking with reasonable accuracy [39–41,45]. With a sufficiently large number of preview steps, the error can be made arbitrarily small. However, similar to the TS method, the preview or pre-actuation needed for exact inversion techniques [36,39,43] increases as the uncancellable zero approaches the unit circle in the z-plane, and is infinite for zeros on the unit circle (i.e., for nonhyperbolic systems) [41]. Methods have been proposed to solve this problem [41–43,46,47]. However, such methods are applicable to only a restrictive set of systems [47] or desired trajectories [41,46]; alternatively, stable inversion is achieved by perturbation of the unstable inverse system, at the cost of tracking accuracy [42].

The tracking accuracy of the methods discussed above, for a given desired trajectory, varies significantly with the location of the NMP zeros in the z-plane (for a given preview or pre-actuation time interval or weighting filter). Most of the methods discussed in this review cannot be applied to nonhyperbolic systems. The methods that can be applied for tracking control of nonhyperbolic systems have restrictions in terms of the desired trajectories that they can track or in terms of their tracking performance.

To overcome these shortcomings, Ref. [48] proposed the FBF approach. The FBF approach expresses the control input as a linear combination of user-defined basis functions having unknown coefficients. The basis functions are forward filtered through the plant dynamics and the coefficients are selected such that the tracking error is minimized. The FBF approach finds its origins in iterative learning control (ILC) [49] but was not applied to feedforward tracking control of NMP systems until recently [20,48,50]. In addition, Lunenburg et al. [18] presented a tracking approach based on inversion of the lifted system representation (LSR) of plant dynamics *G*. This method is a special case of FBF where the vector space spanned by the basis functions contains the vector space spanned by all possible desired trajectories. Jetto et al. [46] employed a special case of FBF based on spline segments as basis functions to track transient portions of desired trajectories for NMP systems. However, as noted previously, their method is effective only for restrictive class of desired trajectories. In addition, it requires the use of feedback control to be effective. The FBF approach is seen in literature to be very versatile and consistent – it is applicable to all discrete-time linear systems and its tracking accuracy does not vary significantly depending on plant dynamics [20,48,50,51]. However, a fundamental understanding of the FBF approach including the role of the basis functions is lacking in the literature [20,48,50,51]. There is a wide variety of basis functions that can be used with the FBF approach but there is no work to date on how to select the best of basis functions. For example, the approach by Lunenburg et al. [18] (a special case of FBF) results in perfect tracking but results in high control input if the system has NMP zeros. Hence, a methodology for selecting the best set of basis functions to achieve an optimal tradeoff between FBF's (nominal) tracking accuracy and control effort is required.

1.2.2 Feedforward Tracking Control of Uncertain Systems

Model-inversion based FF control can be made more robust by either using some form of feedback to complement FF [47,52–58] or without using feedback [14,59–64]. Feedback based approaches include real-time feedback [52–54], iterative learning control (ILC) with iteration-level feedback [47,55–57], and adaptive control with feedback applied to model parameter estimation [58]. ILC typically assumes that the task is repetitive in nature [65] which might not hold true for many applications, whereas, adaptive control might not be effective if the control signals used for parameter estimation lack sufficient level of persistence of excitation [66,67]. In addition, as discussed in Section 1.1, this dissertation is motivated by applications where FF control is the sole

or primary recourse for control and hence, the rest of the review will focus on improving the robustness of FF controllers.

The robustness of FF tracking control can be improved by using low pass filters [59,60], H_∞ model matching approach [14,61] and direct inversion based robust controllers [62–64]. Refs. [59,60] append low pass filters to FF controllers to reduce the effect of high frequency uncertainties and disturbances on tracking error. However, introduction of low pass filters makes the FF control causal, which reduces the controller's effectiveness for tracking control of NMP systems (as seen in Section 1.2.1). In addition, the manner of selection of the low pass filter parameters is quite arbitrary, which could make the controller sub-optimal. The limitations of the H_∞ model matching approach concerning computational complexity and dependence of performance on weighting filters have already been discussed in Section 1.2.1 and hold for the robust versions as well. Devasia [62] analyzed the effect of uncertainty on direct inversion based tracking control and proposed a controller that used direct inversion at frequencies where the magnitude of uncertainty is small and does not use FF at other frequencies. Wu and Zou [63] proposed a gain modulated direct inversion approach where the gain modulation is obtained by worst case optimization of tracking error due to dynamic uncertainty (in the frequency domain) and showed its effectiveness as compared to Devasia's approach [62]. Lunenburg [64] proposed an approach that focused on finding an optimal controller using an optimization that minimized the average tracking error over the uncertainty (in the frequency domain) and implemented the approach using direct inversion [39]. However, similar to the nominal model based direct inversion approach [39], discussed in Section 1.2.1, its robust versions [62–64] suffer from dependence of required preview time on zero location in the z-plane. In addition, these robust direct inversion-based approaches cannot be used if any of the uncertain systems is nonhyperbolic.

As discussed in the previous section, FBF overcomes the limitations faced by nominal versions of the above robust approaches. Therefore, a robust version of FBF could potentially overcome the problems faced by abovementioned robust tracking controllers. Inspired by abovementioned robust control approaches, methods to improve robustness of FBF to uncertainties have been proposed in the literature [68–70]. Ref. [68] formulated the coefficient selection process as a constrained game-type problem where the control objective is to minimize the tracking error in the presence of uncertainties and the solution is obtained by solving a set of nonlinear coupled equations. This nonlinear solution is cumbersome as compared to the elegant least squares solution

of the FBF approach and is not amenable to the LPFBS algorithm (a computationally efficient implementation of the FBF method). Hence, Refs. [69,70] proposed an approach that improves the robustness of FBF and retains the elegance associated with least squares solution. An optimal FF controller that minimizes the tracking error in the frequency domain, in the presence of uncertainties, is designed. The inverse of the optimal FF controller is used to filter the basis functions and coefficients are selected such that the tracking error is minimized. However, the literature has not explored the effect of basis functions on robustness of the FBF approach and lacks a methodology for selection of optimal basis functions to improve robustness of the FBF approach.

1.3 Dissertation Contributions and Outline

To address shortcomings faced by other FF tracking controllers and develop a fundamental understanding of the FBF approach, this dissertation (based on publications [71–75]) makes the following contributions:

C1. In Chapter 2, it presents and studies the FBF approach for tracking control of NMP systems. Existence and uniqueness of the least squares solution is explored. As compared to other methods in the literature, it is shown that the FBF method is effective in tracking any desired trajectory, irrespective of the location of NMP zeros in the *z*-plane (including nonhyperbolic systems). Also, FBF maintains consistent tracking accuracy compared to popular linear time invariant (LTI) discrete-time tracking controllers irrespective of the location of the NMP zero in the *z*-plane.

C2. Also in Chapter 2, it proposes the Frobenius norm of the LSR of the dynamics as a metric for comparing the performance of LTI and linear time varying (LTV) controllers, like the FBF controller.

C3. Also in Chapter 2, it is shown analytically that, for the FBF controller, the metric for FBF's error dynamics is independent of the plant dynamics and choice of basis functions, thus explaining the consistent performance of FBF as compared to other methods.

C4. In Chapter 3, it is demonstrated that the metric for FBF's control effort dynamics is dependent on the system dynamics and choice of basis functions used. A methodology for determining the optimal set of basis functions for achieving a desired level of tracking accuracy with minimum control effort is derived analytically. The superior performance of

the optimal basis functions as compared to popular basis functions in the literature is demonstrated in simulations, and in experiments on a 3D printer.

C5. In Chapter 4, it analyzes the effect of basis functions, nominal model used for filtering the basis functions and the known model uncertainty on the tracking accuracy of the FBF approach. Based on the analysis, a methodology for optimal selection of the nominal model and the basis functions is proposed. The superior performance of the proposed optimal nominal model and optimal basis functions for robust tracking control, as compared to arbitrary selection of nominal model and popular basis functions is demonstrated in simulations, and in experiments on a 3D printer.

Chapter 5 summarizes the dissertation, presents conclusions and discusses recommendations for future research.

Chapter 2

Filtered Basis Functions Approach for Tracking Control of NMP Systems

2.1 Overview

This chapter studies the FBF for feedforward tracking control of NMP systems, presents a fundamental study of the tracking accuracy of the FBF approach and compares the FBF approach with popular methods in the literature, viz., zero phase error tracking control (ZPETC) and truncated series (TS). Since, FBF is an LTV controller, even if the plant is LTI, the Frobenius norm of the LSR of the error dynamics is proposed as a metric for evaluation and comparison of tracking accuracy of FBF as compared to LTI controllers ZPETC and TS. The analysis is illustrated in simulations using a simple first order example.

This chapter is organized as follows: The tracking control problem is introduced in Section 2.2 and the FBF approach is presented in Section 2.3. Since the FBF approach depends on the least squares solution, conditions for uniqueness and existence of the solution are explored in Section 2.4. The Frobenius norm metric is proposed in Section 2.5 and Section 2.6 analyzes tracking accuracy of the FBF approach using the Frobenius norm metric. Section 2.7 uses simulations to validate the discussion in this chapter and Section 2.8 summarizes the chapter.

2.2 Feedforward Tracking Control Problem

Given a discrete-time linear time invariant (LTI) single input single output (SISO) system $G(q)$, as shown in Figure 2.1, which may represent an open loop plant or a closed loop-controlled system, we can write

$$y(k) = G(q)u(k) \tag{2.1}$$

where k is the time index, q is the forward shift operator, y and u are the output and control input, respectively. The objective of tracking control is to design the feedforward controller $C(q)$ or find the control input $u(k)$ given by

$$u(k) = C(q)y_d(k) \tag{2.2}$$

where $y_d(k)$ is the desired trajectory, such that the tracking error $e(k)$

$$\begin{aligned} e(k) &= y_d(k) - y(k) \\ &= (1 - \underbrace{G(q)C(q)}_{L(q)})y_d(k) = E_{ff}(q)y_d(k) \end{aligned} \tag{2.3}$$

is minimized, where $L(q)$ and $E_{ff}(q)$ are the overall and the error dynamics of the controlled system, respectively.

For finite time, $0 \le k \le M$ (M+1 is the number of discrete points in the trajectory), the desired trajectory, control input, tracking error and output trajectory can be expressed using vectors

$$\begin{aligned} \mathbf{y}_d &= \begin{bmatrix} y_d(0) & y_d(1) & \dots & y_d(M) \end{bmatrix}^{\mathrm{T}}, \\ \mathbf{u} &= \begin{bmatrix} u(0) & u(1) & \dots & u(M) \end{bmatrix}^{\mathrm{T}}, \\ \mathbf{e} &= \begin{bmatrix} e(0) & e(1) & \dots & e(M) \end{bmatrix}^{\mathrm{T}}, \\ \mathbf{y} &= \begin{bmatrix} y(0) & y(1) & \dots & y(M) \end{bmatrix}^{\mathrm{T}} \end{aligned} \tag{2.4}$$

Accordingly, Eqs. (2.1), (2.2) and (2.3) can be expressed as

$$\mathbf{y} = \mathbf{G}\mathbf{u}; \quad \mathbf{u} = \mathbf{C}\mathbf{y}_d; \quad \mathbf{e} = \underbrace{(\mathbf{I} - \mathbf{L})}_{\mathbf{E}_{ff}}\mathbf{y}_d \tag{2.5}$$

where $\mathbf{G}$, $\mathbf{C}$, $\mathbf{L}$ and $\mathbf{E}_{ff}$ are the lifted system representations [65] of G, C, L and E_{ff}, respectively (see Appendix A for more details), and $\mathbf{I}$ is the identity matrix of appropriate size. The use of boldface symbols to represent LSR of systems is maintained hereinafter.

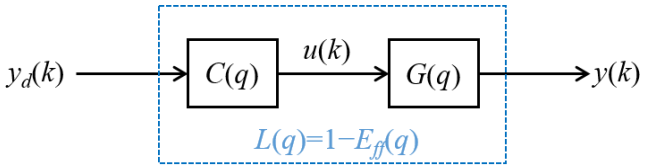

Figure 2.1 Block diagram for feedforward tracking control

2.3 Filtered Basis Functions (FBF) Approach

The FBF approach relies on two assumptions:

- The desired trajectory is known a priori
- The control input $u(k)$ is expressed as a linear combination of n+1 user-defined basis functions $\varphi_i(k)$

$$u(k) = \sum_{i=0}^{n} \gamma_i \varphi_i(k) \tag{2.6}$$

where γ_i are unknown coefficients. Using vectors, Eq. (2.6) can be expressed as

$$\begin{aligned} &\mathbf{u} = \boldsymbol{\Phi}\boldsymbol{\gamma}; \\ &\boldsymbol{\Phi} = \begin{bmatrix} \boldsymbol{\varphi}_0 & \boldsymbol{\varphi}_1 & \cdots & \boldsymbol{\varphi}_n \end{bmatrix}, \\ &\boldsymbol{\varphi}_i = \begin{bmatrix} \varphi_i(0) & \varphi_i(1) & \cdots & \varphi_i(M) \end{bmatrix}^{\mathrm{T}}, \\ &\boldsymbol{\gamma} = \begin{bmatrix} \gamma_0 & \gamma_1 & \cdots & \gamma_n \end{bmatrix}^{\mathrm{T}} \end{aligned} \tag{2.7}$$

For a linear system $G(q)$ (with lifted system representation $\mathbf{G}$), $\mathbf{y}$ can be expressed as

$$\begin{aligned} &\mathbf{y} = \tilde{\boldsymbol{\Phi}}\boldsymbol{\gamma}; \\ &\tilde{\boldsymbol{\Phi}} = \mathbf{G}\boldsymbol{\Phi}; \quad \tilde{\boldsymbol{\varphi}}_i = \mathbf{G}\boldsymbol{\varphi}_i; \\ &\tilde{\boldsymbol{\Phi}} = \begin{bmatrix} \tilde{\boldsymbol{\varphi}}_0 & \tilde{\boldsymbol{\varphi}}_1 & \cdots & \tilde{\boldsymbol{\varphi}}_n \end{bmatrix} \end{aligned} \tag{2.8}$$

where $\tilde{\mathbf{\Phi}}$ represents the filtered basis functions matrix, obtained by filtering $\mathbf{\Phi}$ using the model of the system *G*, as shown in Figure 2.2. The control objective is to find the optimal coefficient vector $\boldsymbol{\gamma}$ such that the 2-norm of the tracking error

$$\mathbf{e}^{\mathrm{T}}\mathbf{e} = \left(\mathbf{y}_d - \tilde{\mathbf{\Phi}}\boldsymbol{\gamma}\right)^{\mathrm{T}}\left(\mathbf{y}_d - \tilde{\mathbf{\Phi}}\boldsymbol{\gamma}\right) \tag{2.9}$$

is minimized; the optimal solution is given by

$$\boldsymbol{\gamma}^{*} = \left(\tilde{\mathbf{\Phi}}^{\mathrm{T}}\tilde{\mathbf{\Phi}}\right)^{-1}\tilde{\mathbf{\Phi}}^{\mathrm{T}}\mathbf{y}_d \tag{2.10}$$

Based on Eqs. (2.5), (2.7), (2.8) and (2.10), the lifted system representations of the controller and error dynamics can be expressed as

$$\begin{aligned}\mathbf{C}_{FBF} &= \mathbf{\Phi}\left(\tilde{\mathbf{\Phi}}^{\mathrm{T}}\tilde{\mathbf{\Phi}}\right)^{-1}\tilde{\mathbf{\Phi}}^{\mathrm{T}} \\ \mathbf{E}_{ff,FBF} &= \mathbf{I} - \underbrace{\tilde{\mathbf{\Phi}}\left(\tilde{\mathbf{\Phi}}^{\mathrm{T}}\tilde{\mathbf{\Phi}}\right)^{-1}\tilde{\mathbf{\Phi}}^{\mathrm{T}}}_{\mathbf{L}_{FBF}}\end{aligned} \tag{2.11}$$

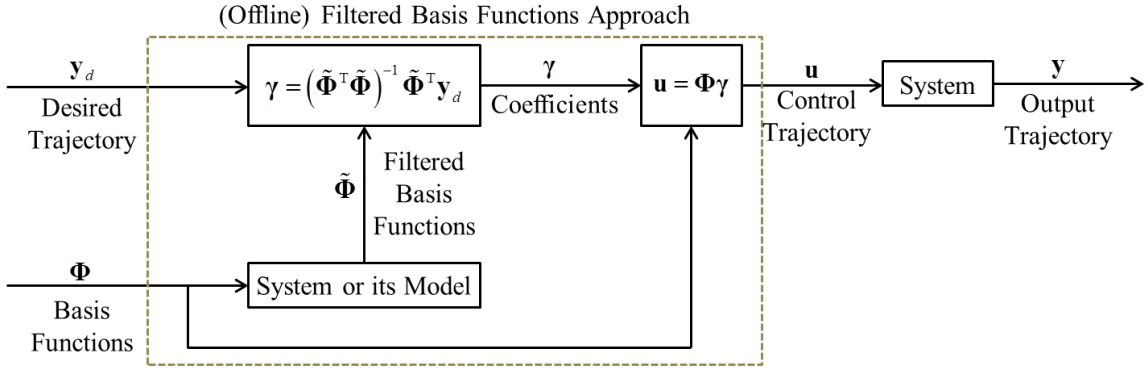

Figure 2.2 Flow chart of the FBF approach

Remark 2.1: $\mathbf{C}_{FBF}$ and $\mathbf{E}_{ff,FBF}$ both depend on the system as well as the selected basis functions. Both matrices are, in general, non-Toeplitz and non-triangular implying that the FBF controller is, in general, LTV and non-causal.

Remark 2.2: The LTV system resulting from the FBF approach is bounded input bounded output (BIBO) stable for stable G and finite n and M. Interested readers can see Appendix B for more details.

Remark 2.3: Although the above discussion focuses on the FBF approach in the context of LTI SISO systems, it is applicable to other types of linear systems such as LTV and MIMO systems. Ref. [20] relaxes the assumption on a priori knowledge of the desired trajectory using B-spline basis functions. As shown in Section 1.1, this variant of the FBF approach called the limited preview filtered B-splines (LPFBS) approach can significantly reduce tracking errors and print time in commercial 3D printers (see Figure 1.3 and Table 1.1).

The FBF approach is observed to be quite effective for a wide range of desired trajectories and plants including nonhyperbolic systems, for example, systems with zeros on the unit circle in the z-plane [20,48,50], square and non-square multi input multi output (MIMO), linear parameter varying (LPV) and LTV systems [51], etc. This versatility of FBF could help control designers to effectively track multi-axis systems with significantly different dynamics along its axes using the same tracking control method, i.e., FBF, along different axes. However, a fundamental understanding of the approach including the role of the basis functions is lacking in the literature and is explored in Refs. [71–75]. This dissertation (based on Refs. [71–75]) focuses on understanding the FBF approach, and starts with establishing the conditions for existence and uniqueness of the least squares solution (Eq. (2.10)), presented in the following section.

2.4 Existence and Uniqueness of Least Squares Solution

A unique solution to Eq. (2.10) exists if $\left(\tilde{\mathbf{\Phi}}^{\mathrm{T}}\tilde{\mathbf{\Phi}}\right)^{-1}$ exists, i.e., if $\tilde{\mathbf{\Phi}}^{\mathrm{T}}\tilde{\mathbf{\Phi}}$ is invertible. The matrix $\tilde{\mathbf{\Phi}}^{\mathrm{T}}\tilde{\mathbf{\Phi}}$ is invertible provided $\tilde{\mathbf{\Phi}}$ has linearly independent columns, meaning that the rank of the matrix $\tilde{\mathbf{\Phi}}$ is equal to n+1 [76]. The linear dependence of filtered basis functions $\{\tilde{\varphi}_i(k)\}$ implies the existence of non-zero $\{\eta_i\}$ such that

$$\begin{aligned} y(k) &= \sum_{i=0}^{n} \eta_i \tilde{\varphi}_i(k) = 0; \\ u(k) &= \sum_{i=0}^{n} \eta_i \varphi_i(k) \neq 0 \end{aligned} \tag{2.12}$$

given that $\{\varphi_i(k)\}$ are linearly independent by definition. Hence, $\{\tilde{\varphi}_i(k)\}$ are linearly dependent if there exists a non-zero $u(k)$ such that

$$y(k) = Gu(k) = 0 \tag{2.13}$$

implying that a non-zero $u(k)$ belongs to the null space of the system.

For further analysis, the state-space representation of the system G (with state, input, output and feedforward matrices denoted by $\mathbf{A}_d$, $\mathbf{B}_d$, $\mathbf{C}_d$ and D_d) is used, because it accounts for non-zero initial conditions. The output $y(k)$ is composed of a zero input response (ZIR) and a zero state response (ZSR) [77], i.e.,

$$y(k) = \underbrace{\mathbf{C}_d \mathbf{A}_d^k \mathbf{x}(0)}_{\text{Zero Input Response (ZIR)}} + \underbrace{\mathbf{C}_d \sum_{q=0}^{k-1} \mathbf{A}_d^{k-q-1} \mathbf{B}_d u(q) + D_d u(k)}_{\text{Zero State Response (ZSR)}} \tag{2.14}$$

Consequently, the linear dependence of the filtered basis functions requires the determination of $u(k) \neq 0$ and $\mathbf{x}(0)$ such that $y(k) = 0$ for $0 \leq k \leq M$; i.e.,

$$0 = \mathbf{C}_d \mathbf{A}_d^k \mathbf{x}(0) + \mathbf{C}_d \sum_{q=0}^{k-1} \mathbf{A}_d^{k-q-1} \mathbf{B}_d u(q) + D_d u(k) \tag{2.15}$$

The system of equations given by Eq. (2.15) represents an underdetermined system [77] (with M+1 equations and M+1+n_o unknowns) with infinitely many solutions. The solutions to Eq. (2.15) form a vector space (denoted as $\widehat{U}$) which is n_o dimensional. If $\mathbf{x}_0(0)$, $\mathbf{x}_1(0)$, ..., $\mathbf{x}_n(0)$ represent the initial states used to forward filter basis functions $\varphi_0(k)$, $\varphi_1(k)$, ..., $\varphi_n(k)$, respectively, then the filtered basis functions are linearly dependent if there exists non-zero $\{\eta_i\}$ and $\begin{bmatrix} \widehat{\mathbf{u}}^{\mathrm{T}} & \widehat{\mathbf{x}}^{\mathrm{T}}(0) \end{bmatrix}^{\mathrm{T}} \in \widehat{U}$, such that

$$\begin{bmatrix} \boldsymbol{\Phi} \\ \mathbf{X} \end{bmatrix} \boldsymbol{\eta} = \begin{bmatrix} \hat{\mathbf{u}} \\ \hat{\mathbf{x}}(0) \end{bmatrix};$$
$$\mathbf{X} = \begin{bmatrix} \mathbf{x}_0(0) & \mathbf{x}_1(0) & \dots & \mathbf{x}_n(0) \end{bmatrix}$$
$$\boldsymbol{\eta} = \begin{bmatrix} \eta_0 & \eta_1 & \dots & \eta_n \end{bmatrix}^{\mathrm{T}} \tag{2.16}$$
$$\hat{\mathbf{u}} = \begin{bmatrix} \hat{u}(0) & \hat{u}(1) & \dots & \hat{u}(M) \end{bmatrix}^{\mathrm{T}}$$

Therefore, the filtered basis functions $\{\tilde{\varphi}_i(k)\}$ are linearly dependent if and only if the basis functions $\{\varphi_i(k)\}$ and filter initial states $\{\mathbf{x}_i(0)\}$ satisfy the condition

$$\operatorname{rank}\left(\begin{bmatrix} \boldsymbol{\Phi} \\ \mathbf{X} \end{bmatrix}\right) = \operatorname{rank}\left(\begin{bmatrix} \boldsymbol{\Phi} & \hat{\mathbf{u}} \\ \mathbf{X} & \hat{\mathbf{x}}(0) \end{bmatrix}\right) \tag{2.17}$$

Note that $\hat{\mathbf{u}}$ and $\hat{\mathbf{x}}(0)$ are dependent on the dynamics of a given system whereas $\boldsymbol{\Phi}$ and $\mathbf{X}$ can be freely selected by the user.

Remark 2.4: Linear dependence of filtered basis functions is quite rare. However, if the conditions given by Eq. (2.17) are satisfied by a given $\boldsymbol{\Phi}$ and $\mathbf{X}$, then the control designer can easily modify either $\boldsymbol{\Phi}$ or $\mathbf{X}$ to establish linear independence of the filtered basis functions, as demonstrated using an example in Appendix C. For $\mathbf{X} = \mathbf{0}_{n+1}^{\mathrm{T}}$, linear dependence can typically occur if the LSR of the system $\mathbf{G}$ has very small singular values. Very small singular values are quite prevalent if the system has NMP zeros or a relative degree (i.e., more poles than zeros). Selection of basis functions $\boldsymbol{\Phi}$ (for $\mathbf{X} = \mathbf{0}_{n+1}^{\mathrm{T}}$) to avoid these small singular values is further explored in Chapter 3.

2.5 Frobenius Norm Metric for Analyzing Performance of Linear Controllers

As discussed in Section 2.3 (Remark 2.1), the FBF approach results in an LTV controller and hence, FBF is fundamentally different than popular LTI control methods in the literature (discussed in Section 1.2.1), viz., NPZ-ignore, ZPETC, ZMETC, EBZPETC, TS, direct inversion, etc. The tracking performance of these popular methods in the literature has been quantified and analyzed using frequency-domain metrics like Bode diagrams [25], magnitude at Nyquist frequency [29] and 2-norm of error dynamics [18,25]. However, such frequency-domain metrics

are not applicable to the FBF approach because it is an LTV controller. To address this shortcoming, this dissertation proposes the following metric based on the LSR of tracking error dynamics

$$J_e \triangleq \frac{1}{\sqrt{M+1}} \left\| \mathbf{E}_{ff} \right\|_F ; \qquad \left\| \mathbf{E}_{ff} \right\|_F = \sqrt{\mathrm{Tr}\left(\mathbf{E}_{ff} \mathbf{E}_{ff}^{\mathrm{T}} \right)} = \sqrt{\sum_i \left\{ \sigma_i (\mathbf{E}_{ff}) \right\}^2} \tag{2.18}$$

The Frobenius norm is selected because it takes into account all singular values/gains (σ_i) of $\mathbf{E}_{ff}$, as opposed to $\|\mathbf{E}_{ff}\|_2$, which considers only the maximum singular value/gain. The square root of (M+1) in the metric ensures that the metric is uniformly bounded as the length of the trajectory grows.

Note that for a normalized desired trajectory ($\|\mathbf{y}_d\|_2 = 1$),

$$\mathbf{e}_{RMS} = \frac{\| \mathbf{e} \|_2}{\sqrt{M+1}} \leq \frac{\left\| \mathbf{E}_{ff} \right\|_F}{\sqrt{M+1}} = J_e \tag{2.19}$$

The implication is that J_e is an upper bound on the RMS tracking error ($\mathbf{e}_{RMS}$). Moreover, it is shown in Appendix D, that for an LTI system

$$\frac{\left\| \mathbf{E}_{ff} \right\|_F}{\sqrt{M+1}} \to \left\| E_{ff}(q) \right\|_2 \quad \text{as } M \to \infty \tag{2.20}$$

In other words, J_e approaches the system error 2-norm criterion (sometimes used in the design and analysis of tracking controllers [25]).

Remark 2.5: The lifted system representation is employed for the proposed metric because it applies to both LTI and LTV controllers [65]. Moreover, the lifted system representation is applicable to feedforward as well as feedback controllers, SISO as well as multi-input multi-output (MIMO) controllers. As a result, the proposed metric is broadly applicable to any linear, discrete-time tracking controller.

2.6 Analysis of Tracking Accuracy of FBF using Frobenius Norm Metric

This section analyzes the FBF approach using the Frobenius norm metric applied to its error dynamics.

Proposition 2.1*:* The metric of Eq. (2.18) applied to the FBF error dynamics (i.e., $J_{e,FBF}$) is given by

$$J_{e,FBF} = \sqrt{1 - \frac{n+1}{M+1}} \tag{2.21}$$

Proof*:* The filtered basis functions matrix $\tilde{\mathbf{\Phi}}$ in Eq. (2.8) can be transformed to the decoupled filtered basis functions matrix $\tilde{\mathbf{\Psi}}$ using transformation $\mathbf{\Omega}$ (for more details see Appendix E)

$$\begin{aligned} \tilde{\mathbf{\Phi}} &= \tilde{\mathbf{\Psi}}\mathbf{\Omega} \\ \mathbf{\Phi} &= \mathbf{\Psi}\mathbf{\Omega} \end{aligned} \tag{2.22}$$

such that

$$\begin{aligned} &\tilde{\mathbf{\Psi}}^{\mathrm{T}}\tilde{\mathbf{\Psi}} = \mathbf{I}_{n+1}; \\ &\mathbf{C}_{FBF} = \mathbf{\Psi}\tilde{\mathbf{\Psi}}^{\mathrm{T}}; \\ &\mathbf{E}_{ff,FBF} = \mathbf{I}_{M+1} - \tilde{\mathbf{\Psi}}\tilde{\mathbf{\Psi}}^{\mathrm{T}} \end{aligned} \tag{2.23}$$

Based on Eq. (2.20), it is known that $\mathbf{L}_{FBF}$, which depends on the selected basis functions and the plant dynamics, can be expressed as

$$\mathbf{L}_{FBF} = \sum_{i=1}^{n+1} \tilde{\mathbf{\psi}}_i \tilde{\mathbf{\psi}}_i^{\mathrm{T}} \tag{2.24}$$

where $\tilde{\mathbf{\psi}}_i$ are the decoupled filtered basis functions that satisfy

$$\tilde{\boldsymbol{\psi}}_i^{\mathrm{T}}\tilde{\boldsymbol{\psi}}_j = \delta_{ij}$$
$$\delta_{ij} = \begin{cases} 1 & i = j \\ 0 & i \neq j \end{cases} \tag{2.25}$$

Hence,

$$\begin{aligned} J_{e,FBF} &= \frac{\left\| \mathbf{I} - \mathbf{L}_{FBF} \right\|_F}{\sqrt{M+1}} \\ &= \frac{\left\| \sum_{i=1}^{M+1} \tilde{\boldsymbol{\psi}}_i \tilde{\boldsymbol{\psi}}_i^{\mathrm{T}} - \sum_{i=1}^{n+1} \tilde{\boldsymbol{\psi}}_i \tilde{\boldsymbol{\psi}}_i^{\mathrm{T}} \right\|_F}{\sqrt{M+1}} \\ &= \frac{\left\| \sum_{i=n+2}^{M+1} \tilde{\boldsymbol{\psi}}_i \tilde{\boldsymbol{\psi}}_i^{\mathrm{T}} \right\|_F}{\sqrt{M+1}} \\ &= \sqrt{\frac{M-n}{M+1}} \\ &= \sqrt{1 - \frac{n+1}{M+1}} \end{aligned} \tag{2.26}$$

(End of proof)

Remark 2.6: Note that $J_{e,FBF}$ is independent of $G(q)$ and the type of basis functions employed. It depends only on the number of basis functions (relative to the number of discrete points in the trajectory). As the number of basis functions increases, the tracking accuracy of the FBF approach improves. As will be shown in Section 2.7, the independence of J_e from $G(q)$ cannot be taken for granted with other tracking controllers. The consistent tracking accuracy of FBF stems from the unique structure of $\mathbf{E}_{ff,FBF}$ and it provides an analytical explanation of the relative independence of the FBF method's tracking accuracy from $G(q)$ observed in Refs. [20,48], and demonstrated in Section 2.7. Also, the result of Proposition 2.1 holds for any linear plant dynamics, i.e., it also applies to LTV and LPV plants.

Remark 2.7: Note that, $\|\mathbf{E}_{ff,FBF}\|_2$ is equal to 1, irrespective of the number of basis functions used, which is not a reasonable representation of the tracking accuracy of the FBF method, which varies

significantly with n [20,48]. Hence, the proposed metric is more appropriate compared to 2-norm metrics like those used in convergence analysis in ILC [78].

2.7 Examples

To demonstrate the effectiveness of the FBF approach, it is compared with popular methods in the literature, viz., zero phase error tracking control (ZPETC) and truncated series (TS), using time-domain examples and the proposed Frobenius norm metric applied to their respective error dynamics. For comparison a simple first-order plant studied by Butterworth et al. [79] is used.

$$G(q) = \frac{q-a}{q-p} \tag{2.27}$$

where a (a real number) and $p = 0.5$ are the zero and pole of the plant, respectively. The ZPETC [13] is a widely discussed technique in the literature, and TS [25] is the optimal solution to the constrained minimization of weighted integral of squared magnitude of the error dynamics; it is one of the most versatile controllers with regards to its ability to deliver excellent tracking irrespective of the plant dynamics.

As shown in the preceding section, the Frobenius norm metric J_e for FBF is independent of the plant dynamics (see Eq. (2.26)). For ZPETC, the error dynamics $E_{ff}(q)$ and metric J_e are given by

$$\left.\begin{aligned} L_{ZPETC}(q) &= \frac{(q-a)\left(q^{-1}-a\right)}{(1-a)^2} \\ \Rightarrow E_{ff,ZPETC}(q) &= \frac{aq^{-1}-2a+aq}{(1-a)^2} \\ \Rightarrow J_{e,ZPETC} &= \sqrt{6-\frac{2}{M+1}}\,\frac{|a|}{(1-a)^2} \end{aligned}\right\} a \neq 1 \tag{2.28}$$

For TS, the expressions are given by

$$
\begin{aligned}
L_{TS}(q) &= \begin{cases} 1-a^{-n_1}q^{n_1} & |a|>1 \\ 1-a^{n_1}q^{-n_1} & |a|<1 \end{cases} \\
\Rightarrow E_{ff,TS}(q) &= \begin{cases} a^{-n_1}q^{n_1} & |a|>1 \\ a^{n_1}q^{-n_1} & |a|<1 \end{cases} \\
\Rightarrow J_{e,TS} &= \begin{cases} \sqrt{1-\dfrac{n_1}{M+1}}\,|a|^{-n_1} & |a|>1 \\ \sqrt{1-\dfrac{n_1}{M+1}}\,|a|^{n_1} & |a|<1 \end{cases}
\end{aligned}
\tag{2.29}
$$

where n_1 is the number of terms in the series.

Remark 2.8: The expressions of J_e for ZPETC and TS given by Eqs. (2.28) and (2.29), respectively, are valid beyond the first order plant in Eq. (2.27) and hold for all systems with one real NMP zero. For ZPETC and TS, the error dynamics depends on the NMP zero and is independent of the cancellable (stable) part of the dynamics. This dependence of ZPETC and TS error dynamics on NMP zero dynamics holds irrespective of the number of NMP zero(s). The value of J_e for FBF is independent of the NMP zero(s) location, whereas, for ZPETC and TS it depends on the NMP zero(s) location.

Figure 2.3 compares the FBF approach with ZPETC and TS for $a \in [-5,5]$ based on parameter values M = 1000, n = 990 and n_1 = 5, using the normalized RMS tracking error $\mathbf{e}_{RMS}/\mathbf{y}_{d,RMS}$. A zero-mean white noise signal, with variance equal to 1, M = 1000 and sampling frequency 10 kHz, as the desired trajectory (y_d). The white noise nature of the desired trajectory ensures that it has equal intensity at different frequencies. There is a wide range of BFs available for use with the FBF method. Here, two types of BFs are used: (i) discrete cosine transform (DCT) [80] and (ii) B-splines [81]. The DCT is a frequency-based transform that is widely used in signal processing [82–84]. B-splines are commonly used to parameterize commands sent to manufacturing machines and robots [85]. The mathematical expressions for the basis functions are provided in Appendix F. The variation of $\mathbf{e}_{RMS}/\mathbf{y}_{d,RMS}$ with a seen in Figure 2.3 for FBF, ZPETC and TS are in agreement with observations made in the literature; i.e.:

- The FBF method demonstrates very consistent tracking performance irrespective of plant dynamics [20,48].

- The performance of ZPETC for left hand plane (LHP) zeros is better than that for right hand plane (LHP) zeros and the worst case is around $a = 1$ [29].
- The performance of TS for RHP and LHP zeros is the same, i.e., its performance is symmetric with respect to the imaginary axis. However, its performance degrades drastically as $|a| \rightarrow 1$ for a fixed n_1. To improve its performance as $|a| \rightarrow 1$, n_1 must approach infinity [25].

Remark 2.9: For $n = M$, FBF can achieve perfect tracking in theory. Hence, the relative accuracy between FBF and the other methods is not of particular interest, since the accuracy of FBF can always be improved by using higher n.

Remark 2.10: Note that FBF is defined for all zero locations, whereas, ZPETC and TS are not applicable for $a = 1$ and $|a| = 1$, respectively. It must be pointed out that approximate inversion is not generally used for tracking control in the minimum phase (MP) region because $C = G^{-1}$ can be employed (providing a is not poorly damped [13]). However, the MP region is included in Figure 2.3 for the sake of completeness.

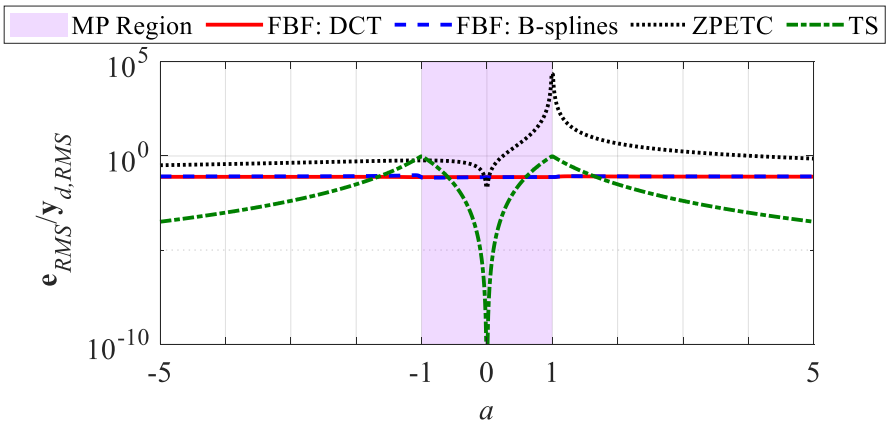

Figure 2.3 Effect of zero location on tracking error for FBF (DCT and B-splines), ZPETC and TS ($M = 1000$, $n = 990$, $n_1 = 5$). ZPETC is not applicable for $a = 1$ and TS is not applicable for $|a| = 1$. The methods are also simulated for the MP region but the plant can also be inverted in this region.

The J_e values for FBF, ZPETC and TS are plotted in Figure 2.4, for the same values of parameters as used above ($M = 1000$, $n = 990$ and $n_1 = 5$). Notice that the trends in J_e for the various methods are very similar to those observed in Figure 2.3, which validates the effectiveness of the proposed metric. It confirms that the tracking performance of FBF does not vary much with zero

location and type of basis functions. However, the tracking performances of ZPETC and TS change drastically with zero location in the pattern predicted by their respective J_e values. It must be noted that there might be instances when the performance trends might not exactly follow insights drawn from the Frobenius norm metric. For example, FBF might have much better tracking performance than predicted by J_e if one purposely (or accidently) uses filtered basis functions that span the desired trajectory (y_d). But, in general, the proposed Frobenius norm metric provides good insights about tracking performance and one can expect a more consistent performance (with respect to the zero location) with FBF compared to ZPETC and TS.

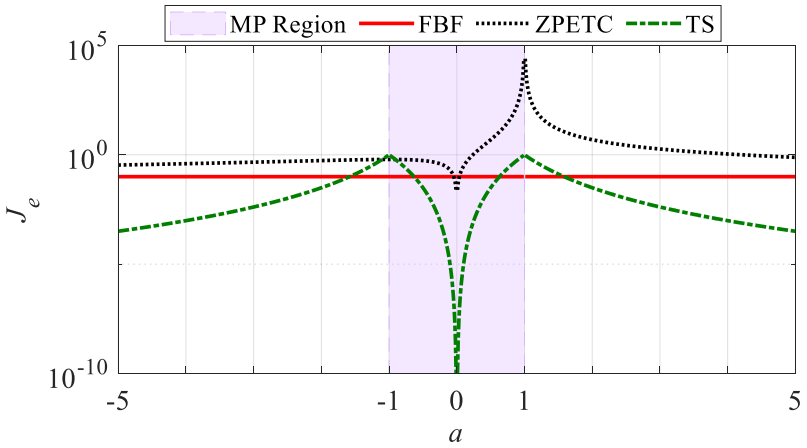

Figure 2.4 Effect of zero location on Frobenius norm metric for FBF, ZPETC and TS (M = 1000, n = 990, n_1 = 5). ZPETC is not applicable for a = 1 and TS is not applicable for $|a|$ = 1

Remark 2.11: The inconsistent performance of ZPETC and TS shown by $\mathbf{e}_{RMS}/\mathbf{y}_{d,RMS}$ and J_e in Figure 2.3 and Figure 2.4, respectively, is faced by most other tracking control methods [29]. Therefore, the consistent tracking performance of FBF predicted by $J_{e,FBF}$ and validated in Figure 2.3, as well as in Refs. [20,48], sets it apart from most other tracking control methods. This consistent tracking property of FBF presents an opportunity to effectively track multi-axis systems with significantly different dynamics along its axes using the same tracking control method, i.e., FBF, along different axes.

2.8 Summary

In this chapter, the proposed filtered basis functions (FBF) approach for tracking control of discrete-time linear systems with NMP zeros is studied. In the FBF method, it is assumed that the desired trajectory to be tracked is entirely known. Accordingly, the control input is expressed as a linear combination of linearly independent basis functions which are forward filtered using the system model, and their coefficients selected to minimize the norm of the tracking error. It is shown that the FBF solution exists and is unique if the FBFs are linearly independent. A rank test is established to ascertain linear independence of FBFs, based on the unfiltered basis functions, filter initial states and system parameters.

The analyses in this chapter show that the FBF method generally results in an LTV system, indicating its fundamental difference from methods like ZPETC and TS which always result in LTI systems. To evaluate and compare LTV controlled systems such as FBF with LTI controlled systems such as ZPETC and TS, this chapter proposes a metric based on the Frobenius norm of the LSR of system dynamics. It is shown that the proposed Frobenius norm metric is closely related to the 2-norm of the system dynamics; the metric also establishes an upper bound on the corresponding output of the system dynamics. It is very interesting that, for FBF, the proposed Frobenius norm metric applied to error dynamics is independent of the plant dynamics and the type of basis functions, whereas, for ZPETC and TS the metric is dependent on plant dynamics (specifically, zero location). The observations made using the proposed metric regarding FBF, ZPETC and TS are in agreement with those made in the literature. Analysis and simulations based on a plant with varying zero locations are used to validate the effectiveness of the FBF approach as compared to popular methods in the literature such as ZPETC and TS, and the proposed metric as a tool for evaluating the tracking performance of LTI and LTV discrete-time linear controllers.

Chapter 3

Optimal Selection of Basis Functions for Minimum-Effort Tracking Control

3.1 Overview

The previous chapter analyzed the tracking error dynamics of FBF using the Frobenius norm metric and demonstrated that the tracking accuracy of the FBF approach is independent of the type of basis functions and plant dynamics. This chapter applies the Frobenius norm metric to FBF's controller dynamics and shows that the control effort required by the FBF approach depends on the basis functions and the plant dynamics. Based on the analysis, an optimal set of basis functions that minimize the control effort without sacrificing tracking accuracy is proposed. This is especially useful in the context of control of NMP systems which are known to require large control effort. Large control efforts are not desirable because of the large amounts of energy that needs to be supplied by actuators to achieve them. In many cases where this energy cannot be supplied, saturation occurs and the tracking performance suffers. The effectiveness of the proposed optimal basis functions as compared to popular basis functions in the literature, viz. DCT and B-splines is demonstrated using simulations and experiments on a desktop 3D printer.

This chapter is organized as follows: The problem of optimal basis function selection for minimum control effort-based tracking is motivated in Section 3.2 using a simple example. Section 3.3 applies the Frobenius norm metric to FBF's controller dynamics and Section 3.4 presents a methodology for optimal selection of basis functions. The effectiveness of the proposed optimal basis functions is demonstrated in Section 3.5 using simulations and experiments on a 3D printer. Section 3.6 summarizes the chapter.

3.2 Motivation

This section motivates the rest of the chapter using the example from Section 2.7. In addition to the tracking accuracy of DCT and B-spline based FBF controllers, this section focuses

on their control inputs. Figure 3.1(a) compares the normalized root mean square (RMS) tracking error $\mathbf{e}_{RMS}/\mathbf{y}_{d,RMS}$ for the DCT and B-splines basis functions for various values of a (Figure 3.1(a) is identical to Figure 2.3 except for the omission of ZPETC and TS). As discussed in Chapter 2, the FBF approach demonstrates consistent tracking accuracy with respect to zero location and the type of basis functions. Figure 3.1(b) compares the normalized RMS control effort of the DCT and B-splines basis functions applied to the FBF approach. Notice that there is significant variation in control effort for various basis functions, even when tracking accuracy is similar. For instance, at $a = 1.02$, both the basis functions achieve similar levels of tracking accuracy, but the control effort required by B-splines is 11800 times that required by DCT. In contrast, all the basis functions have very similar values of $\mathbf{e}_{RMS}$ and $\mathbf{u}_{RMS}$ for $-1 \leq a \leq 1$. This suggests that the system dynamics and choice of basis functions play a significant role in the control effort required to achieve a desired level of tracking accuracy using the FBF approach. Hence, a methodology for determining the best set of basis functions for a given plant dynamics and desired level of tracking accuracy is needed.

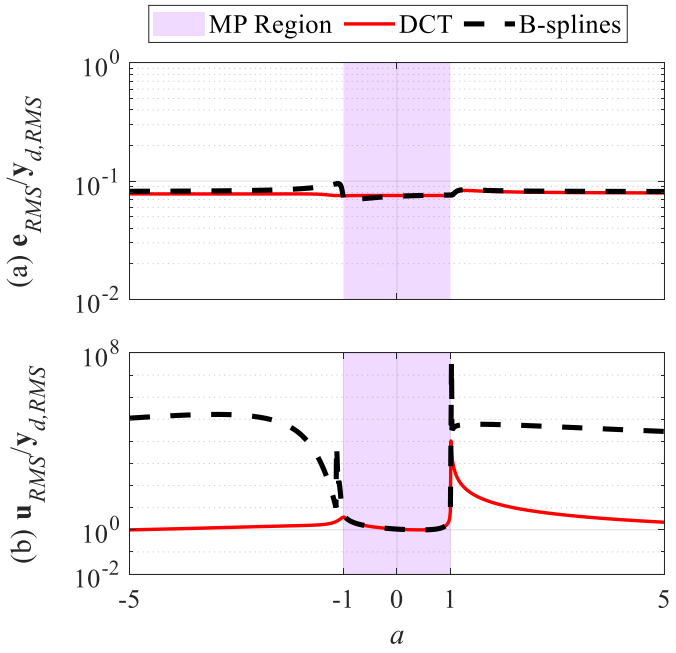

Figure 3.1 Effect of basis functions (DCT and B-splines) on: (a) normalized RMS tracking error and (b) normalized RMS control input for various values of a (M = 1000, n = 990).

3.3 Analysis of Control Effort using Frobenius Norm Metric

Based on Eq. (2.26), we can see that $J_{e,FBF} = 0$, i.e., perfect tracking can be achieved at $n = M$. However, $n = M$ implies $\mathbf{C} = \mathbf{G}^{-1}$ which might be undesirable if $G(q)$ contains uncancellable zeros because such zeros result in very small singular values of **G,** and large control signals [18]. Also, if a system has more poles than zeros, then **G** has very small singular values. The FBF approach is rank constrained minimization of the metric applied to error dynamics (see Appendix G). A rank constraint, which in the LSR implies a restricted space of input and output, is used to avoid inversion of the full **G**, while also reducing the computational demands of the control problem [80,86,87]. However, the rank constraint does not necessarily result in minimization of control input and hence, analysis of FBF controller dynamics (discussed in this section) and selection of an optimal set of basis functions (presented in Section 3.4) is necessary.

The LSR of the plant, **G**, can be decomposed using singular value decomposition (SVD) [88] as follows

$$\begin{aligned}
&\mathbf{G} = \mathbf{V}\boldsymbol{\Sigma}\mathbf{W}^{\mathrm{T}} = \sum_{i=1}^{M+1} \sigma_i \mathbf{v}_i \mathbf{w}_i^{\mathrm{T}}; \\
&\mathbf{V} = \begin{bmatrix} \mathbf{v}_1 & \mathbf{v}_2 & \dots & \mathbf{v}_{M+1} \end{bmatrix}; \\
&\mathbf{W} = \begin{bmatrix} \mathbf{w}_1 & \mathbf{w}_2 & \dots & \mathbf{w}_{M+1} \end{bmatrix}; \\
&\boldsymbol{\Sigma} = diag\left(\begin{bmatrix} \sigma_1 & \sigma_2 & \dots & \sigma_{M+1} \end{bmatrix} \right); \\
&\sigma_1 > \sigma_2 > \ldots > \sigma_{M+1} > 0
\end{aligned} \tag{3.1}$$

Without loss of generality, this paper assumes that **G** has distinct singular values.

The Frobenius norm of $\mathbf{C}_{FBF}$ can be expressed as

$$\begin{aligned}
\left\| \mathbf{C}_{FBF} \right\|_F &= \sqrt{\mathrm{Tr}(\mathbf{C}_{FBF}^{\mathrm{T}} \mathbf{C}_{FBF})} = \sqrt{\mathrm{Tr}(\tilde{\boldsymbol{\Psi}}\boldsymbol{\Psi}^{\mathrm{T}}\boldsymbol{\Psi}\tilde{\boldsymbol{\Psi}}^{\mathrm{T}})} \\
&= \sqrt{\mathrm{Tr}(\boldsymbol{\Psi}^{\mathrm{T}}\boldsymbol{\Psi}\tilde{\boldsymbol{\Psi}}^{\mathrm{T}}\tilde{\boldsymbol{\Psi}})} = \sqrt{\mathrm{Tr}(\boldsymbol{\Psi}^{\mathrm{T}}\boldsymbol{\Psi})} \\
&= \left\| \boldsymbol{\Psi} \right\|_F \\
&= \left\| \mathbf{G}^{-1}\tilde{\boldsymbol{\Psi}} \right\|_F = \left\| \mathbf{W}\boldsymbol{\Sigma}^{-1}\mathbf{V}^{\mathrm{T}}\tilde{\boldsymbol{\Psi}} \right\|_F = \left\| \boldsymbol{\Sigma}^{-1}\mathbf{V}^{\mathrm{T}}\tilde{\boldsymbol{\Psi}} \right\|_F \\
&= \left\| \boldsymbol{\Sigma}^{-1}\tilde{\boldsymbol{\Xi}} \right\|_F
\end{aligned} \tag{3.2}$$

where

$$\begin{aligned}
&\tilde{\boldsymbol{\Xi}} = \mathbf{V}^{\mathrm{T}}\tilde{\boldsymbol{\Psi}} \\
&\tilde{\boldsymbol{\Xi}} = \begin{bmatrix} \tilde{\xi}_{10} & \tilde{\xi}_{11} & \cdots & \tilde{\xi}_{1n} \\ \tilde{\xi}_{20} & \tilde{\xi}_{21} & \cdots & \tilde{\xi}_{2n} \\ \vdots & \vdots & \ddots & \vdots \\ \tilde{\xi}_{M+1,0} & \tilde{\xi}_{M+1,1} & \cdots & \tilde{\xi}_{M+1,n} \end{bmatrix} \\
&\tilde{\boldsymbol{\psi}}_j = \sum_{i=1}^{M+1} \tilde{\xi}_{ij}\mathbf{v}_i
\end{aligned} \tag{3.3}$$

The implication is that $\tilde{\xi}_{ij}$ represents the contribution of $\mathbf{v}_i$ towards $\tilde{\boldsymbol{\psi}}_j$ and vice-versa. Hence,

$$J_{c,FBF} = \frac{\left\|\mathbf{C}_{FBF}\right\|_F}{\sqrt{M+1}} = \sqrt{\frac{1}{M+1}\sum_{i=1}^{M+1}\frac{1}{\sigma_i^2}\left(\sum_{j=0}^{n}\tilde{\xi}_{ij}^2\right)} \tag{3.4}$$

Since, $\mathbf{v}_i$ and $\tilde{\boldsymbol{\psi}}_j$ are unitary vectors

$$\begin{aligned}
&\left|\tilde{\xi}_{ij}\right| \le 1 \\
&\Rightarrow \tilde{\xi}_{ij}^2 \le \left|\tilde{\xi}_{ij}\right| \\
&\Rightarrow \sum_{j=0}^{n}\tilde{\xi}_{ij}^2 \le \sum_{j=0}^{n}\left|\tilde{\xi}_{ij}\right| \le \left\|\tilde{\boldsymbol{\Xi}}\right\|_\infty \le \left\|\tilde{\boldsymbol{\Xi}}\right\|_2
\end{aligned} \tag{3.5}$$

Based on Eqs. (2.23) and (3.3)

$$\begin{aligned}
&\left\|\tilde{\boldsymbol{\Xi}}\right\|_2 = 1 \\
&\Rightarrow \sum_{j=0}^{n}\tilde{\xi}_{ij}^2 \le 1
\end{aligned} \tag{3.6}$$

The squared Frobenius norm of the FBF controller dynamics $\|\mathbf{C}_{FBF}\|_F^2$ is a linear combination of the inverse of squared singular values of **G**, i.e., $\left\{1/\sigma_i^2\right\}_{i=1}^{M+1}$ with coefficients of the linear combination $\sum_{j=0}^{n}\tilde{\xi}_{ij}^2$ determined by interaction between filtered basis functions $\tilde{\boldsymbol{\psi}}_j$ and system dynamics **G**. The coefficients are bounded between 0 and 1 and need to satisfy orthogonality condition

$$\tilde{\boldsymbol{\Xi}}^{\mathrm{T}}\tilde{\boldsymbol{\Xi}} = \mathbf{I}_{n+1} \tag{3.7}$$

3.4 Optimal Selection of Basis Functions for Minimal Control Effort

It has been shown in Section 2.6 that the tracking accuracy of the FBF method (measured by J_e) is always fixed for a given number of basis functions, irrespective of the type of basis functions or the plant dynamics. In addition, as discussed in the preceding section, for a given number of basis functions, the control effort of the FBF method (measured by J_c) is dependent on the plant dynamics and type of basis functions. In this section, the optimal set of basis functions that minimizes J_c for a given J_e are presented, i.e., find $\boldsymbol{\Psi}$ such that

$$\begin{aligned} &\min_{\boldsymbol{\Psi}} J_c\left(\boldsymbol{\Psi}, \mathbf{G}\right) \\ &\text{s.t. } J_e = J_e^*(n) \end{aligned} \tag{3.8}$$

and the resulting controller is called the control effort optimal (CE-Opt) FBF controller.

Proposition 3.1: For n+1 basis functions, the minimum value of the squared Frobenius norm of LSR of FBF controller dynamics, $\|\mathbf{C}_{FBF}\|_F^2$, is given by

$$\min\left(\|\mathbf{C}_{FBF}\|_F^2\right) = \sum_{i=1}^{n+1}\frac{1}{\sigma_i^2} \tag{3.9}$$

Proof: Proposition 3.1 is substantiated by

- proving by contradiction that there is no $\tilde{\xi}_{ij}$ such that

$$\left\|\mathbf{C}_{FBF}\right\|_F^2 < \sum_{i=1}^{n+1} \frac{1}{\sigma_i^2} \tag{3.10}$$

- showing there exists $\tilde{\xi}_{ij}$ such that

$$\left\|\mathbf{C}_{FBF}\right\|_F^2 = \sum_{i=1}^{n+1} \frac{1}{\sigma_i^2} \tag{3.11}$$

Assume

$$\begin{aligned} &\left\|\mathbf{C}_{FBF}\right\|_F^2 = \sum_{i=1}^{M+1} \frac{1}{\sigma_i^2} \chi_i < \sum_{i=1}^{n+1} \frac{1}{\sigma_i^2}; \\ &\chi_i = \sum_{j=0}^{n} \tilde{\xi}_{ij}^2 \le 1 \end{aligned} \tag{3.12}$$

Therefore,

$$\sum_{i=n+2}^{M+1} \frac{1}{\sigma_i^2} \chi_i < \sum_{i=1}^{n+1} \frac{1}{\sigma_i^2} (1 - \chi_i) \tag{3.13}$$

From Eqs. (2.23) and (3.3),

$$\mathrm{Tr}(\tilde{\mathbf{\Xi}}^{\mathrm{T}} \tilde{\mathbf{\Xi}}) = \sum_{i=1}^{M+1} \chi_i = n+1 = \mathrm{Tr}(\mathbf{I}_{n+1}) \tag{3.14}$$

Hence,

$$\sum_{i=n+2}^{M+1} \chi_i = \sum_{i=1}^{n+1} (1-\chi_i) \tag{3.15}$$

Multiplying Eq. (3.13) by σ_{n+1}^2 gives

$$\sum_{i=n+2}^{M+1} \frac{\sigma_{n+1}^2}{\sigma_i^2} \chi_i < \sum_{i=1}^{n+1} \frac{\sigma_{n+1}^2}{\sigma_i^2} (1-\chi_i) \tag{3.16}$$

Subtracting Eq. (3.15) from Eq. (3.16) results in

$$\sum_{i=n+2}^{M+1} \left(\frac{\sigma_{n+1}^2}{\sigma_i^2} - 1 \right) \chi_i < \sum_{i=1}^{n+1} \left(\frac{\sigma_{n+1}^2}{\sigma_i^2} - 1 \right) (1-\chi_i) \tag{3.17}$$

Note that

$$\begin{aligned} &\left(\frac{\sigma_{n+1}^2}{\sigma_i^2} - 1 \right) > 0 \quad \text{for} \quad i = n+2, n+3, \ldots M+1 \\ &\left(\frac{\sigma_{n+1}^2}{\sigma_i^2} - 1 \right) \leq 0 \quad \text{for} \quad i = 1, 2, \ldots, n+1 \\ &\chi_i \geq 0 \\ &(1-\chi_i) \geq 0 \end{aligned} \tag{3.18}$$

which implies that left hand side of Eq. (3.17) is always greater than or equal to zero whereas, the right hand side is always less than or equal to zero, which is a contradiction and hence, the assumption given by Eq. (3.12) is incorrect.

The minimum value of Eq. (3.9)

$$\left\| \mathbf{C}_{FBF} \right\|_F^2 = \sum_{i=1}^{n+1} \frac{1}{\sigma_i^2} \tag{3.19}$$

can be realized when

$$\tilde{\xi}_{ij} = \begin{cases} \pm 1 & i = j+1, 0 \le j \le n \\ 0 & \text{otherwise} \end{cases} \tag{3.20}$$

and hence,

$$\left\| \mathbf{C}_{FBF} \right\|_F^2 \ge \sum_{i=1}^{n+1} \frac{1}{\sigma_i^2} \tag{3.21}$$

The minimum can be achieved at

$$\begin{aligned} \tilde{\boldsymbol{\psi}}_i &= \pm \mathbf{v}_i \\ \boldsymbol{\psi}_i &= \pm \frac{\mathbf{w}_i}{\sigma_i} \\ i &= 1, 2, \ldots, n+1 \end{aligned} \tag{3.22}$$

The implication is that the decoupled filtered basis functions $\tilde{\boldsymbol{\psi}}_i$ are the left singular vectors (SV) of the LSR of the plant, **G**. Hence, the minimum value of metric $J_{c,FBF}$ is given by

$$\min J_{c,FBF} = \min \frac{\left\| \mathbf{C}_{FBF} \right\|_F}{\sqrt{M+1}} = \sqrt{\frac{1}{M+1} \sum_{i=1}^{n+1} \frac{1}{\sigma_i^2}} \tag{3.23}$$

(End of proof)

For $n = M$, i.e., the number of basis functions equals the number of trajectory points, the value of J_e and J_c are independent of the choice of basis functions and given by

$$\begin{aligned} J_e &= 0 \\ J_c &= \sqrt{\frac{1}{M+1} \sum_{i=1}^{M+1} \frac{1}{\sigma_i^2}} \end{aligned} \tag{3.24}$$

However, when $n = M$, the control input is undesirably high if system G contains NMP zero(s) [18,89].

Remark 3.1: The singular vectors (SV) based basis functions (given by Eq. (3.22)) are the optimal set of basis functions which result in minimum J_c for given J_e. Note that these optimal basis functions are system dependent. Inversion of the LSR, $\mathbf{G}^{-1}$ for NMP systems can be realized, approximately, by truncating the smallest singular values from the SVD of $\mathbf{G}$ [18,89]. The truncated SVD-based approximation of $\mathbf{G}^{-1}$ is a special case of the optimal FBF controller (i.e., it uses the SVs of $\mathbf{G}$ as basis functions with $n = M-r$, where r is the number of NMP zero(s) of system G).

Remark 3.2: For FBF, the fact that J_e is independent of plant dynamics and basis functions, whereas, J_c is dependent on the plant dynamics and basis functions permits a sequential two-stage design procedure for achieving the optimal FBF controller. In the first stage, the user selects the number of basis functions (n+1) to achieve a desired level of tracking accuracy (J_e). Then, in the second stage, the control effort (J_c) is minimized by selecting n+1 of the highest M+1−r SV components of $\mathbf{G}$ as the optimal set of basis functions.

Remark 3.3: While the proposed two-step methodology is general in that it is independent of desired trajectory, it can accommodate special cases where information (e.g., frequency spectrum) of a specific desired trajectory to be tracked is available. For instance, the dynamics can be pre-multiplied with a weighting filter that emphasizes the frequency content of the desired trajectory and the proposed methodology can be applied to the augmented dynamics.

3.5 Examples

3.5.1 Simulations

Section 3.2 motivated Section 3.4 using a first order plant and two different basis functions, viz., discrete cosine transform (DCT) and B-splines. This section continues with the same example and compares the two basis functions mentioned above, with the optimal basis functions CE-Opt proposed in Section 3.4. The desired trajectory and other parameters (M = 1000, n = 990) are same as Section 3.2.

Figure 3.2 plots J_e and J_c for different basis functions and Figure 3.3 plots the normalized tracking error $\mathbf{e}_{RMS}/\mathbf{y}_{d,RMS}$ and normalized control input $\mathbf{u}_{RMS}/\mathbf{y}_{d,RMS}$. Note that Figures 3.2 and 3.3 validate the discussion in Section 3.4. The trend for $\mathbf{e}_{RMS}/\mathbf{y}_{d,RMS}$ and $\mathbf{u}_{RMS}/\mathbf{y}_{d,RMS}$ in Figure 3.3 are quite similar to those of J_e and J_c, respectively, in Figure 3.2, which demonstrates the effectiveness of the proposed metric. Note that there might be instances when performance trends may not exactly follow the predictions of J_e or J_c. For example, FBF might have much better tracking accuracy than predicted by J_e or smaller control effort than predicted by J_c if one purposely (or accidentally) uses filtered basis functions that span the desired trajectory (y_d). However, in general, the proposed metric provides good insights on the upper limits of RMS tracking performance and control effort. As discussed in Section 3.4, all the three basis functions have similar tracking error (see Figure 3.3(a)) but different control efforts (see Figure 3.3(b)). Table 3.1 shows the mean values of $\mathbf{e}_{RMS}/\mathbf{y}_{d,RMS}$ and $\mathbf{u}_{RMS}/\mathbf{y}_{d,RMS}$ over all a. For $\mathbf{e}_{RMS}/\mathbf{y}_{d,RMS}$, the values of the mean for different basis functions are of the same order of magnitude. This validates the discussion about consistent tracking accuracy of the FBF approach. However, when it comes to $\mathbf{u}_{RMS}/\mathbf{y}_{d,RMS}$, the value of the mean for B-splines is four orders of magnitude higher than the value of the mean for DCT and the value of the mean for DCT is two orders of magnitude higher than the proposed CE-Opt basis functions. The example demonstrates the effectiveness of the proposed CE-Opt basis functions, proposed in Section 3.4, in tracking the desired trajectory with minimal control effort.

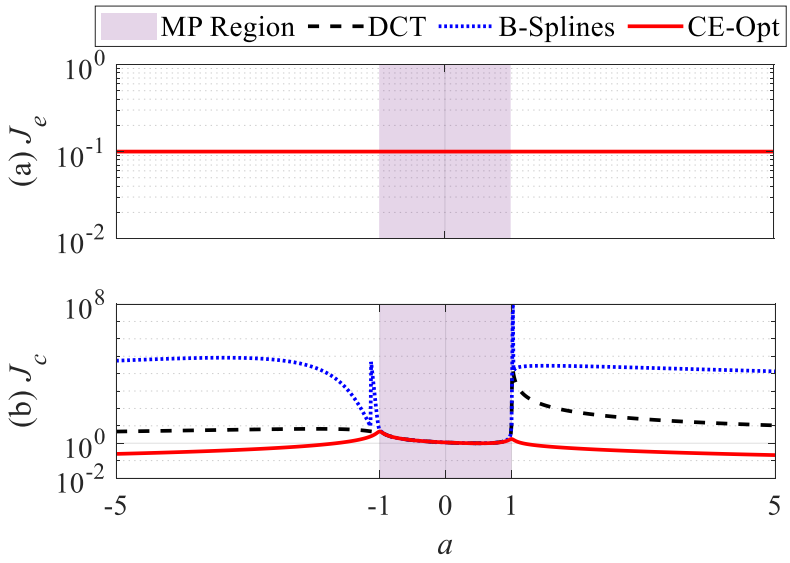

Figure 3.2 Effect of basis functions (DCT, B-splines and CE-Opt) on (a) J_e and (b) J_c for various values of a (M = 1000, n = 990).

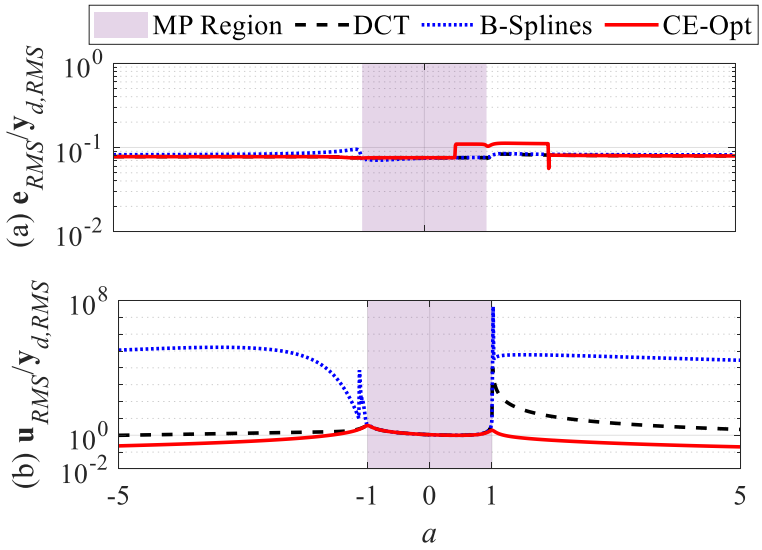

Figure 3.3 Effect of basis functions (DCT, B-splines and CE-Opt) on: (a) normalized RMS tracking error and (b) normalized RMS control input for various values of a (M = 1000, n = 990).

Table 3.1 Mean values of $\mathbf{e}_{RMS}/\mathbf{y}_{d,RMS}$ and $\mathbf{u}_{RMS}/\mathbf{y}_{d,RMS}$ over all a for different basis functions

Attribute	DCT	B-splines	CE-Opt
$\mathbf{e}_{RMS}/\mathbf{y}_{d,RMS}$	7.83×10^{-2}	8.14×10^{-2}	8.28×10^{-2}
$\mathbf{u}_{RMS}/\mathbf{y}_{d,RMS}$	2.76×10^{1}	1.02×10^{5}	7.06×10^{-1}

3.5.2 Experiments

This section demonstrates the practical benefits of optimal basis functions in experiments. The Lulzbot Taz 6 desktop 3D printer, shown in Figure 3.4, is used for the experiments. For system identification and control, motion commands are sent to the printer's stepper motors at 1 kHz sampling rate using a real-time controller (dSPACE 1202) via stepper motor drivers (Pololu DRV8825). The relative position of the print head and the bed is observed from their accelerations measured using two accelerometers (SparkFun ADXL335 triple-axis).

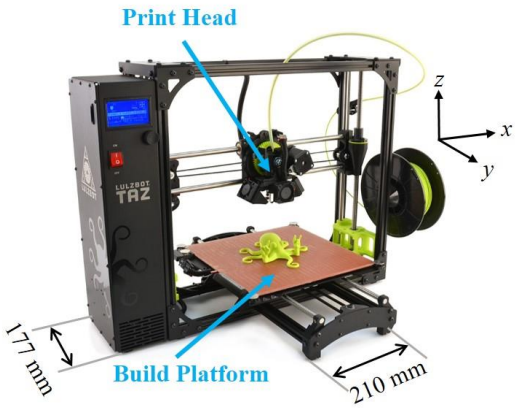

Figure 3.4 Lulzbot Taz 6 desktop 3D printer.

Figure 3.5 shows the frequency response function (FRF) of the dynamics of the *x*-axis of the 3D printer, generated by applying swept sine acceleration inputs to the printer and measuring the relative accelerations of the print head and the build platform using the accelerometers. Using *invfreqs* function in MATLAB, the dynamics is modeled as

$$G(q) = \frac{0.0874q^4 - 0.3415q^3 + 0.5118q^2 - 0.3481q + 0.09063}{q^5 - 4.54q^4 + 8.283q^3 - 7.583q^2 + 3.479q - 0.639} \tag{3.25}$$

The modeled dynamics has a pair of complex NMP zeros at 0.9924 ± 0.3176*j*, where *j* is the unit imaginary number. Figure 3.5 shows a good match between the measured and modeled FRFs. Based on the methodology discussed in Appendix A, the LSR of the modeled dynamics is generated. The position signal shown in Figure H.6(a) is used as desired trajectory. The duration of the trajectory is 1 second (i.e., M = 1000, based on 1 kHz sampling frequency).

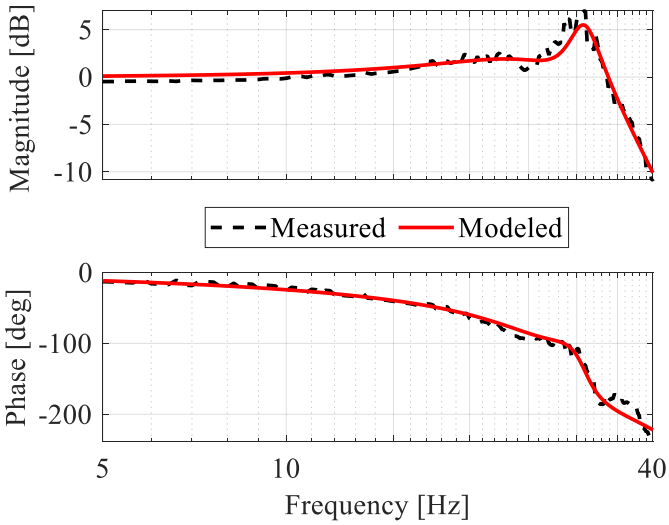

Figure 3.5 Measured and modeled frequency response functions of the *x* axis of the Taz 6 3D printer

For experiments, the optimal basis functions proposed in Section 3.4 are compared with popular basis functions DCT and B-splines. Figure 3.6 shows the control input (i.e., modified position commands) sent to the *x*-axis for the two sets of basis functions (for $n = 500$). Also, shown are the resultant tracking errors, which are based on position signals derived from measured acceleration signals using an observer. Note that the B-splines and DCT based control inputs show rapid growth in magnitude towards the end of the signal because of the small singular values of the LSR corresponding to the NMP zeros and the relative degree. For safety reasons, a limit of ± 10 mm is placed on the position commands, as shown in Figure 3.6; the B-splines and DCT based control inputs saturates at the limits. Notice that, before saturation, the control inputs for the proposed optimal basis functions and B-splines are quite similar which results in similar tracking errors. In the time interval between 0 and 0.947 s (the first-time saturation occurs), the RMS tracking errors for optimal basis functions, B-splines and DCT are 125.52 μm, 131.69 μm and 126.63 μm, respectively. However, because of saturation, the DCT and B-splines based commands generate large tracking errors, as shown in Figure 3.6. Consequently, the overall RMS tracking error for B-splines and DCT are respectively, 10% and 83% higher than the RMS tracking error for the optimal basis functions (see Table 3.2). In addition, the maximum tracking errors for B-splines and DCT are respectively, 1.82 and 6.73 times the maximum tracking error for the optimal basis functions. Moreover, the optimal basis functions require 5% and 11% lower control effort

than B-splines and DCT, respectively. The proposed optimal basis functions track better than B-splines and DCT and require less control effort.

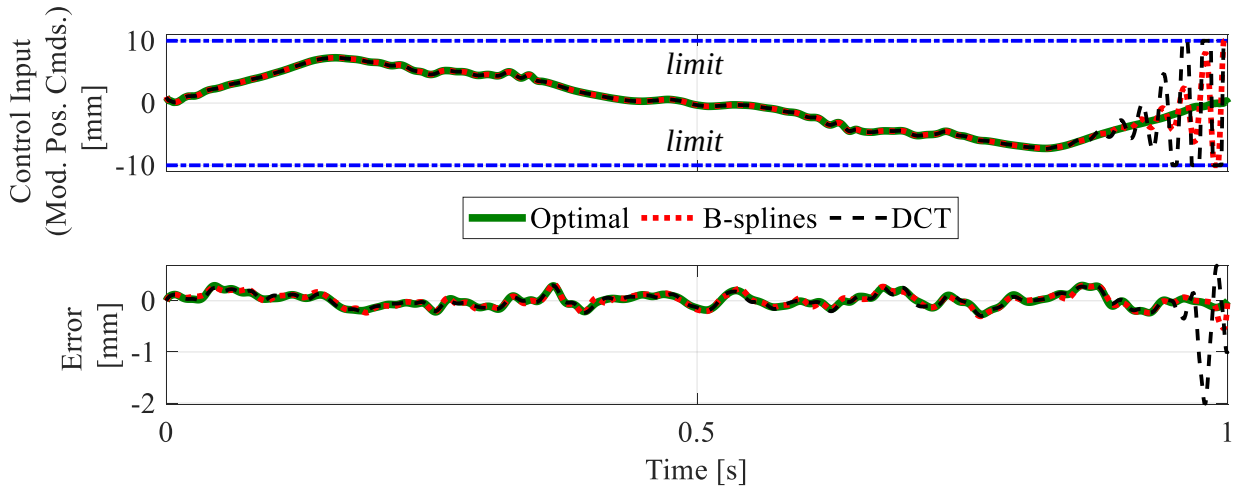

Figure 3.6 Control inputs (i.e., modified position command) signals and tracking errors for optimal basis functions, B-splines and DCT (M = 1000, n = 500)

Table 3.2 Summary of tracking error and control effort for experiments

Basis Functions	$\mathbf{e}_{RMS}/\mathbf{y}_{d,RMS}$	$\mathbf{u}_{RMS}/\mathbf{y}_{d,RMS}$	$\max(\lvert\mathbf{e}\rvert)/\mathbf{y}_{d,RMS}$
Optimal	0.0287	0.9993	0.0699
B-splines	0.0316	1.0480	0.1270
DCT	0.0525	1.1227	0.4701

Remark 3.4: The violation of actuator limits by B-splines observed in the results of Figure 3.6 can be mitigated by formulating the FBF approach as a constrained optimization problem using the constraint handling capabilities of B-splines, as done in prior work of the authors [90]. However, all things being equal, it is theoretically and practically preferable to avoid large control signals altogether than to contain them via constraints.

Appendix H presents experiments on a biaxial linear motor driven stage. The dynamics of the biaxial stage has one real NMP zero along each axis and B-splines based control input demonstrates saturation, similar to the example in this section. The proposed optimal basis functions are shown to improve the tracking error by up to 19 times as compared to the B-splines basis functions.

3.6 Summary

This chapter analyzes the control effort of the FBF approach by applying the Frobenius norm metric to FBF's controller dynamics. Although the metric applied to error dynamics of FBF shows independence from plant dynamics and basis functions (shown in Chapter 2), application of the metric to FBF's controller dynamics shows that the control effort depends on the plant dynamics as well as the basis functions. Leveraging the analysis, a two-step procedure for selection of optimal basis functions that minimize the control effort for a given tracking accuracy is proposed. In the first step, the number of basis functions is selected to satisfy a desired level of tracking accuracy regardless of the type of basis functions; in the second step, the optimal set of basis functions – which are related to the singular vectors of the controlled system – are determined for minimum control effort. Simulations and experiments are used to demonstrate the effectiveness of the proposed optimal basis functions. Simple first-order plants with varying zero locations in the *z*-plane are used in simulations and the proposed basis functions are compared with other commonly used basis functions (DCT and B-splines). The results demonstrate the effectiveness of the proposed metric as well as the superiority of the optimal basis functions as compared to popular basis functions. Experiments on a Lulzbot Taz 6 desktop 3D printer, are used to show that the proposed basis functions can effectively track a desired trajectory with minimal control effort, as compared to popular basis functions DCT and B-splines which require much higher control effort, resulting in control saturation and degradation of tracking accuracy.

Chapter 4

Optimal Selection of Basis Functions and Nominal Model for Robust Tracking Control

4.1 Overview

As discussed in Section 1.1, a key challenge with inversion based feedforward control methods, including FBF, is how to improve their tracking accuracy, in the presence of uncertainties. Section 1.2.2 presents various methods used in the literature to improve tracking accuracy of feedforward control methods, in the presence of uncertainties. Inspired by these methods in the literature, various approaches such as optimal selection of coefficients [68] and optimal filtering of basis functions [69,70] (also presented in Appendix I with simulation and experimental examples) have been explored as avenues to improve the robustness of the FBF approach. However, optimal selection of basis functions also presents an opportunity for improving the robustness of the FBF approach that is unavailable to other feedforward tracking control methods. This chapter proposes a methodology for finding an optimal set of basis functions for robust tracking control using the Frobenius norm metric discussed in Chapter 2, in a manner similar to the use of the metric to find basis functions for minimum control effort in Chapter 3. The proposed methodology for selection of basis functions could be used as an alternative or in complement to existing methods. This chapter complements optimal basis functions selection with optimal nominal model selection, derived using lifted domain optimization.

This chapter is organized as follows: Section 4.2 motivates the rest of the chapter. Section 4.3 analyzes the tracking accuracy of the FBF approach, in the presence of known uncertainties, using the Frobenius norm metric. Based on the analysis in Section 4.3, Sections 4.4 and 4.5 propose methodologies for optimal selection of basis functions and optimal nominal model, respectively. Section 4.6 demonstrates the effectiveness of the approach as compared to standard FBF and popular basis functions and Section 4.7 summarizes the chapter.

4.2 Motivation

This section motivates the rest of the chapter, using a damped oscillator with parametric uncertainty:

$$\begin{aligned} &G(s) = \frac{\omega_n^2}{s^2 + 2\zeta\omega_n s + \omega_n^2}; \\ &\omega_{n,nom} = 200\text{Hz}, \;\; \zeta_{nom} = 0.01, \\ &\omega_n \in [180, \quad 220]\text{Hz}, \;\; \zeta \in [0.001, \quad 0.1] \end{aligned} \tag{4.1}$$

where ω_n and ζ denote the natural frequency and damping ratio, and the subscript '*nom*' denotes the nominal value. The system is sampled at 1 kHz. The set of actual plant dynamics, is generated by selecting 410 evenly distributed realizations of the plant defined by Eq. (4.1). The nominal values of the plant parameters are used to generate the nominal model for filtering the basis functions. Similar to the discussion in Chapters 2 and 3, the desired signal $\mathbf{y}_d$ is a white noise signal with zero mean and unit variance. This example uses popular basis functions DCT and B-splines, and CE-Opt basis functions (the optimal basis functions for control effort, proposed in Chapter 3).

Figure 4.1 shows the normalized RMS tracking error $\mathbf{e}_{RMS}/\mathbf{y}_{d,RMS}$ for DCT, B-splines and CE-Opt basis functions, for various numbers of basis functions (n = 10 to 990), using the 410 realizations of the actual plant dynamics G, described above. The metrics used for comparison are the mean, standard deviation and nominal values (assuming the plant model is perfect) of $\mathbf{e}_{RMS}/\mathbf{y}_{d,RMS}$. It is observed that for the same n, the nominal tracking accuracy of FBF does not vary significantly with the type of basis functions. This observation is in agreement with the discussion in Chapter 2. However, it is observed that the tracking accuracy of the FBF approach deteriorates in the presence of uncertainty and varies significantly depending on the type of basis functions. This example suggests that although different basis functions give the same nominal tracking accuracy, their tracking accuracy, in the presence of uncertainties, varies significantly with the choice of basis functions used for tracking. Hence, a methodology for selecting an optimal set of basis functions for robust tracking control using FBF is needed.

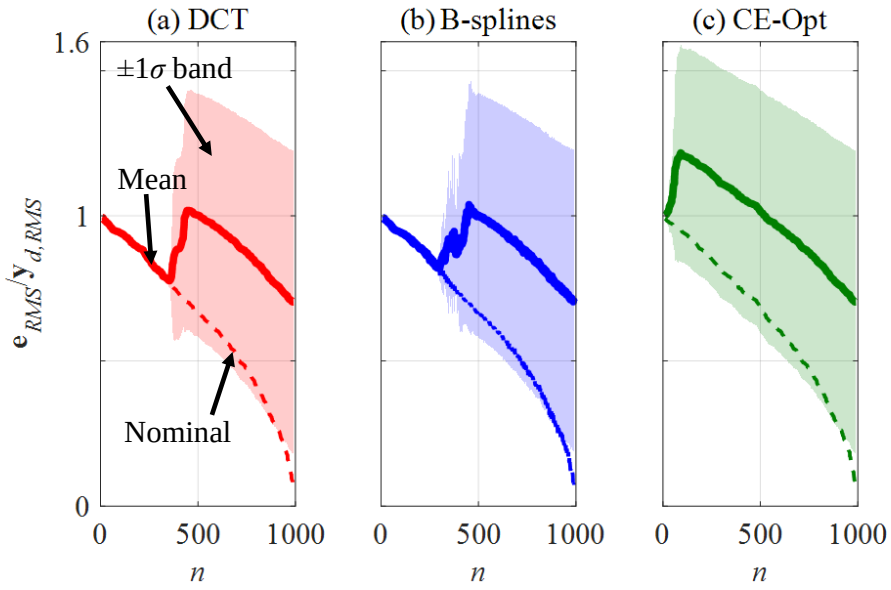

Figure 4.1 Comparison of normalized RMS tracking error for DCT, B-splines and CE-Opt basis functions, in the absence (nominal) and presence of uncertainty, for various values of number of basis functions, n

4.3 Analysis of Robustness of FBF using Frobenius Norm Metric

Section 2.6 analyzed tracking accuracy of FBF, using the Frobenius norm metric, assuming the plant model is perfect. This section analyzes the tracking accuracy of the FBF approach for known uncertainty, using the Frobenius norm metric. Assume that the actual plant dynamics belongs to the set $\{G_{aj}\}$, j =1, 2, …, l. The set could represent a plant with additive uncertainty, multiplicative uncertainty, parametric uncertainty, etc. Without loss of generality, this paper assumes that the set is discrete. Sampling of uncertainty has been used in literature [57,64] for robust controller design. If the controller C (see Figure 2.1) is designed based on nominal plant dynamics G_{nom} and the error dynamics corresponding to G_{aj} is given by E_{ffj}, then to analyze the robustness of tracking controllers, the Frobenius norm metric $J_{e,r}$ can be expressed as

$$
\begin{aligned}
J_{e,r}^2 &= \sum_{j=1}^{l} \lambda_j J_{ej}^2; \\
J_{ej} &= \frac{\left\| \mathbf{E}_{ffj} \right\|_F}{\sqrt{M+1}} = \frac{\left\| \mathbf{I} - \mathbf{G}_{aj}\mathbf{C} \right\|_F}{\sqrt{M+1}}; \\
\sum_{j=1}^{l} \lambda_j &= 1
\end{aligned}
\tag{4.2}
$$

where $\{\lambda_j\}$ denotes weights associated with the distribution of the uncertainty. Note that the nominal plant dynamics G_{nom} may or may not belong to the set $\{G_{aj}\}$.

Remark 4.1: This dissertation focuses on FBF, hence, the modified metric will only be explored in the context of FBF in the remainder of this dissertation. However, the metric can be used to analyze robustness of other tracking controllers.

If the FBF controller C is designed using the nominal plant dynamics G_{nom}, then its LSR $\mathbf{C}$ is given by

$$
\mathbf{C} = \mathbf{\Phi}\left(\tilde{\mathbf{\Phi}}_{nom}^{\mathrm{T}} \tilde{\mathbf{\Phi}}_{nom} \right)^{-1} \tilde{\mathbf{\Phi}}_{nom}^{\mathrm{T}} \tag{4.3}
$$

Analysis using the pseudoinverse is quite cumbersome and hence, the filtered basis functions matrix $\tilde{\mathbf{\Phi}}_{nom} = \mathbf{G}_{nom}\mathbf{\Phi}$ is transformed into the decoupled filtered basis functions matrix $\tilde{\mathbf{\Psi}}_{nom} = \mathbf{G}_{nom}\mathbf{\Psi}_{nom}$ (for more details see Appendix E). After transformation, the LSRs $\mathbf{C}$ and $\mathbf{E}_{ffj}$ can be expressed as

$$
\begin{aligned}
\mathbf{C} &= \mathbf{\Psi}_{nom} \tilde{\mathbf{\Psi}}_{nom}^{\mathrm{T}}; \\
\tilde{\mathbf{\Psi}}_{nom}^{\mathrm{T}} \tilde{\mathbf{\Psi}}_{nom} &= \mathbf{I}_{n+1}; \\
\mathbf{E}_{ffj} &= \mathbf{I}_{M+1} - \tilde{\mathbf{\Psi}}_{aj,nom} \tilde{\mathbf{\Psi}}_{nom}^{\mathrm{T}}
\end{aligned}
\tag{4.4}
$$

where $\tilde{\mathbf{\Psi}}_{aj,nom}$ is obtained by filtering $\mathbf{\Psi}_{nom}$ using LSR of the possible actual plant dynamics $\mathbf{G}_{aj}$.

Proposition 4.1: For the set of possible actual plant dynamics $\{G_{aj}\}$ and associated weights $\{\lambda_j\}$, $j = 1, 2, \ldots, l$, the metric $J_{e,r}$ can be expressed in terms of the uncertainty and basis functions as

$$J_{e,r}^2 = 1 - \frac{n+1}{M+1} + \sum_{j=1}^{l} \lambda_j \frac{\left\| \left(\mathbf{G}_{aj} - \mathbf{G}_{nom} \right) \mathbf{\Psi}_{nom} \right\|_F^2}{M+1} \tag{4.5}$$

Proof: This proof first finds the metric J_{ej} and then finds $J_{e,r}$ using Eq. (4.2). Based on Eqs. (4.2) and (4.4)

$$\begin{aligned}
\left\| \mathbf{E}_{ffj} \right\|_F^2 &= trace\left(\mathbf{E}_{ffj}^{\mathrm{T}} \mathbf{E}_{ffj} \right) \\
&= trace\begin{pmatrix} (\mathbf{I}_{M+1} - \tilde{\mathbf{\Psi}}_{aj,nom} \tilde{\mathbf{\Psi}}_{nom}^{\mathrm{T}})^{\mathrm{T}} \\ (\mathbf{I}_{M+1} - \tilde{\mathbf{\Psi}}_{aj,nom} \tilde{\mathbf{\Psi}}_{nom}^{\mathrm{T}}) \end{pmatrix} \\
&= trace\begin{pmatrix} \mathbf{I}_{M+1} - \tilde{\mathbf{\Psi}}_{aj,nom} \tilde{\mathbf{\Psi}}_{nom}^{\mathrm{T}} \\ -\tilde{\mathbf{\Psi}}_{nom} \tilde{\mathbf{\Psi}}_{aj,nom}^{\mathrm{T}} \\ +\tilde{\mathbf{\Psi}}_{nom} \tilde{\mathbf{\Psi}}_{aj,nom}^{\mathrm{T}} \tilde{\mathbf{\Psi}}_{aj,nom} \tilde{\mathbf{\Psi}}_{nom}^{\mathrm{T}} \end{pmatrix} \\
&= trace\begin{pmatrix} \mathbf{I}_{M+1} \\ -\left\{ \tilde{\mathbf{\Psi}}_{nom} + \tilde{\mathbf{\Psi}}_{aj-nom,nom} \right\} \tilde{\mathbf{\Psi}}_{nom}^{\mathrm{T}} \\ -\tilde{\mathbf{\Psi}}_{nom} \left\{ \tilde{\mathbf{\Psi}}_{nom} + \tilde{\mathbf{\Psi}}_{aj-nom,nom} \right\}^{\mathrm{T}} \\ +\tilde{\mathbf{\Psi}}_{nom} \left\{ \tilde{\mathbf{\Psi}}_{nom} + \tilde{\mathbf{\Psi}}_{aj-nom,nom} \right\}^{\mathrm{T}} \\ \left\{ \tilde{\mathbf{\Psi}}_{nom} + \tilde{\mathbf{\Psi}}_{aj-nom,nom} \right\} \tilde{\mathbf{\Psi}}_{nom}^{\mathrm{T}} \end{pmatrix}; \\
\tilde{\mathbf{\Psi}}_{aj-nom,nom} &\triangleq \tilde{\mathbf{\Psi}}_{aj,nom} - \tilde{\mathbf{\Psi}}_{nom}
\end{aligned} \tag{4.6}$$

Using the fact that *trace* is a linear mapping and is invariant under cyclic permutations

$$\left\| \mathbf{E}_{ffj} \right\|_F^2 = \left(M+1 \right) - \left(n+1 \right) + \left\| \tilde{\mathbf{\Psi}}_{aj-nom,nom} \right\|_F^2 \tag{4.7}$$

Substituting Eq. (4.7) in Eq. (4.2) gives

$$
\begin{aligned}
J_{e,r}^2 &= \sum_{j=1}^{l} \lambda_j J_{ej}^2 \\
&= 1 - \frac{n+1}{M+1} + \sum_{j=1}^{l} \lambda_j \frac{\left\| \left(\mathbf{G}_{aj} - \mathbf{G}_{nom} \right) \mathbf{\Psi}_{nom} \right\|_F^2}{M+1}
\end{aligned}
\tag{4.8}
$$

(End of Proof)

Remark 4.2: The metric can be expressed as

$$
\begin{aligned}
J_{e,r}^2 &= J_{e,nom}^2 + J_{e,unc}^2 \\
J_{e,nom}^2 &\triangleq 1 - \frac{n+1}{M+1} \\
J_{e,unc}^2 &\triangleq \sum_{j=1}^{l} \lambda_j \frac{\left\| \left(\mathbf{G}_{aj} - \mathbf{G}_{nom} \right) \mathbf{\Psi}_{nom} \right\|_F^2}{M+1}
\end{aligned}
\tag{4.9}
$$

The implication is that the metric is the summation of two components – nominal and uncertainty-related. The nominal component is identical to the value of the metric in the absence of the uncertainty (discussed in Section 2.6); it only depends on the number of basis functions and is independent of the plant dynamics and the choice of basis functions. However, the uncertainty-related component depends on the uncertainty, choice of nominal model and the type and number of basis functions. With increase in n, the nominal component decreases monotonically. Whereas, the uncertainty-related component generally increases with increase in n. The implication is that the tracking error for FBF, in the presence of uncertainty, does not vary monotonically with the number of basis functions (as seen in Figure 4.1).

4.4 Optimal Selection of Basis Functions for Robust Tracking Control

This section finds an optimal set of basis functions that minimize $J_{e,r}$ for a given nominal model $\mathbf{G}_{nom}$ and known uncertainty $\{\mathbf{G}_{aj}\}$. Towards achieving this objective, this section first finds an optimal set of basis functions that minimize the uncertainty-related component of the metric $J_{e,unc}$, for a given value of the nominal component of the metric $J_{e,nom}$. This objective is achieved

while ensuring that the control input does not contain components from the very small singular values (a result of NMP zeros and relative degree) of the LSR of nominal model $\mathbf{G}_{nom}$. Mathematically, the problem can be expressed as finding $\mathbf{\Psi}_{nom}$ such that

$$\begin{aligned} &\min_{\mathbf{\Psi}_{nom}} J_{e,unc}\left(\mathbf{\Psi}_{nom}, \mathbf{G}_{nom}, \{\mathbf{G}_{aj}\}\right) \\ &\text{s.t. } J_{e,nom} = J^{*}_{e,nom}(n) \\ &J_c \le J^{*}_c(\mathbf{G}_{nom}, r) \end{aligned} \tag{4.10}$$

where the first constraint denotes achieving a desired value of nominal tracking accuracy by selecting a particular value of n and the second constraint signifies that the control input does not contain the r smallest singular components of $\mathbf{G}_{nom}$. Proposition 4.2 formulates the problem described above and presents a solution.

Proposition 4.2: For the set of possible actual plant dynamics $\{G_{aj}\}$, associated weights $\{\lambda_j\}$, j =1, 2, …, l, and nominal model G_{nom} (with r very small singular values in its LSR), the n+1 basis functions $\mathbf{\Psi}_{nom}$ that minimize $J_{e,unc}$ are given by

$$\begin{aligned} &\mathbf{\Psi}_{nom} = \mathbf{W}_{nom}\mathbf{\Sigma}_{nom}^{-1}\left[\mathbf{W}_{\bar{\mathbf{\Delta}}_{nom,s}}\begin{bmatrix}\mathbf{0}_{(M-n-r)\times(n+1)}\\ \mathbf{I}_{n+1}\end{bmatrix}; \right. \\ &\qquad\qquad \left. \mathbf{0}_{r\times(n+1)}\right] \\ &\mathbf{G}_{nom} = \mathbf{V}_{nom}\mathbf{\Sigma}_{nom}\mathbf{W}_{nom}^{\mathrm{T}}; \\ &\bar{\mathbf{\Delta}}_{nom} = \mathbf{\Delta}\mathbf{W}_{nom}\mathbf{\Sigma}_{nom}^{-1} = \left[\bar{\mathbf{\Delta}}_{nom,s} \quad \bar{\mathbf{\Delta}}_{nom,r}\right]; \\ &\bar{\mathbf{\Delta}}_{nom,s} = \mathbf{V}_{\bar{\mathbf{\Delta}}_{nom,s}}\mathbf{\Sigma}_{\bar{\mathbf{\Delta}}_{nom,s}}\mathbf{W}_{\bar{\mathbf{\Delta}}_{nom,s}}^{\mathrm{T}}; \\ &\mathbf{\Delta}^{\mathrm{T}}\mathbf{\Delta} = \sum_{j=1}^{l}\lambda_j\left(\mathbf{G}_{aj}-\mathbf{G}_{nom}\right)^{\mathrm{T}}\left(\mathbf{G}_{aj}-\mathbf{G}_{nom}\right) \end{aligned} \tag{4.11}$$

where $\mathbf{V}_{nom}$, $\mathbf{\Sigma}_{nom}$ and $\mathbf{W}_{nom}$ denote the left singular vector matrix, singular value matrix and right singular vector matrix of $\mathbf{G}_{nom}$, respectively. Similarly, $\mathbf{V}_{\bar{\mathbf{\Delta}}_{nom,s}}$, $\mathbf{\Sigma}_{\bar{\mathbf{\Delta}}_{nom,s}}$ and $\mathbf{W}_{\bar{\mathbf{\Delta}}_{nom,s}}$ denote the left singular vector matrix, singular value matrix and right singular vector matrix of $\bar{\mathbf{\Delta}}_{nom,s}$, respectively. Also, $\bar{\mathbf{\Delta}}_{nom,s}$ and $\bar{\mathbf{\Delta}}_{nom,r}$ are the first M+1−r columns and last r columns of $\bar{\mathbf{\Delta}}_{nom}$, respectively.

Proof: The problem of minimizing $J_{e,unc}$ for a given value of n can be expressed as (using Eqs. (4.4) and (4.9))

$$\min_{\boldsymbol{\Psi}_{nom}} \left[J_{e,unc}^2 = \sum_{j=1}^{l} \lambda_j \frac{\left\| \left(\mathbf{G}_{aj} - \mathbf{G}_{nom} \right) \boldsymbol{\Psi}_{nom} \right\|_F^2}{M+1} \right] \quad \text{s.t.} \quad \tilde{\boldsymbol{\Psi}}_{nom}^{\mathrm{T}} \tilde{\boldsymbol{\Psi}}_{nom} = \mathbf{I}_{n+1} \tag{4.12}$$

Note that the constraint is a result of the decoupling process (Eq. (4.4)). The objective of the problem, given by Eq. (4.12), can alternatively be expressed as

$$\begin{aligned} J_{e,unc}^2 &= \sum_{j=1}^{l} \lambda_j \frac{\left\| \left(\mathbf{G}_{aj} - \mathbf{G}_{nom} \right) \boldsymbol{\Psi}_{nom} \right\|_F^2}{M+1} \\ &= \frac{trace\left(\boldsymbol{\Psi}_{nom}^{\mathrm{T}} \left\{ \sum_{j=1}^{l} \lambda_j \left(\mathbf{G}_{aj} - \mathbf{G}_{nom} \right)^{\mathrm{T}} \left(\mathbf{G}_{aj} - \mathbf{G}_{nom} \right) \right\} \boldsymbol{\Psi}_{nom} \right)}{M+1} \end{aligned} \tag{4.13}$$

Defining

$$\boldsymbol{\Delta}^{\mathrm{T}} \boldsymbol{\Delta} \triangleq \sum_{j=1}^{l} \lambda_j \left(\mathbf{G}_{aj} - \mathbf{G}_{nom} \right)^{\mathrm{T}} \left(\mathbf{G}_{aj} - \mathbf{G}_{nom} \right) \tag{4.14}$$

Eq. (4.13) can be expressed as

$$
\begin{aligned}
J_{e,unc}^2 &= \frac{\left\|\boldsymbol{\Delta\Psi}_{nom}\right\|_F^2}{M+1} \\
&= \frac{\left\|\boldsymbol{\Delta}\mathbf{G}_{nom}^{-1}\tilde{\boldsymbol{\Psi}}_{nom}\right\|_F^2}{M+1} \\
&= \frac{\left\|\boldsymbol{\Delta}\mathbf{W}_{nom}\boldsymbol{\Sigma}_{nom}^{-1}\mathbf{V}_{nom}^{\mathrm{T}}\tilde{\boldsymbol{\Psi}}_{nom}\right\|_F^2}{M+1} \\
&= \frac{\left\|\bar{\boldsymbol{\Delta}}_{nom}\tilde{\boldsymbol{\Xi}}_{nom}\right\|_F^2}{M+1}; \\
\bar{\boldsymbol{\Delta}}_{nom} &\triangleq \boldsymbol{\Delta}\mathbf{W}_{nom}\boldsymbol{\Sigma}_{nom}^{-1}; \\
\tilde{\boldsymbol{\Xi}}_{nom} &\triangleq \mathbf{V}_{nom}^{\mathrm{T}}\tilde{\boldsymbol{\Psi}}_{nom}
\end{aligned}
\tag{4.15}
$$

The constraint in Eq. (4.12) can be expressed as

$$
\begin{aligned}
&\tilde{\boldsymbol{\Psi}}_{nom}^{\mathrm{T}}\tilde{\boldsymbol{\Psi}}_{nom} = \mathbf{I}_{n+1} \\
&\Rightarrow \tilde{\boldsymbol{\Psi}}_{nom}^{\mathrm{T}}\mathbf{V}_{nom}\mathbf{V}_{nom}^{\mathrm{T}}\tilde{\boldsymbol{\Psi}}_{nom} = \mathbf{I}_{n+1} \\
&\Rightarrow \tilde{\boldsymbol{\Xi}}_{nom}^{\mathrm{T}}\tilde{\boldsymbol{\Xi}}_{nom} = \mathbf{I}_{n+1}
\end{aligned}
\tag{4.16}
$$

Hence, the optimization problem given by Eq. (4.12) can be re-written as

$$
\begin{aligned}
&\min_{\tilde{\boldsymbol{\Xi}}_{nom}} \left[J_{e,unc}^2 = \frac{\left\|\bar{\boldsymbol{\Delta}}_{nom}\tilde{\boldsymbol{\Xi}}_{nom}\right\|_F^2}{M+1} \right] \\
&\text{s.t. } \tilde{\boldsymbol{\Xi}}_{nom}^{\mathrm{T}}\tilde{\boldsymbol{\Xi}}_{nom} = \mathbf{I}_{n+1}
\end{aligned}
\tag{4.17}
$$

This optimization problem is similar to the optimization problem for finding CE-Opt basis functions (see Section 3.4) and using the methodology described in Proposition 3.1, the optimal basis functions for robustness is the set of right singular vectors of the matrix $\bar{\boldsymbol{\Delta}}_{nom}$, corresponding to its n+1 smallest singular values. Although, the basis functions obtained by solving Eq. (4.17) are optimal in terms of robustness, they might result in large control inputs, especially if $\mathbf{G}_{nom}$ has very small singular values. Very small singular values might result in an unrealizable robust controller (as seen in Section 3.5.2) and hence, the optimal basis functions should be designed to

avoid components corresponding to these very small singular values. Based on the discussion in Section 3.3 and Eq. (4.15), the components corresponding to r very small singular values of $\mathbf{G}_{nom}$ can be avoided by equating the elements of last r rows of $\tilde{\boldsymbol{\Xi}}_{nom}$ to zero:

$$\begin{aligned} \min_{\tilde{\boldsymbol{\Xi}}_{nom}} & \left[J_{e,unc}^2 = \frac{\left\| \bar{\boldsymbol{\Delta}}_{nom} \tilde{\boldsymbol{\Xi}}_{nom} \right\|_F^2}{M+1} \right] \\ \text{s.t. } & \tilde{\boldsymbol{\Xi}}_{nom}^{\mathrm{T}} \tilde{\boldsymbol{\Xi}}_{nom} = \mathbf{I}_{n+1} \\ & \text{the last } r \text{ rows of } \tilde{\boldsymbol{\Xi}}_{nom} \text{ have elements equal to } 0 \end{aligned} \tag{4.18}$$

The new constraint can be embedded into the objective and orthogonality constraint by

$$\begin{aligned} \bar{\boldsymbol{\Delta}}_{nom} \tilde{\boldsymbol{\Xi}}_{nom} &= \begin{bmatrix} \bar{\boldsymbol{\Delta}}_{nom,s} & \bar{\boldsymbol{\Delta}}_{nom,r} \end{bmatrix} \begin{bmatrix} \tilde{\boldsymbol{\Xi}}_{nom,s} \\ \mathbf{0}_{r\times(n+1)} \end{bmatrix} = \bar{\boldsymbol{\Delta}}_{nom,s} \tilde{\boldsymbol{\Xi}}_{nom,s} \\ \tilde{\boldsymbol{\Xi}}_{nom}^{\mathrm{T}} \tilde{\boldsymbol{\Xi}}_{nom} &= \begin{bmatrix} \tilde{\boldsymbol{\Xi}}_{nom,s}^{\mathrm{T}} & \mathbf{0}_{(n+1)\times r} \end{bmatrix} \begin{bmatrix} \tilde{\boldsymbol{\Xi}}_{nom,s} \\ \mathbf{0}_{r\times(n+1)} \end{bmatrix} = \tilde{\boldsymbol{\Xi}}_{nom,s}^{\mathrm{T}} \tilde{\boldsymbol{\Xi}}_{nom,s} \end{aligned} \tag{4.19}$$

where $\bar{\boldsymbol{\Delta}}_{nom,s}$ and $\bar{\boldsymbol{\Delta}}_{nom,r}$ are the matrices formed from first M+1−r columns and last r columns of $\bar{\boldsymbol{\Delta}}_{nom}$, respectively. The optimization problem, given by Eq. (4.18), can be re-written as

$$\begin{aligned} \min_{\tilde{\boldsymbol{\Xi}}_{nom,s}} & \left\| \bar{\boldsymbol{\Delta}}_{nom,s} \tilde{\boldsymbol{\Xi}}_{nom,s} \right\|_F^2 \\ \text{s.t. } & \tilde{\boldsymbol{\Xi}}_{nom,s}^{\mathrm{T}} \tilde{\boldsymbol{\Xi}}_{nom,s} = \mathbf{I}_{n+1} \end{aligned} \tag{4.20}$$

The optimal solution to Eq. (4.20), is the set of right singular vectors of the matrix $\bar{\boldsymbol{\Delta}}_{nom,s}$ corresponding to its n+1 smallest singular values (based on Proposition 3.1).

$$\begin{aligned} \tilde{\boldsymbol{\Xi}}_{nom,s} &= \mathbf{W}_{\bar{\boldsymbol{\Delta}}_{nom,s}} \begin{bmatrix} \mathbf{0}_{(M-n-r)\times(n+1)} \\ \mathbf{I}_{n+1} \end{bmatrix}; \\ \bar{\boldsymbol{\Delta}}_{nom,s} &= \mathbf{V}_{\bar{\boldsymbol{\Delta}}_{nom,s}} \boldsymbol{\Sigma}_{\bar{\boldsymbol{\Delta}}_{nom,s}} \mathbf{W}_{\bar{\boldsymbol{\Delta}}_{nom,s}}^{\mathrm{T}} \end{aligned} \tag{4.21}$$

and the corresponding basis functions are

$$\begin{aligned}\boldsymbol{\Psi}_{nom} &= \mathbf{W}_{nom}\boldsymbol{\Sigma}_{nom}^{-1}\mathbf{V}_{nom}^{\mathrm{T}}\tilde{\boldsymbol{\Psi}}_{nom} \\ &= \mathbf{W}_{nom}\boldsymbol{\Sigma}_{nom}^{-1}\tilde{\boldsymbol{\Xi}}_{nom} \\ &= \mathbf{W}_{nom}\boldsymbol{\Sigma}_{nom}^{-1}\begin{bmatrix}\tilde{\boldsymbol{\Xi}}_{nom,s} \\ \mathbf{0}_{r\times(n+1)}\end{bmatrix} \\ &= \mathbf{W}_{nom}\boldsymbol{\Sigma}_{nom}^{-1}\begin{bmatrix}\mathbf{W}_{\bar{\boldsymbol{\Delta}}_{nom,s}}\begin{bmatrix}\mathbf{0}_{(M-n-r)\times(n+1)} \\ \mathbf{I}_{n+1}\end{bmatrix} \\ \mathbf{0}_{r\times(n+1)}\end{bmatrix}; \\ \mathbf{G}_{nom} &= \mathbf{V}_{nom}\boldsymbol{\Sigma}_{nom}\mathbf{W}_{nom}^{\mathrm{T}}\end{aligned} \tag{4.22}$$

(End of Proof)

Remark 4.3: Since, the choice of basis functions only affects the uncertainty-related component and does not affect the nominal component (Remark 4.2), the proposed optimal basis functions are selected such that robust tracking is realized without significantly affecting the nominal tracking accuracy of FBF (Proposition 4.2). This is unlike many other robust tracking controllers in the literature [63,69], whose improved robustness in tracking is achieved at the cost of deterioration in nominal tracking accuracy.

Remark 4.4: For the basis functions given by Eq. (4.22), the value of metric $J_{e,unc}$ is given by

$$J_{e,unc}^2 = \frac{\sum_{i=M-r-n+1}^{M+1-r}\sigma_{\bar{\boldsymbol{\Delta}}_{nom,s},i}^2}{M+1} \tag{4.23}$$

where $\{\sigma_{\bar{\boldsymbol{\Delta}}_{nom,s},i}\}$, $i = 1, 2, \ldots, M+1-r$ are the singular values of the matrix $\bar{\boldsymbol{\Delta}}_{nom,s}$ in the descending order. For $n = 0$ (1 basis function), $J_{e,unc}$ only depends on the smallest singular value of $\bar{\boldsymbol{\Delta}}_{nom,s}$. The implication is that in an $M+1$ dimensional vector space, the basis function is aligned with the most robust vector; i.e., the vector that ensures that the uncertainty has the least effect on the tracking accuracy of FBF. As n increases, new basis functions are added such that the next higher singular values are added to $J_{e,unc}$ and the next most robust vectors in the $M+1$ dimensional vector space are selected. Among all the $n+1$ dimensional vector spaces (for $M+1$ length vectors), the effect of the

uncertainty on tracking accuracy of FBF is minimum in the vector space created by these n+1 basis functions.

The value of $J_{e,r}$ for the proposed optimal basis functions is given by

$$J_{e,r}^2 = \underbrace{1 - \frac{n+1}{M+1}}_{J_{e,nom}^2} + \underbrace{\frac{\sum_{i=M-r-n+1}^{M+1-r} \sigma_{\bar{\Delta}_{nom,s},i}^2}{M+1}}_{J_{e,unc}^2} \tag{4.24}$$

The difference in values of $J_{e,r}^2$ as n increases from $n = n_1$ to $n = n_1$+1 is given by

$$J_{e,r}^2\left[n_1+1\right] - J_{e,r}^2\left[n_1\right] = \frac{\sigma_{\bar{\Delta}_{nom,s},M-r-n_1}^2 - 1}{M+1} \tag{4.25}$$

where $J_{e,r}^2[n_1]$ denotes the value of $J_{e,r}^2$ for $n = n_1$. Hence, the value of the metric decreases (i.e., tracking accuracy improves) if $\sigma_{\bar{\Delta}_{nom,s},M-r-n_1} < 1$ and increases (i.e., tracking accuracy deteriorates) if $\sigma_{\bar{\Delta}_{nom,s},M-r-n_1} > 1$.

Remark 4.5: Based on the above discussion, following three scenarios are possible with the proposed optimal basis functions:

(i) If all singular values $\{\sigma_{\bar{\Delta}_{nom,s},i}\}$ are less than 1, then $J_{e,r}^2$ is a non-increasing function of n and $n = M - r$ results in the most robust optimal basis functions for known uncertainty and given nominal model.

(ii) If all singular values $\{\sigma_{\bar{\Delta}_{nom,s},i}\}$ are greater than 1, then $J_{e,r}^2$ is a non-decreasing function of n and $n = 0$ results in the most robust optimal basis functions for known uncertainty and given nominal model.

(iii) If $\{\sigma_{\bar{\Delta}_{nom,s},i}\}$ has values dispersed on either side of 1, then for lower values of n, $J_{e,r}^2$ is a non-increasing function of n, until $\sigma_{\bar{\Delta}_{nom,s},M+1-r-n} < 1$ and for higher values of n, $J_{e,r}^2$ is a non-decreasing function of n. The most robust optimal basis functions, for known uncertainty and given nominal model, are achieved at the highest value of n where $\sigma_{\bar{\Delta}_{nom,s},M+1-r-n} < 1$.

For a given uncertainty, scenario (i) would be the most desirable, since the optimal value is achieved for highest value of *n* (the most optimal nominal tracking accuracy and spans the entire possible trajectory space). This analysis demonstrates that smaller singular values $\{\sigma_{\bar{\mathbf{\Delta}}_{nom,s},i}\}$ are desirable.

Since, the singular values depend on the uncertainty and the nominal model, an ideal way to optimize tracking accuracy of FBF, in addition to optimal selection of basis functions, would be to optimize the nominal model to minimize the singular values. The following section presents a methodology for selecting an optimal nominal model based on minimizing the sum of the square of singular values.

4.5 Optimal Selection of Nominal Model for Robust Tracking Control

This section finds a nominal model such that the following cost function *J* is minimized (see Eq. (4.15))

$$\begin{aligned} J &= \left\| \bar{\mathbf{\Delta}}_{nom} \right\|_F^2 \\ &= \left\| \mathbf{\Delta W}_{nom} \mathbf{\Sigma}_{nom}^{-1} \mathbf{V}_{nom}^{\mathrm{T}} \right\|_F^2 \\ &= \left\| \mathbf{\Delta G}_{nom}^{-1} \right\|_F^2 \\ &= trace\left(\mathbf{G}_{nom}^{-\mathrm{T}} \left\{ \sum_{j=1}^{l} \lambda_j \left(\mathbf{G}_{aj} - \mathbf{G}_{nom} \right)^{\mathrm{T}} \left(\mathbf{G}_{aj} - \mathbf{G}_{nom} \right) \right\} \mathbf{G}_{nom}^{-1} \right) \\ &= trace\left(\sum_{j=1}^{l} \lambda_j \left(\mathbf{G}_{aj} \mathbf{G}_{nom}^{-1} - \mathbf{I}_{M+1} \right)^{\mathrm{T}} \left(\mathbf{G}_{aj} \mathbf{G}_{nom}^{-1} - \mathbf{I}_{M+1} \right) \right) \end{aligned} \tag{4.26}$$

The optimal nominal model is obtained by differentiating the cost function *J* w.r.t. the inverse of the nominal model $\mathbf{G}_{nom}$, and equating the result to zero

$$\begin{aligned} &\frac{\partial J}{\partial \mathbf{G}_{nom}^{-1}} = \sum_{j=1}^{l} \left(-2\mathbf{G}_{aj} + 2\mathbf{G}_{nom}^{-\mathrm{T}} \mathbf{G}_{aj}^{\mathrm{T}} \mathbf{G}_{aj} \right) = 0 \\ &\Rightarrow \mathbf{G}_{nom,opt} = \left(\sum_{j=1}^{l} \lambda_j \mathbf{G}_{aj}^{\mathrm{T}} \right)^{-1} \left(\sum_{j=1}^{l} \lambda_j \mathbf{G}_{aj}^{\mathrm{T}} \mathbf{G}_{aj} \right) \end{aligned} \tag{4.27}$$

The optimal nominal model given by Eq. (4.27) might not be realizable if the members of the set $\{\mathbf{G}_{aj}\}$ have very small singular values, which holds true for systems with NMP zeros. Hence, this dissertation proposes the following approximate nominal model

$$\mathbf{G}_{nom,opt} \approx \left(\sum_{j=1}^{l} \lambda_j \mathbf{G}_{aj}^{\mathrm{T}} \right)^{\dagger} \left(\sum_{j=1}^{l} \lambda_j \mathbf{G}_{aj}^{\mathrm{T}} \mathbf{G}_{aj} \right) \tag{4.28}$$

Remark 4.6: The approach presented in this section for selection of nominal model minimizes the sum of the singular values and obtains the solution in one optimization in the lifted domain. Whereas, the approach proposed in Ref. [69,70] (also presented in Appendix I) for selection of nominal model, focuses on optimizing for each frequency. Since the method presented in this section uses a lifted domain approach, the method can be applied to any linear system, including time and parameter varying systems. However, the method presented in Appendix I is restricted to time invariant systems only.

Remark 4.7: Since the methodology adopted in this section for selection of nominal model does not consider the basis functions used, a robust FBF controller can be designed using a two-step procedure: (i) select an optimal nominal model based on the discussion in this section (ii) select an optimal set of basis functions for the nominal model obtained in step (i) using Proposition 4.2.

4.6 Examples

4.6.1 Simulations

The discussion in this chapter was motivated using a simple example in Section 4.2 and this section continues with the same example. The robust optimal basis functions proposed in Section 4.4 are compared with DCT, B-splines and CE-Opt basis functions. While DCT and B-splines are defined independent of the plant dynamics (see Appendix F), the CE-Opt basis functions are designed based on the nominal model of the plant dynamics (see Section 3.4) and the proposed robust optimal basis functions are designed based on the nominal model as well as the known uncertainty in the plant dynamics (see Section 4.4). The system and desired trajectory parameters are same as that in Section 4.2. For design of the robust optimal basis functions, the set

of possible actual plant dynamics $\{G_{aj}\}$, is generated by selecting l = 410 evenly distributed realizations of the plant defined by Eq. (4.1) such that $\lambda_j = 1/l$. Also, the LSRs of members of the set of possible actual plant dynamics $\{\mathbf{G}_{aj}\}$ have one very small singular value and hence, $r = 1$.

Figure 4.2 shows the normalized RMS tracking error $\mathbf{e}_{RMS}/\mathbf{y}_{d,RMS}$ for DCT, B-splines, CE-Opt and the proposed robust optimal basis functions, for various numbers of basis functions (n = 10 to 990), using the 410 realizations of actual plant dynamics G, described above. The metrics used for comparison are the mean and standard deviation of $\mathbf{e}_{RMS}/\mathbf{y}_{d,RMS}$. It is observed that for all values of n, the proposed robust optimal basis functions result in minimum values of mean and standard deviation as compared to DCT, B-splines and CE-OPT. For example, at n = 500, compared to DCT, B-splines and CE-Opt, the optimal basis functions result in improvements in mean and standard deviations of $\mathbf{e}_{RMS}/\mathbf{y}_{d,RMS}$ by up to 1.5 times and 77 times, respectively. The nominal values of $\mathbf{e}_{RMS}/\mathbf{y}_{d,RMS}$ for DCT, B-splines, CE-Opt and optimal basis functions are 0.6686, 0.6662, 0.6800 and 0.6794, respectively. This demonstrates that the significant improvement in mean and standard deviations of $\mathbf{e}_{RMS}/\mathbf{y}_{d,RMS}$ is achieved without significantly affecting nominal tracking accuracy of the FBF approach. Figure 4.3 shows the singular values of $\overline{\mathbf{\Delta}}_{nom,s}$ for the known uncertainty and nominal model. It is observed that the singular values are dispersed on either side of 1 and hence, this case represents scenario (iii) in Remark 4.5. Using the singular values, the optimal value of n for the proposed robust optimal basis functions should be achieved at n = 891 (see Remark 4.5 for more details). The time-domain simulations (see Figure 4.2) show that the minimum value of mean($\mathbf{e}_{RMS}/\mathbf{y}_{d,RMS}$) for proposed robust optimal basis functions is achieved at n = 890. The values of mean($\mathbf{e}_{RMS}/\mathbf{y}_{d,RMS}$) for n = 890 and 891 are 0.3935 and 0.394, respectively. This small difference in estimation of n could be attributed to the fact that the Frobenius norm metric only represents a trend and does not consider the effect of the desired trajectory. As compared to the other three basis functions, DCT, B-splines and CE-Opt, the proposed robust optimal basis functions achieve improvement in minimum value of mean($\mathbf{e}_{RMS}/\mathbf{y}_{d,RMS}$) by up to 1.8 times.

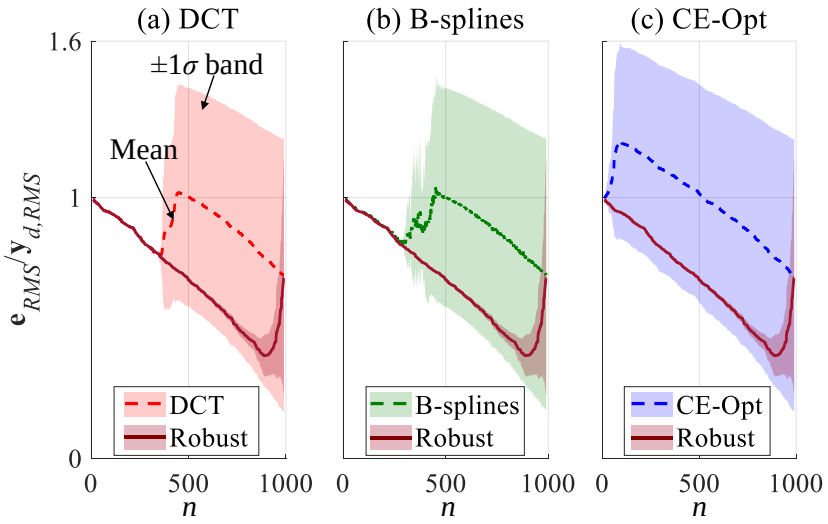

Figure 4.2 Comparison of normalized RMS tracking error for proposed robust optimal basis functions, DCT, B-splines and CE-Opt basis functions, in the presence of uncertainty, for various values of number of basis functions, n

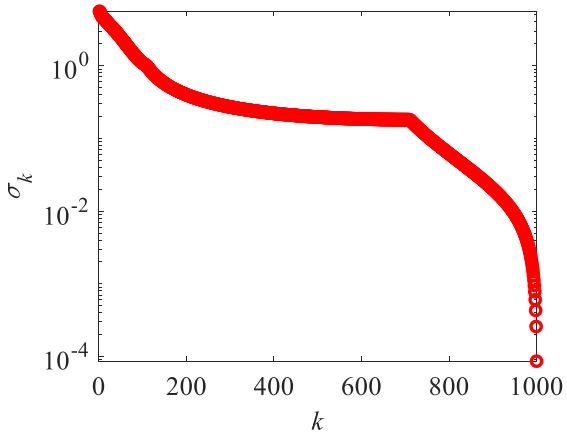

Figure 4.3 Singular values of $\overline{\mathbf{\Delta}}_{nom,s}$

Figure 4.4 shows the singular values of $\overline{\mathbf{\Delta}}_{nom,s}$ for the optimized nominal model proposed in Section 4.5. The maximum singular value of $\overline{\mathbf{\Delta}}_{nom,s}$ is 0.9748, which implies that this case represents scenario (i) of Remark 4.5 and optimal tracking control is achieved for the highest possible value of n. Figure 4.5 shows the normalized RMS tracking error $\mathbf{e}_{RMS}/\mathbf{y}_{d,RMS}$ for standard (arbitrarily selected in Section 4.2) nominal model and the optimal nominal model (proposed in Section 4.5) using DCT, B-splines, CE-Opt and the proposed robust optimal basis functions, for

various numbers of basis functions (n = 10 to 990). It is observed that the proposed nominal model has improved the tracking accuracy of the FBF approach, both in terms of mean and standard deviation of $\mathbf{e}_{RMS}/\mathbf{y}_{d,RMS}$, as compared to the standard nominal model, for different types and number of basis functions. To quantify the improvement, mean(mean($\mathbf{e}_{RMS}/\mathbf{y}_{d,RMS}$)) over n, for each combination of nominal model and type of basis functions, is used as a metric and the values are shown in Table 4.1. The proposed nominal model has resulted in improvement in tracking error as compared to the standard approach for selection of nominal model. For DCT, B-splines and CE-Opt, the improvement is significant with the proposed nominal model. However, it is observed that the value of mean(mean($\mathbf{e}_{RMS}/\mathbf{y}_{d,RMS}$)) for the above three type of basis functions with the proposed nominal model is still higher than the value of mean(mean($\mathbf{e}_{RMS}/\mathbf{y}_{d,RMS}$)) for the standard nominal model combined with the robust optimal basis functions. This demonstrates that the proposed robust optimal basis functions have improved the tracking accuracy of the FBF approach as compared to popular basis functions, irrespective of the nominal model (standard or proposed) used. Among the various combinations of types of basis functions and nominal models, the proposed two-step robust controller (Remark 4.7) is the best and the CE-Opt basis functions with a standard nominal model are the worst. The proposed two-step robust controller has resulted in improvement in tracking error by as much as 32% compared to the popular basis functions with the standard nominal model.

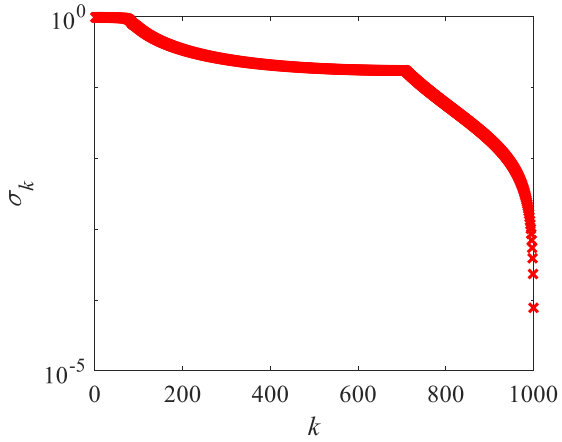

Figure 4.4 Singular values of $\overline{\mathbf{\Lambda}}_{nom,s}$ for optimized nominal model

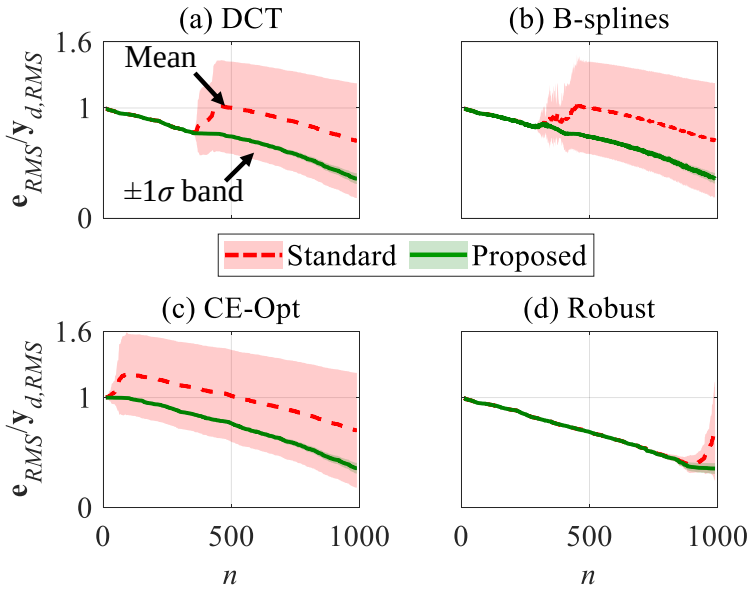

Figure 4.5 Comparison of the standard (arbitrarily selected) nominal model and proposed optimal nominal model for four different types of basis functions, (a) DCT, (b) B-splines, (c) CE-Opt, (d) proposed robust optimal basis functions, for various values of number of basis functions, n

Table 4.1 Summary of mean(mean($\mathbf{e}_{RMS}/\mathbf{y}_{d,RMS}$)) for different combinations of nominal models (Standard and Proposed) and types of basis functions (DCT, B-splines, CE-Opt and Robust)

Basis Functions	Standard	Proposed
DCT	0.88	0.71
B-splines	0.89	0.72
CE-Opt	0.99	0.74
Robust	0.69	0.67

Figure 4.6 shows the normalized RMS control input $\mathbf{u}_{RMS}/\mathbf{y}_{d,RMS}$ for the combinations of different nominal models and basis functions, for various numbers of basis functions (n = 10 to 990) and Table 4.2 shows max($\mathbf{u}_{RMS}/\mathbf{y}_{d,RMS}$) over values of n. The CE-Opt basis functions are the most optimal in terms of the control effort required. It is observed that the proposed nominal model results in lower max($\mathbf{u}_{RMS}/\mathbf{y}_{d,RMS}$) as compared to the standard nominal model, for all types of basis functions. Among the basis functions, the value of max($\mathbf{u}_{RMS}/\mathbf{y}_{d,RMS}$) is highest (for both nominal models) for B-splines, followed by DCT, proposed robust and CE-Opt. The high values for B-

splines and DCT can be attributed to the contribution of the very small singular value, whereas, proposed robust and CE-Opt basis functions avoid the small singular values by using constraints and optimization, respectively. The maximum control effort required by the proposed robust basis functions is 2.58 times and 1.18 times the maximum control effort required by CE-Opt basis functions, using standard and proposed nominal models, respectively. This demonstrates that the proposed robust FBF controller achieves significant improvement in tracking accuracy without unduly sacrificing on control effort, as compared to the popular basis functions like DCT and B-splines.

(a)

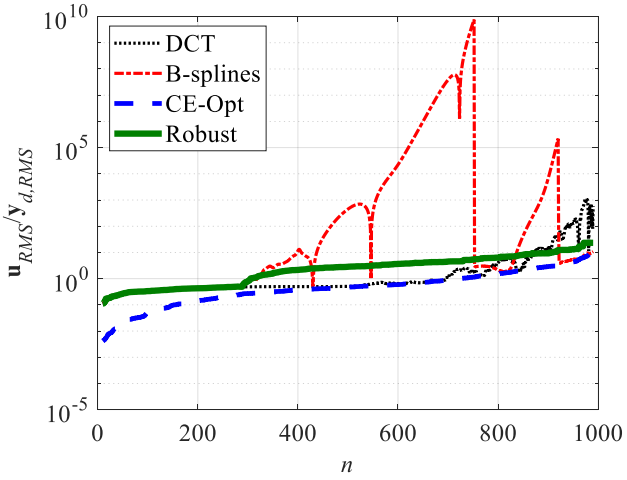

(b)

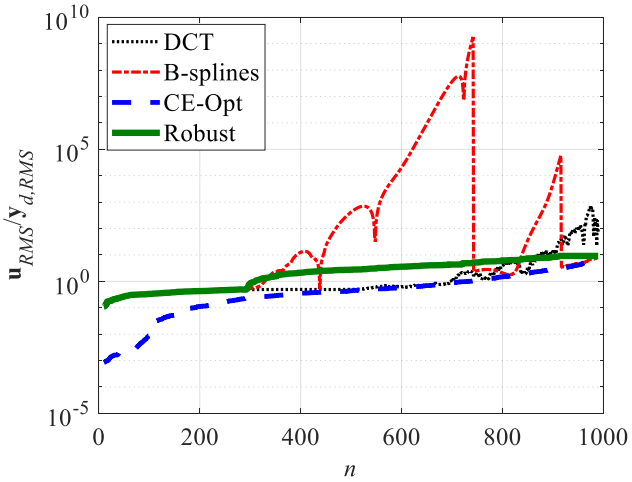

Figure 4.6 Comparison of normalized RMS control input for (a) standard (b) proposed nominal models for different types of basis functions, DCT, B-splines, CE-Opt basis functions and proposed robust basis functions, for various values of number of basis functions, n

Table 4.2 Summary of max($\mathbf{u}_{RMS}/\mathbf{y}_{d,RMS}$) for different combinations of nominal models and types of basis functions

Basis Functions	Standard	Proposed
DCT	1.10×10^3	6.81×10^2
B-splines	7.64×10^9	1.78×10^9
CE-Opt	9.26×10^0	7.77×10^0
Robust	2.39×10^1	9.16×10^0

4.6.2 Experiments

This section demonstrates the effectiveness of the proposed robust FBF controller as compared to CE-Opt basis functions using a Lulzbot Taz 6 desktop 3D printer (see Section 3.5.2). The experiments use CE-Opt for comparison because of the potential hazards with the high control input values associated with popular basis functions such as DCT and B-splines, as shown in Sections 3.5.2 and 4.6.1. The frequency response functions (FRFs) of the 3D printer are obtained by applying swept sine acceleration signals (with amplitudes ranging from 2 m/s^2 to 5 m/s^2 in increments of 0.2 m/s^2) to the printer's stepper motors (each having 10 μm stepping resolution) and measuring the relative acceleration of the build platform and print head using accelerometers (SparkFun ADXL335 triple-axis). Figure 4.7 shows the uncertainty and FRFs for 2 m/s^2, 3 m/s^2, 4 m/s^2 and 5 m/s^2. For robust FBF controller, the set $\{G_{aj}\}$ consists of the plant dynamics obtained from 16 FRFs (l = 16) described above, $\lambda_j = 1/l$ and r = 2, i.e., two very small singular values in the LSRs. The proposed robust optimal basis functions and CE-Opt basis functions are designed for nominal models based on FRFs corresponding to 2 m/s^2, 3 m/s^2, 4 m/s^2 and 5 m/s^2, and the proposed robust nominal model. A signal with frequency content distributed between 5 and 50 Hz, is used as the desired trajectory. The length of the signal is 2.474 seconds, resulting in 2475 discrete points (i.e., M = 2474) based on sampling time T_s = 1 ms. The control inputs generated for various combinations of basis functions (n = 125) and nominal models, are scaled and sent to the 3D printer to emulate 30 different uncertain plant dynamics.

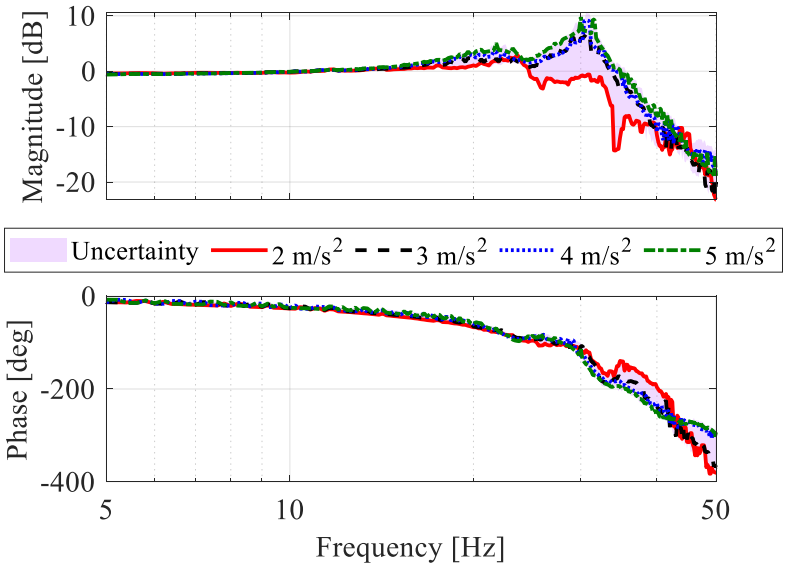

Figure 4.7 Frequency response functions (FRFs) corresponding to uncertainty and 2 m/s^2, 3 m/s^2, 4 m/s^2 and 5 m/s^2

Figure 4.8 shows bee-swarm plots comparing the normalized RMS tracking error ($\mathbf{e}_{RMS}/\mathbf{y}_{d,RMS}$) for the proposed robust and CE-Opt basis functions using four standard nominal models (FRFs corresponding to 2 m/s^2, 3 m/s^2, 4 m/s^2 and 5 m/s^2) and the proposed robust nominal model. Table 4.3 provides the mean and standard deviation values for the different cases. It is observed that the proposed robust basis functions perform better than the CE-Opt basis functions in terms of mean as well as standard deviation. The improvement in mean and standard deviation with the proposed robust basis functions is as high as 1.58 times and 3.73 times as compared to the CE-Opt basis functions. The robust nominal model improves the mean and standard deviation for robust basis functions by up to 1.34 times and 2.57 times, respectively, as compared to the standard nominal models. Whereas, for CE-Opt basis functions, the improvement in mean and standard deviation for robust nominal model as compared to standard nominal models is as high as 1.65 times and 2.73 times, respectively. Among all the cases, the proposed two-step robust FBF tracking controller performs best in terms of both mean as well as standard deviation. As compared to combination of CE-Opt basis functions with standard nominal models, the proposed two-step robust controller improves the mean and standard deviation by up to 1.84 times and 7.32 times, respectively.

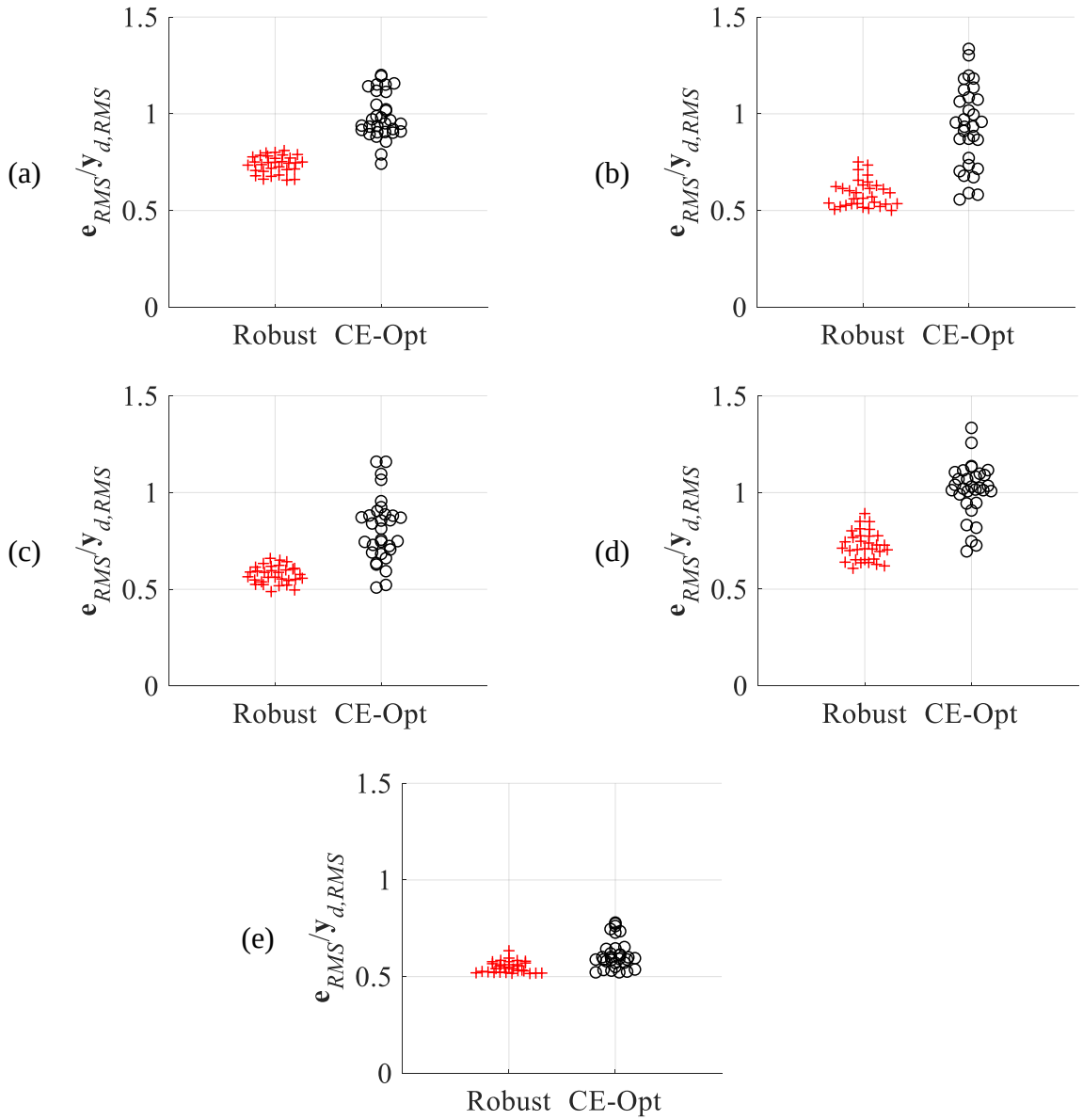

Figure 4.8 Bee-swarm plots showing comparison of normalized RMS tracking error for proposed robust basis functions and CE-Opt basis functions using five different nominal models: corresponding to (a) 2 m/s^2 FRF (b) 3 m/s^2 FRF (c) 4 m/s^2 FRF (d) 5 m/s^2 FRF, and (e) proposed robust nominal model (n = 125, M = 2474)

Table 4.3 Summary of mean ± standard deviation of $\mathbf{e}_{RMS}/\mathbf{y}_{d,RMS}$ for robust basis functions and CE-Opt basis functions using five different nominal models: corresponding to (a) 2 m/s^2 FRF (b) 3 m/s^2 FRF (c) 4 m/s^2 FRF (d) 5 m/s^2 FRF, and (e) proposed robust nominal model

Nominal Models	Robust	CE-Opt
2 m/s^2 FRF	0.7383 ± 0.0436	0.9858 ± 0.1160
3 m/s^2 FRF	0.5874 ± 0.0681	0.9308 ± 0.2078
4 m/s^2 FRF	0.5756 ± 0.0441	0.8096 ± 0.1646
5 m/s^2 FRF	0.7246 ± 0.0731	1.0137 ± 0.1284
Proposed Robust	0.5494 ± 0.0284	0.6160 ± 0.0761

4.7 Summary

This chapter analyzes the effect of known uncertainty, basis functions and nominal model on tracking accuracy of the FBF approach using the Frobenius norm metric. Similar to other methods for feedforward control, the tracking accuracy of FBF suffers in the presence of uncertainty. However, basis functions present a tuning parameter exclusive to FBF, which can be used to improve its tracking accuracy in the presence of uncertainty. Based on the Frobenius norm metric, a methodology for optimal selection of basis functions is presented. The basis functions are selected such that the effect of uncertainty on tracking accuracy is minimized, for known uncertainty and nominal model. This minimization is achieved while ensuring that the nominal tracking accuracy is not affected, and the control input is not very high due to NMP zeros. In addition, a procedure for finding the optimal number of basis functions for robust control is presented. The Frobenius norm metric is used to find an optimal nominal model for robustness. The distinction between the nominal model presented in this chapter and other similar methods in the literature, is its applicability to all types of linear systems, including time and parameter varying ones, as compared to other methods which are restricted to LTI systems. Combining the optimal selection of basis functions and nominal model, a two-step methodology for design of a robust FBF controller is proposed. The effectiveness of the optimal basis functions, optimal nominal model and their combination as compared to popular basis functions in the literature, viz. DCT and B-splines, and the control effort optimal basis functions (CE-Opt), proposed in Chapter 3, is demonstrated in simulations as well as experiments. A simple damped oscillator with uncertainties

is used in simulations, to demonstrate the effectiveness of proposed robust FBF controller as compared to popular basis functions. Experiments on a Taz 6 desktop 3D printer show that the proposed two-step robust controller is more effective than using CE-Opt basis functions with different arbitrary nominal models.

Chapter 5

Summary, Conclusions and Future Work

5.1 Summary and Conclusions

Tracking control is a fundamental problem in control engineering. It has broad practical applications in several industries, like manufacturing, automotive, robotics and aerospace. This dissertation focuses on feedforward tracking control. It is motivated by applications like 3D printing where feedforward techniques are very often the only recourse for tracking control due to the absence of feedback sensors. There are also several applications where, relative to feedback control, feedforward plays an outsized role in achieving excellent tracking control.

A major issue in achieving excellent tracking control using feedforward approaches is the presence of NMP zeros in the dynamics of the controlled plant. Existing methods for feedforward tracking control demonstrate varying levels of effectiveness depending on the location of the NMP zeros in the complex plane; several of them are not applicable to non-hyperbolic systems (i.e., systems with zeros on the unit circle). This dissertation has demonstrated analytically and numerically that the FBF approach overcomes this shortcoming of most existing approaches - i.e., its effectiveness is not significantly affected by NMP zero location and it is applicable to non-hyperbolic systems. These findings are very significant in practice because a feedforward controller may have to deal with plants with zeros anywhere in the complex plane, and it is not uncommon to have plants with one or more zeros on the unit circle. Having an approach that is agnostic to zero location nullifies the need to treat each plant specially, e.g., by designing a different controller for each plant.

Although this dissertation has primarily focused on LTI plants to understand and analyze the FBF approach and demonstrate its effectiveness, the FBF approach can easily be applied to other types of linear systems, for example, LTV, LPV, MIMO (including non-square systems), etc. This is unlike many other tracking control methods in the literature which are restricted to LTI systems, SISO systems or square MIMO systems. The versatility of the FBF approach combined

with its effectiveness for tracking different plant dynamics (irrespective of the zero location in the *z*-plane) make it suitable for tackling a wide range of tracking control problems and simplifies the controller design process.

To analytically compare the effectiveness of the FBF approach, an LTV control method, to that of LTI controllers in the literature, this dissertation (Chapter 2) proposes a metric based on the Frobenius norm of the LSR of system dynamics. The Frobenius norm metric is used to evaluate and compare the FBF approach with popular control methods in the literature, viz. ZPETC and TS. The effectiveness of the metric is validated using observations and analytical results from the literature. The metric explains the consistency of the FBF approach by showing that the metric applied to FBF's error dynamics is independent of its plant dynamics and basis functions. Its genesis from the LSR allows the Frobenius norm metric to be applied to all types of linear dynamics. This is unlike many frequency domain based metrics in the literature which are restricted to LTI systems. Hence, the Frobenius norm metric presents an opportunity to design and analyze linear controllers for specific control objectives. This dissertation presents examples for design of controllers using the Frobenius norm metric by proposing methodologies for optimal selection of basis functions for minimal control effort and robust tracking using FBF.

In the literature, basis functions are used by various control methods but their selection is generally ad-hoc. This dissertation (Chapter 3) presents a systematic optimization-based methodology for optimal selection of basis functions for FBF to achieve a desired level of tracking accuracy with minimum control effort. In most tracking control methods, perfect tracking while ensuring boundedness (stability) of the control input is the objective. Alternatively, the tracking error is minimized while subjecting the control input to satisfy some constraint(s). Many times these control methods result in perfect tracking or almost perfect tracking and utilize the maximum achievable control input. However, many engineering applications do not require perfect tracking. For example, manufactured parts can tolerate a certain amount of error. For such applications, the two-step optimal FBF controller proposed in this dissertation (Chapter 3) can help achieve optimal control effort with desired (tolerable) level of tracking accuracy. In the first step, the number of basis functions is selected to achieve a desired level of tracking accuracy and in step two, optimal set of basis functions – based on singular vectors of plant dynamics – are determined for minimum control effort. Simulations using a simple first order system with varying zero location and experiments on a desktop 3D printer are used to demonstrate the effectiveness of the proposed

optimal basis functions as compared to popular basis functions such as DCT and B-splines. In many cases, it is observed that the proposed basis functions result in orders of magnitude improvement in control effort of FBF tracking controller for the same tracking error, as compared to popular basis functions in the literature.

Chapters 2 and 3 assumed that the plant model is known precisely. However, plant dynamics always has some uncertainty and the tracking accuracy of feedforward methods such as FBF suffers in the presence of such uncertainty. However, unlike other methods in the literature, the FBF approach presents an additional tuning parameter, i.e., the basis functions, which can be used to improve the robustness of the FBF approach. Using the Frobenius norm metric, this dissertation presents an understanding of the effect of the choice of basis functions and uncertainty on the tracking accuracy of FBF. It is observed that the metric comprises of two components – nominal and uncertainty-related. The nominal component is independent of the type of basis functions and plant dynamics, whereas, the uncertainty-related component depends on the known uncertainty, nominal model used for filtering and the type of basis functions. An optimal set of basis functions that minimize the uncertainty-related component, while maintaining the desired level of nominal tracking accuracy and bounds on control effort, are selected. The proposed basis functions try to ensure that the deviation between the tracking error due to the uncertainty and the nominal tracking error is minimal. In many applications, this property of the proposed basis functions could ensure that the uncertainty does not affect tracking accuracy significantly, resulting in near consistent tracking even in the presence of uncertainty. In addition, the proposed robust basis functions can be complemented with other methods to improve the robustness of the FBF approach. This dissertation explores one such approach by proposing an optimal nominal model, which is obtained by minimizing a Frobenius norm metric. Combining the proposed basis functions and the nominal model, this dissertation proposes a two-step procedure to improve the robustness of the FBF approach. In step one, the nominal model is selected to minimize the effect of the uncertainty and in step two, the basis functions are selected to minimize the effect of the uncertainty. The effectiveness of the proposed two-step robust FBF controller as compared to popular basis functions in the literature and arbitrary selection of nominal model, is demonstrated using simulation examples and experiments on a desktop 3D printer.

The discussion in this dissertation has shown the effectiveness of the FBF approach for feedforward tracking control, as compared to popular methods in the literature. Also, the

effectiveness of the Frobenius norm metric as a tool for design and evaluation of controllers is explored through analysis of the FBF approach and methodologies for selection of basis functions. The FBF approach as well as the metric has shown tremendous potential and the following section provides some avenues to further explore this potential.

5.2 Recommendations for Future Research

Chapter 4 proposed an optimal two-step robust FBF controller which avoided large control inputs through use of constraints. A possible future research direction could be to find basis functions and nominal model such that robustness and control effort are simultaneously optimized. This dissertation focused on feedforward control but in many applications feedback is available, either in real-time [63] or at regular intervals [47]. Understanding the interaction between FBF FF controller and typical FB controllers using the Frobenius norm metric could provide useful insights which could be leveraged to improve the design of tracking controllers. This dissertation has entirely focused on linear systems but there are many applications in manufacturing [91], robotics [92] and aerospace [93] where the dynamics is nonlinear. Many such applications use FF control and FF tracking control of nonlinear NMP systems using direct inversion has been explored in the literature [94]. A possible future research topic could be application of the FBF approach, predicated on linear systems theory, to tracking control of nonlinear systems. As discussed in Section 2.3, FBF finds its origins in ILC [49] and basis functions are also used in model predictive control (MPC) [95]. Use of the methodology presented in this dissertation for selection of optimal basis functions, could be potentially used to address challenges in basis functions based ILC and MPC. As discussed in Section 2.3, B-splines are used to relax the assumption on desired trajectory of FBF. However, the analysis in Chapters 3 and 4 shows that B-splines result in significant loss in control effort and robustness as compared to the optimal basis functions. Although the optimal basis functions are efficient, a significant challenge will be implementing them in practice because of the associated high computational costs. Addressing this challenge could help in realization of practical and efficient FBF controllers.

APPENDICES

Appendix A

Lifted System Representation (LSR)

An LTI SISO causal plant G can be expressed as

$$G(q) = g_0 + g_1 q^{-1} + g_2 q^{-2} + \ldots \tag{A.1}$$

where the coefficients g_l are the Markov parameters of G. The sequence $g_0, g_1, g_2, \ldots$ also represent the impulse response of G. Then

$$\underbrace{\begin{bmatrix} y(0) \\ y(1) \\ \vdots \\ y(M) \end{bmatrix}}_{\mathbf{y}} = \underbrace{\begin{bmatrix} g_0 & 0 & \ldots & 0 \\ g_1 & g_0 & \ldots & 0 \\ \vdots & \vdots & \ddots & \vdots \\ g_M & g_{M-1} & \ldots & g_0 \end{bmatrix}}_{\mathbf{G}} \underbrace{\begin{bmatrix} u(0) \\ u(1) \\ \vdots \\ u(M) \end{bmatrix}}_{\mathbf{u}} \tag{A.2}$$

For an LTI non-causal controller C

$$C(q) = \ldots + c_{-2} q^2 + c_{-1} q^1 + c_0 + c_1 q^{-1} + c_2 q^{-2} + \ldots \tag{A.3}$$

the LSR of C can be expressed as

$$\underbrace{\begin{bmatrix} u(0) \\ u(1) \\ \vdots \\ u(M) \end{bmatrix}}_{\mathbf{u}} = \underbrace{\begin{bmatrix} c_0 & c_{-1} & \ldots & c_{-M} \\ c_1 & c_0 & \ldots & c_{-M+1} \\ \vdots & \vdots & \ddots & \vdots \\ c_M & c_{M-1} & \ldots & c_0 \end{bmatrix}}_{\mathbf{C}} \underbrace{\begin{bmatrix} y_d(0) \\ y_d(1) \\ \vdots \\ y_d(M) \end{bmatrix}}_{\mathbf{y}_d} \tag{A.4}$$

Similarly, overall dynamics L and error dynamics E_{ff} can be expressed in LSR as $\mathbf{L}$ and $\mathbf{E}_{ff}$. For LTI systems, the LSR is Toeplitz. For LTV systems or controllers, the construction of the LSR for L and E_{ff} follows a similar process but the resulting matrices are not Toeplitz [65].

Appendix B

BIBO Stability of the FBF Approach

This appendix examines the stability of the LTV system resulting from the FBF method using a BIBO stability approach. Let the bound on the desired trajectory, $y_d(k)$, be given by

$$\begin{aligned} &|y_d(k)| \le B_{y_d} \\ &0 < B_{y_d} < \infty \end{aligned} \tag{B.1}$$

Let us denote the elements of the LSR of FBF's overall dynamics $\mathbf{L}_{FBF}$ as $l_{FBF}(j,k)$ $(0 \le j \le M,\ 0 \le k \le M)$ and hence output $y(j)$ can be expressed as

$$y(j) = \begin{bmatrix} l_{FBF}(j,0) & l_{FBF}(j,1) & \dots & l_{FBF}(j,M) \end{bmatrix} \begin{bmatrix} y_d(0) \\ y_d(1) \\ \vdots \\ y_d(M) \end{bmatrix} \tag{B.2}$$

From Eqs. (B.1) and (B.2) one can conclude that

$$|y(j)| \le \sum_{k=0}^{M} |l_{FBF}(j,k)| B_{y_d} \tag{B.3}$$

Hence, $y(k)$ is bounded by

$$
\begin{aligned}
\left|y(k)\right| &\le \max_{0\le j\le M}\left(\sum_{k=0}^{M}\left|l_{FBF}(j,k)\right|B_{y_d}\right)\\
&\le \max_{0\le j\le M}\left(\sum_{k=0}^{M}\left|l_{FBF}(j,k)\right|\right)B_{y_d}\\
&\le \left\|\mathbf{L}_{FBF}\right\|_{\infty} B_{y_d}
\end{aligned}
\tag{B.4}
$$

where $\left\|\mathbf{L}_{FBF}\right\|_{\infty}$ represents the infinity norm of matrix $\mathbf{L}_{FBF}$. Similarly, $u(k)$ is bounded by

$$
\left|u(k)\right| \le \left\|\mathbf{C}_{FBF}\right\|_{\infty} B_{y_d} \tag{B.5}
$$

The implication is that a bounded desired trajectory, $y_d(k)$, results in output, $y(k)$, and control trajectories, $u(k)$, which are bounded by the infinity norms of $\mathbf{L}_{FBF}$ and $\mathbf{C}_{FBF}$, respectively. The bounds on the trajectories depend on matrices $\mathbf{L}_{FBF}$ and $\mathbf{C}_{FBF}$, and hence on the system and the selected basis functions. This implies that, for BIBO stability, the infinity norms of $\mathbf{L}_{FBF}$ and $\mathbf{C}_{FBF}$ should be bounded. The matrices $\mathbf{L}_{FBF}$ and $\mathbf{C}_{FBF}$ defined by Eq. (2.11), are quite cumbersome to analyze due to the presence of $\left(\tilde{\mathbf{\Phi}}^{\mathrm{T}}\tilde{\mathbf{\Phi}}\right)^{-1}$. As discussed in [49], the analysis can be simplified by use of decoupled filtered basis functions $\left\{\tilde{\boldsymbol{\psi}}_i\right\}$ in place of filtered basis functions $\left\{\tilde{\boldsymbol{\varphi}}_i\right\}$. For more details on decoupled filtered basis functions, see Appendix E. Based on the discussion in Appendix E (Eq. (E.7)), the matrix $\mathbf{L}_{FBF}$ can be expressed in terms of decoupled filtered basis functions, as [88]

$$
\mathbf{L}_{FBF} = \sum_{i=0}^{n}\tilde{\boldsymbol{\psi}}_i\tilde{\boldsymbol{\psi}}_i^{\mathrm{T}} = \sum_{i=0}^{n}\mathbf{L}_{FBF,i} \tag{B.6}
$$

where $\mathbf{L}_{FBF,i} = \tilde{\boldsymbol{\psi}}_i\tilde{\boldsymbol{\psi}}_i^{\mathrm{T}}$. Based on Eq. (B.6)

$$
\left\|\mathbf{L}_{FBF}\right\|_{\infty} \le \sum_{i=0}^{n}\left\|\mathbf{L}_{FBF,i}\right\|_{\infty} \tag{B.7}
$$

and $\left\|\mathbf{L}_{FBF,i}\right\|_{\infty}$ is given by

$$\left\|\mathbf{L}_{FBF,i}\right\|_\infty = \left\|\tilde{\boldsymbol{\psi}}_i\right\|_\infty \left\|\tilde{\boldsymbol{\psi}}_i\right\|_1 \tag{B.8}$$

The implication of Eqs. (B.7) and (B.8) is that

$$\left\|\mathbf{L}_{FBF}\right\|_\infty \le \sum_{i=0}^{n} \left\|\tilde{\boldsymbol{\psi}}_i\right\|_\infty \left\|\tilde{\boldsymbol{\psi}}_i\right\|_1 \tag{B.9}$$

Similarly, for matrix $\mathbf{C}_{FBF}$ (based on Appendix E, Eq. (E.7))

$$\left\|\mathbf{C}_{FBF}\right\|_\infty \le \sum_{i=0}^{n} \left\|\boldsymbol{\psi}_i\right\|_\infty \left\|\tilde{\boldsymbol{\psi}}_i\right\|_1 \tag{B.10}$$

For BIBO stability $\left\|\mathbf{L}_{FBF}\right\|_\infty < \infty$, $\left\|\mathbf{C}_{FBF}\right\|_\infty < \infty$. For a finite number of basis functions, this implies that

$$\left\|\boldsymbol{\psi}_i\right\|_\infty < \infty;\ \left\|\tilde{\boldsymbol{\psi}}_i\right\|_1 < \infty \tag{B.11}$$

The decoupled filtered basis functions $\tilde{\psi}_i(\bar{k})$, $-\infty < \bar{k} < \infty$, $\bar{k} \in \mathbb{Z}$, can be expressed as a convolution of corresponding basis function $\psi_i(\bar{k})$ and system $G(q)$ (with a time domain representation $g(\bar{k})$) as follows

$$\tilde{\psi}_i(\bar{k}) = \sum_{\bar{j}=-\infty}^{\infty} \psi_i(\bar{j}) g(\bar{k} - \bar{j}) \tag{B.12}$$

Based on Eq. (B.12)

$$\left\|\tilde{\psi}_i\right\|_1 \le \sum_{\bar{j}=-\infty}^{\infty} \left|\psi_i(\bar{j})\right| \sum_{\bar{k}=-\infty}^{\infty} \left|g(\bar{k} - \bar{j})\right| \tag{B.13}$$

The BIBO stability of $G(z)$ implies

$$\sum_{\bar{k}=-\infty}^{\infty} \left| g(\bar{k}) \right| < \infty \tag{B.14}$$

The implication of Eqs. (B.13) and (B.14) is that $\left\| \boldsymbol{\psi}_i \right\|_1$ (and hence $\left\| \boldsymbol{\varphi}_i \right\|_1$) should be bounded for BIBO stability, i.e., the basis functions should be absolutely summable.

The results of this section demonstrate that the LTV system resulting from the FBF method is BIBO stable for any finite number of absolutely summable basis functions; basis functions with finite length (i.e., for which $M < \infty$) will always satisfy these criteria.

Appendix C

Example: Existence and Uniqueness of Solution

This appendix illustrates the rank test (Eq. (2.17)) using an example. Consider the simple first order NMP system

$$G(q) = K\frac{q-a}{q-p};\;\; K = \frac{1-p}{1-a} \tag{C.1}$$

where K, a and p are the gain, zero and pole of the system, respectively. For the system under consideration, $\hat{u}(k)$ and $\hat{\mathbf{x}}(0)$ can be determined from Eq. (2.15) as

$$\begin{aligned} \hat{u}(k) &= a^k \hat{u}(0) \\ \mathbf{C}_d \hat{\mathbf{x}}(0) &= -D_d \hat{u}(0) \end{aligned} \tag{C.2}$$

Note that $\hat{u}(k)$ is an exponential signal. The initial states are selected as $\mathbf{X} = \mathbf{0}_{n+1}^{\mathrm{T}}$, and for p = 0.5, a = 2, n = 50, M = 100, DCT basis functions (defined in Appendix F)

$$\operatorname{rank}\left(\begin{bmatrix}\boldsymbol{\Phi}\\ \mathbf{X}\end{bmatrix}\right) = 51 \neq \operatorname{rank}\left(\begin{bmatrix}\boldsymbol{\Phi} & \hat{\mathbf{u}}\\ \mathbf{X} & \hat{\mathbf{x}}(0)\end{bmatrix}\right) = 52 \tag{C.3}$$

implying linearly independent filtered basis functions for the two systems. For a pseudorandom binary sequence (PRBS) generated desired trajectory (see Ref. [71] for more details) the RMS tracking error for DCT is 2.49×10^{-4} mm. Selecting $n = M = 100$, for $\mathbf{X} = \mathbf{0}_{n+1}^{\mathrm{T}}$ gives

$$\text{rank}\left(\begin{bmatrix}\boldsymbol{\Phi}\\ \mathbf{X}\end{bmatrix}\right)=\text{rank}\left(\begin{bmatrix}\boldsymbol{\Phi} & \hat{\mathbf{u}}\\ \mathbf{X} & \hat{\mathbf{x}}(0)\end{bmatrix}\right)=101 \tag{C.4}$$

implying linear dependence. However, changing the initial states to $\mathbf{x}_i(0) = 10^{-3}$ results in

$$\text{rank}\left(\begin{bmatrix}\boldsymbol{\Phi}\\ \mathbf{X}\end{bmatrix}\right)=101\neq \text{rank}\left(\begin{bmatrix}\boldsymbol{\Phi} & \hat{\mathbf{u}}\\ \mathbf{X} & \hat{\mathbf{x}}(0)\end{bmatrix}\right)=102 \tag{C.5}$$

i.e., linearly independent filtered basis functions and the RMS tracking error is 2.37×10^{-15}.

For an NMP system or system with relative degree (more poles than zeros), $n = M$ will result in linear dependence because $\mathbf{C}_{FBF} = \mathbf{G}^{-1}$, i.e., the FBF controller is obtained by inversion of the LSR of plant dynamics, and the LSR of plant dynamics has very small singular values.

Appendix D

Relationship between Metric and System Dynamics 2-norm

Based on the discussion in Appendix A, the squared Frobenius norm of the LSR of $\mathbf{E}_{ff}$ can be expressed as

$$\begin{aligned}\left\|\mathbf{E}_{ff}\right\|_F^2 &= \sum_{l=1}^{M+1}\sum_{k=l-1-M}^{l-1} e_{ff,k}^2 \\ &= e_{ff,-M}^2 + e_{ff,-M+1}^2 + \ldots + e_{ff,0}^2 \\ &\quad + e_{ff,-M+1}^2 + e_{ff,-M+2}^2 + \ldots + e_{ff,1}^2 \\ &\quad + \ldots \\ &\quad + e_{ff,0}^2 + e_{ff,1}^2 + \ldots + e_{ff,M}^2\end{aligned} \tag{D.1}$$

According to definition of 2-norm of $E_{ff}(q)$ and Parseval's Theorem [96]

$$\left\|E_{ff}(q)\right\|_2^2 = \frac{\int_0^{2\pi} \left|E_{ff}(e^{j\theta})\right|^2 d\theta}{2\pi} = \sum_{k=-\infty}^{\infty} e_{ff,k}^2; \tag{D.2}$$

$$\text{where } E_{ff}(e^{j\theta}) = \sum_{k=-\infty}^{\infty} e_{ff,-k} e^{jk\theta}$$

Consider

$$
\begin{aligned}
&(M+1)\sum_{k=-\infty}^{\infty} e_{ff,k}^2 \\
&= \sum_{l=1}^{M+1}\sum_{k=-\infty}^{\infty} e_{ff,k}^2 \\
&= \sum_{k=-\infty}^{-M-1} e_{ff,k}^2 + e_{ff,-M}^2 + e_{ff,-M+1}^2 + \ldots + e_{ff,0}^2 + \sum_{k=1}^{M} e_{ff,k}^2 + \sum_{k=M+1}^{\infty} e_{ff,k}^2 \\
&\quad + \ldots \\
&\quad + \sum_{k=-\infty}^{-M-1} e_{ff,k}^2 + \sum_{k=-M}^{h-M-2} e_{ff,k}^2 + e_{ff,h-M-1}^2 + e_{ff,h-M}^2 + \ldots + e_{ff,h-1}^2 + \sum_{k=h}^{M} e_{ff,k}^2 + \sum_{k=M+1}^{\infty} e_{ff,k}^2 \\
&\quad + \ldots \\
&\quad + \sum_{k=-\infty}^{-M-1} e_{ff,k}^2 + \sum_{k=-M}^{-1} e_{ff,k}^2 + e_{ff,0}^2 + e_{ff,1}^2 + \ldots + e_{ff,M}^2 + \sum_{k=M+1}^{\infty} e_{ff,k}^2
\end{aligned}
\tag{D.3}
$$

and using Eq. (D.1),

$$
(M+1)\sum_{k=-\infty}^{\infty} e_{ff,k}^2 = \left\|\mathbf{E}_{ff}\right\|_F^2 + (M+1)\sum_{k=-\infty}^{-M-1} e_{ff,k}^2 + (M+1)\sum_{k=M+1}^{\infty} e_{ff,k}^2 + \sum_{k=-M}^{M} |k| e_{ff,k}^2 \tag{D.4}
$$

Re-arrangement of the terms in the equation results in

$$
\frac{\left\|\mathbf{E}_{ff}\right\|_F^2}{M+1} = \sum_{k=-\infty}^{\infty} e_{ff,k}^2 - \sum_{k=-\infty}^{-M-1} e_{ff,k}^2 - \sum_{k=M+1}^{\infty} e_{ff,k}^2 - \sum_{k=-M}^{M} \frac{|k|}{M+1} e_{ff,k}^2 \tag{D.5}
$$

Consider two different values of M, M_1 and M_2 such that $M_1 > M_2$, then

$$
\begin{aligned}
\frac{\left\|\mathbf{E}_{ff}[M_1]\right\|_F^2}{M_1+1} &= \sum_{k=-\infty}^{\infty} e_{ff,k}^2 - \sum_{k=-\infty}^{-M_1-1} e_{ff,k}^2 - \sum_{k=M_1+1}^{\infty} e_{ff,k}^2 - \sum_{k=-M_1}^{M_1} \frac{|k|}{M_1+1} e_{ff,k}^2 \\
\frac{\left\|\mathbf{E}_{ff}[M_2]\right\|_F^2}{M_2+1} &= \sum_{k=-\infty}^{\infty} e_{ff,k}^2 - \sum_{k=-\infty}^{-M_2-1} e_{ff,k}^2 - \sum_{k=M_2+1}^{\infty} e_{ff,k}^2 - \sum_{k=-M_2}^{M_2} \frac{|k|}{M_2+1} e_{ff,k}^2
\end{aligned}
\tag{D.6}
$$

where $\mathbf{E}_{ff}[M_1]$ and $\mathbf{E}_{ff}[M_2]$ denote the LSRs of $E_{ff}(q)$ for trajectory lengths M_1+1 and M_2+1, respectively. Then

$$
\begin{aligned}
&\frac{\left\|\mathbf{E}_{ff}[M_1]\right\|_F^2}{M_1+1}-\frac{\left\|\mathbf{E}_{ff}[M_2]\right\|_F^2}{M_2+1}\\
&=-\sum_{k=-\infty}^{-M_1-1}e_{ff,k}^2+\sum_{k=-\infty}^{-M_2-1}e_{ff,k}^2-\sum_{k=M_1+1}^{\infty}e_{ff,k}^2+\sum_{k=M_2+1}^{\infty}e_{ff,k}^2\\
&\quad-\sum_{k=-M_1}^{M_1}\frac{|k|}{M_1+1}e_{ff,k}^2+\sum_{k=-M_2}^{M_2}\frac{|k|}{M_2+1}e_{ff,k}^2\\
&=\sum_{k=-M_1}^{-M_2-1}e_{ff,k}^2+\sum_{k=M_2+1}^{M_1}e_{ff,k}^2-\sum_{k=-M_1}^{-M_2-1}\frac{|k|}{M_1+1}e_{ff,k}^2-\sum_{k=M_2+1}^{M_1}\frac{|k|}{M_1+1}e_{ff,k}^2\\
&\quad-\sum_{k=-M_2}^{M_2}\frac{|k|}{M_1+1}e_{ff,k}^2+\sum_{k=-M_2}^{M_2}\frac{|k|}{M_2+1}e_{ff,k}^2\\
&=\sum_{k=-M_1}^{-M_2-1}\left(1-\frac{|k|}{M_1+1}\right)e_{ff,k}^2+\sum_{k=M_2+1}^{M_1}\left(1-\frac{|k|}{M_1+1}\right)e_{ff,k}^2\\
&\quad+\sum_{k=-M_2}^{M_2}\left(\frac{1}{M_2+1}-\frac{1}{M_1+1}\right)|k|e_{ff,k}^2\\
&=\sum_{k=-M_1}^{-M_2-1}\left(1-\frac{|k|}{M_1+1}\right)e_{ff,k}^2+\sum_{k=M_2+1}^{M_1}\left(1-\frac{|k|}{M_1+1}\right)e_{ff,k}^2\\
&\quad+\sum_{k=-M_2}^{M_2}\frac{M_1-M_2}{(M_1+1)(M_2+1)}|k|e_{ff,k}^2\\
&>0
\end{aligned}
\tag{D.7}
$$

The implication is that for $M_1 > M_2$

$$
\frac{\left\|\mathbf{E}_{ff}[M_1]\right\|_F^2}{M_1+1}>\frac{\left\|\mathbf{E}_{ff}[M_2]\right\|_F^2}{M_2+1} \tag{D.8}
$$

i.e., the value of the proposed Frobenius norm metric J_e increases as M increases for a given dynamics $E_{ff}(q)$.

Combining Eqs. (D.2) and (D.5)

$$
\frac{\left\|\mathbf{E}_{ff}\right\|_F^2}{M+1}=\left\|E_{ff}(q)\right\|_2^2-\sum_{k=-\infty}^{-M-1}e_{ff,k}^2-\sum_{k=M+1}^{\infty}e_{ff,k}^2-\sum_{k=-M}^{M}\frac{|k|}{M+1}e_{ff,k}^2 \tag{D.9}
$$

As $M \to \infty$, the first two summation terms on right hand side of Eq. (D.9) tend to 0. Assume that $e_{ff,k}$ is bounded by an exponential function, i.e.,

$$e_{ff,k}^2 \leq Ae^{-\mu|k|} \tag{D.10}$$

where e (on the right hand side) is the Euler's number and A and μ are positive non-zero constants. The implication of the assumption is that the output of dynamics E_{ff} at a particular instant of time depends more on input at the current time instant and inputs immediately preceding or succeeding the current input as compared to inputs which occurred long time back or will occur after a long time in the future. This assumption is true for stable systems. Hence, the third summation term on right hand side of Eq. (D.9) is bounded by

$$\sum_{k=-M}^{M} \frac{|k|}{M+1} e_{ff,k}^2 \leq A \sum_{k=-M}^{M} \frac{|k|}{M+1} e^{-\mu|k|} \tag{D.11}$$

Consider the bound on the summation,

$$A \sum_{k=-M}^{M} \frac{|k|}{M+1} e^{-\mu|k|} = 2A \sum_{k=0}^{M} \frac{k}{M+1} e^{-\mu k} \tag{D.12}$$

The summation on the right hand side represents summation of an arithmetico-geometric sequence [97]. As $M \to \infty$ (based on sum of infinite arithmetico-geometric sequence with absolute value of common ratio of the geometric part of the sequence bounded by 1, i.e., $|e^{-\mu}| < 1$)

$$\lim_{M \to \infty} 2A \sum_{k=0}^{M} \frac{k}{M+1} e^{-\mu k} = \lim_{M \to \infty} 2A \frac{1}{M+1} \frac{e^{-\mu}}{(1-e^{-\mu})^2} = 0 \tag{D.13}$$

which implies that

$$\lim_{M\to\infty}\sum_{k=-M}^{M}\frac{|k|}{M+1}e_{ff,k}^{2}\le\lim_{M\to\infty}A\sum_{k=-M}^{M}\frac{|k|}{M+1}e^{-\mu|k|}=0 \tag{D.14}$$

The implication is that (based on Eqs. (D.9) and (D.14))

$$J_e=\frac{\left\|\mathbf{E}_{ff}\right\|_F}{\sqrt{M+1}}\to\left\|E_{ff}(q)\right\|_2\quad\text{as}\quad M\to\infty \tag{D.15}$$

Appendix E

Decoupled Filtered Basis Functions

As is evident from Eq. (2.10), the coefficients corresponding to any basis function depend on all filtered basis functions which implies that the filtered basis functions are coupled. Hence, Eqs. (2.10) and (2.11) require the inversion of an order n+1 matrix, $\tilde{\mathbf{\Phi}}^{\mathrm{T}}\tilde{\mathbf{\Phi}}$, which is cumbersome numerically and analytically, especially as n increases. The analyses and numerical efficiency of the FBF method is therefore facilitated by decoupling the filtered basis functions.

Let us denote the decoupled filtered basis functions as $\{\tilde{\psi}_i(k)\}$ and the corresponding unfiltered basis functions as $\{\psi_i(k)\}$ such that

$$\begin{aligned} &\tilde{\psi}_i(k) = G\psi_i(k); \\ &\tilde{\mathbf{\Psi}}^{\mathrm{T}}\tilde{\mathbf{\Psi}} = \mathbf{I}_{n+1} \end{aligned} \tag{E.1}$$

where

$$\tilde{\mathbf{\Psi}} = \begin{bmatrix} \tilde{\boldsymbol{\psi}}_0 & \tilde{\boldsymbol{\psi}}_1 & \dots & \tilde{\boldsymbol{\psi}}_n \end{bmatrix} = \begin{bmatrix} \tilde{\psi}_0(0) & \tilde{\psi}_1(0) & \dots & \tilde{\psi}_n(0) \\ \tilde{\psi}_0(1) & \tilde{\psi}_1(1) & \dots & \tilde{\psi}_n(1) \\ \vdots & \vdots & \ddots & \vdots \\ \tilde{\psi}_0(M) & \tilde{\psi}_1(M) & \dots & \tilde{\psi}_n(M) \end{bmatrix} \tag{E.2}$$

The coupled and decoupled filtered basis functions are related by the transformation matrix $\mathbf{\Omega}$ as follows

$$\begin{aligned} \tilde{\mathbf{\Phi}} &= \tilde{\mathbf{\Psi}}\mathbf{\Omega} \\ \mathbf{\Phi} &= \mathbf{\Psi}\mathbf{\Omega} \end{aligned} \tag{E.3}$$

where

$$\boldsymbol{\Psi} = \begin{bmatrix} \boldsymbol{\psi}_0 & \boldsymbol{\psi}_1 & \cdots & \boldsymbol{\psi}_n \end{bmatrix} = \begin{bmatrix} \psi_0(0) & \psi_1(0) & \cdots & \psi_n(0) \\ \psi_0(1) & \psi_1(1) & \cdots & \psi_n(1) \\ \vdots & \vdots & \ddots & \vdots \\ \psi_0(M) & \psi_1(M) & \cdots & \psi_n(M) \end{bmatrix} \tag{E.4}$$

Based on Eqs. (E.1) and (E.3), the matrix $\tilde{\boldsymbol{\Phi}}^{\mathrm{T}}\tilde{\boldsymbol{\Phi}}$ can be expressed as

$$\tilde{\boldsymbol{\Phi}}^{\mathrm{T}}\tilde{\boldsymbol{\Phi}} = \boldsymbol{\Omega}^{\mathrm{T}}\tilde{\boldsymbol{\Psi}}^{\mathrm{T}}\tilde{\boldsymbol{\Psi}}\boldsymbol{\Omega} = \boldsymbol{\Omega}^{\mathrm{T}}\boldsymbol{\Omega} \tag{E.5}$$

Without loss of generality, let us assume that $\boldsymbol{\Omega}$ is an upper triangular matrix that can be obtained from Cholesky decomposition of $\tilde{\boldsymbol{\Phi}}^{\mathrm{T}}\tilde{\boldsymbol{\Phi}}$ [98]. Accordingly, Eq. (2.10) can be written as

$$\boldsymbol{\gamma}_D = \tilde{\boldsymbol{\Psi}}^{\mathrm{T}}\mathbf{y}_d \tag{E.6}$$

and matrices $\mathbf{C}_{FBF}$ and $\mathbf{L}_{FBF}$ can be expressed as

$$\begin{aligned} \mathbf{L}_{FBF} &= \tilde{\boldsymbol{\Psi}}\tilde{\boldsymbol{\Psi}}^{\mathrm{T}} = \sum_{i=0}^{n} \tilde{\boldsymbol{\psi}}_i \tilde{\boldsymbol{\psi}}_i^{\mathrm{T}} \\ \mathbf{C}_{FBF} &= \boldsymbol{\Psi}\tilde{\boldsymbol{\Psi}}^{\mathrm{T}} = \sum_{i=0}^{n} \boldsymbol{\psi}_i \tilde{\boldsymbol{\psi}}_i^{\mathrm{T}} \end{aligned} \tag{E.7}$$

Note that decoupling has replaced the inversion of $\tilde{\boldsymbol{\Phi}}^{\mathrm{T}}\tilde{\boldsymbol{\Phi}}$ with the inversion of $\boldsymbol{\Omega}$. The conditions for the existence of $\boldsymbol{\Omega}^{-1}$ are the same as those for the existence of $\left(\tilde{\boldsymbol{\Phi}}^{\mathrm{T}}\tilde{\boldsymbol{\Phi}}\right)^{-1}$, as discussed in Section 2.4.

Appendix F

Definition of DCT and B-Spline Basis Functions

The DCT is a frequency-based transform that is widely used in signal processing; its basis functions are real-valued cosines defined as [80]

$$\varphi_i(k) = \beta_i \cos\left(\frac{\pi(2k+1)i}{2(M+1)}\right);\ \beta_i = \begin{cases} \dfrac{1}{\sqrt{M+1}} & i = 0 \\ \sqrt{\dfrac{2}{M+1}} & i > 0 \end{cases} \tag{F.1}$$

For a B-spline of degree m, having $n+1 \le M+1$ control points (same as coefficients of basis functions), $\gamma_0, \gamma_1, \ldots, \gamma_n$, and knot vector $[\eta_0\ \eta_1\ \ldots\ \eta_{m+n+1}]^{\mathrm{T}}$, its real-valued basis functions, $\varphi_{i,m}$, are given by [81]

$$\begin{aligned} \varphi_i(k) &:= \varphi_{i,m}(\xi_k) = \frac{\xi_k - \eta_i}{\eta_{i+m} - \eta_i}\varphi_{i,m-1}(\xi) + \frac{\eta_{i+m+1} - \xi_k}{\eta_{i+m+1} - \eta_{i+1}}\varphi_{i+1,m-1}(\xi) \\ \varphi_{i,0}(\xi_k) &= \begin{cases} 1 & \eta_i \le \xi_k \le \eta_{i+1} \\ 0 & \text{otherwise} \end{cases} \end{aligned} \tag{F.2}$$

where $i = 0, 1, \ldots, n$ with $\xi_k \in [0,1]$, representing normalized time, discretized into $M+1$ points, $\xi_0, \xi_1 \ldots \xi_M$, and η_j is a uniform knot vector, selected such that

$$\eta_j = \begin{cases} 0 & 0 \le j \le m \\ \dfrac{j-m}{n-m+1} & m+1 \le j \le n \\ 1 & n+1 \le j \le m+n+1 \end{cases} \tag{F.3}$$

Appendix G

Application of Eckart-Young-Mirsky (EYM) Theorem to Tracking Control

This appendix presents the EYM Theorem [99–101] and shows that the FBF controller is the optimal solution to rank constrained minimization of the Frobenius norm metric applied to tracking error dynamics.

G.1 Eckart-Young-Mirsky (EYM) Theorem

Consider matrix $\mathbf{A}$ ($r_1 \times r_2$, $r_1 \leq r_2$) and $0 < r < r_1$, r is an integer, SVD of $\mathbf{A}$ (assuming full rank) is given by

$$\mathbf{A} = \sum_{i=1}^{r_1} \sigma_{A,i} \mathbf{v}_{A,i} \mathbf{w}_{A,i}^{\mathrm{T}} \tag{G.1}$$

then solution to the following problem

$$\begin{aligned} \hat{\mathbf{A}}^* := \arg\min_{\hat{\mathbf{A}}} & \left\| \mathbf{A} - \hat{\mathbf{A}} \right\|_F \\ \text{s.t.} \quad & rank(\hat{\mathbf{A}}) \leq r \end{aligned} \tag{G.2}$$

is given by

$$\hat{\mathbf{A}}^* = \sum_{i=1}^{r} \sigma_{A,i} \mathbf{v}_{A,i} \mathbf{w}_{A,i}^{\mathrm{T}} \tag{G.3}$$

i.e., a truncated singular value decomposition and

$$\left\|\mathbf{A}-\hat{\mathbf{A}}^{*}\right\|_{F}=\sqrt{\sum_{i=r+1}^{r_1}\sigma_{A,i}^{2}} \tag{G.4}$$

The solution is unique if and only if $\sigma_{A,r+1} \neq \sigma_{A,r}$.

G.2 FBF as Solution to the Rank Constrained Optimization Problem

Consider the rank constrained optimization problem

$$\begin{aligned}&\min_{\mathbf{L}}\left\{J_e=\frac{\left\|\mathbf{I}-\mathbf{L}\right\|_F}{\sqrt{M+1}}\right\}\\&\text{s.t. } rank(\mathbf{L})\le n+1\end{aligned} \tag{G.5}$$

The SVD of **I** is of the form (the SVD is not unique)

$$\mathbf{I}=\sum_{i=1}^{M+1}\boldsymbol{\eta}_i\boldsymbol{\eta}_i^{\mathrm{T}} \tag{G.6}$$

where

$$\begin{aligned}&\boldsymbol{\eta}_i^{\mathrm{T}}\boldsymbol{\eta}_j=\delta_{ij}\\&\delta_{ij}=\begin{cases}1 & i=j\\0 & i\neq j\end{cases}\end{aligned} \tag{G.7}$$

For constant *M*, based on the EYM Theorem, one can conclude that the optimal solution is not unique and is of the form

$$\mathbf{L}_{opt}=\sum_{i=1}^{n+1}\boldsymbol{\eta}_i\boldsymbol{\eta}_i^{\mathrm{T}} \tag{G.8}$$

Based on Eq. (E.7), it is known that the LSR of FBF overall dynamics, which will vary depending on the selected basis functions and the plant, is

$$\mathbf{L}_{FBF} = \tilde{\mathbf{\Psi}}\tilde{\mathbf{\Psi}}^{\mathrm{T}} = \sum_{i=1}^{n+1} \tilde{\boldsymbol{\psi}}_i \tilde{\boldsymbol{\psi}}_i^{\mathrm{T}} \tag{G.9}$$

and based on Eq. (E.1)

$$\tilde{\boldsymbol{\psi}}_i^{\mathrm{T}} \tilde{\boldsymbol{\psi}}_j = \delta_{ij} \tag{G.10}$$

Every optimal solution of Eq. (G.5) is given by Eqs. (G.7) and (G.8) and every FBF overall dynamics can be expressed using Eqs. (G.9) and (G.10). Based on Eqs. (G.7)-(G.10) one can conclude that every optimal solution of Eq. (G.5) represents an FBF overall dynamics and every FBF overall dynamics is an optimal solution of Eq. (G.5).

Appendix H

Experiments on a Biaxial Linear Motor Driven Stage

This appendix presents the experimental results on optimal selection of basis functions for minimum effort tracking control from Ref [73]. The biaxial (X-Y) linear motor driven stage (Aerotech ALS 25010), shown in Figure H.1, is used for the experiments. The stage is controlled using a P/PI feedback controller, augmented with velocity and acceleration feedforward [102] (see Figure H.2). The controller is implemented on a dSPACE 1202 real-time control board with 10 kHz sampling frequency. A flexible fixture consisting of a block mounted on a slender rod is attached to the stage. The block is assumed to represent an apparatus, for example, a tool, a workpiece or a measurement device whose position needs to be tracked accurately despite its flexible structure. The FBF approach is used as a feedforward tracking controller as shown in the block diagram of Figure H.2. The FBF approach takes in the desired position commands y_d for each axis and generates modified position commands u that are sent to the stage to ensure that the actual position of the block y follows y_d accurately, in spite of its inherent structural flexibilities. The actual position of the block is observed from its accelerations measured using two unidirectional accelerometers (PCB piezotronics 393B05).

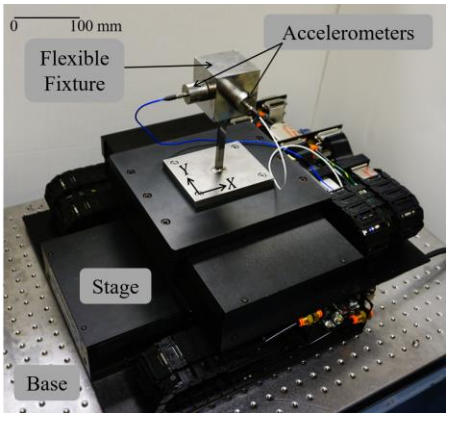

Figure H.1 Biaxial stage with flexible fixture

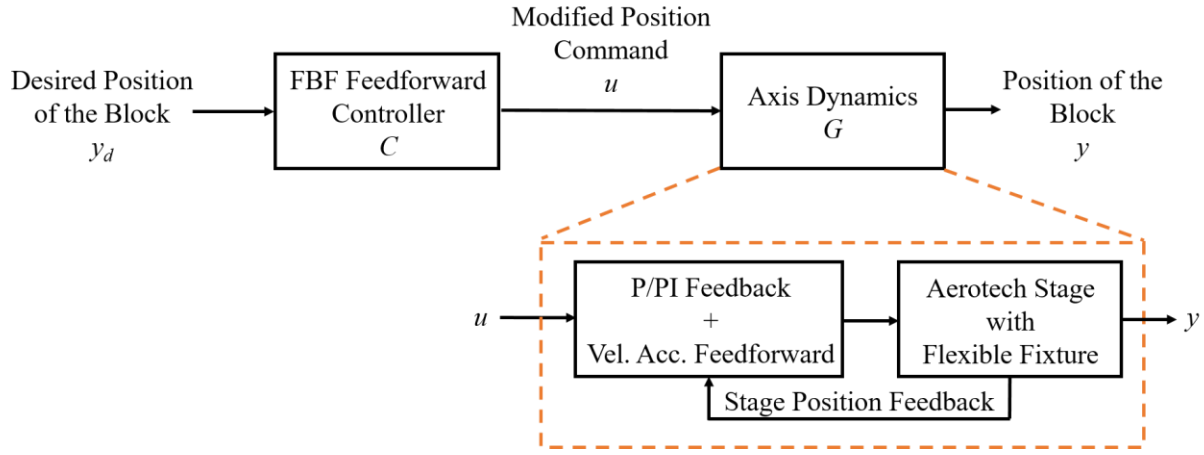

Figure H.2 Block diagram of the FBF controller and experimental setup

Figure H.3 shows the frequency response function (FRF) of the dynamics of each axis of the stage, generated by applying swept sine acceleration inputs to the stage and measuring the corresponding accelerations of the block using the accelerometers. Each axis has 4 modes (two dominant and two less dominant) and hence, the plant dynamics is eighth-order. Prior work of the authors [90] provides more details about a continuous-time model for the system, which indicates the presence of one NMP zero in the dynamics of each axis. The Markov parameters of the dynamics are obtained from the continuous-time model and are used to construct a finite impulse response (FIR) representation of the dynamics along each axis. Figure H.3 shows a good match between the measured FRF and the FRF generated using the FIR representations (modeled). Based on the methodology discussed in Appendix A, the LSR of the dynamics of each axis is generated using the FIR representation. Singular values of the LSRs (for M = 10000) are shown in Figure H.4. Note that each axis has two very small singular values which deviate from the cluster and these singular values result in large control inputs, if the basis functions are not properly selected. One of the two singular values along each axis arises from the NMP zero, whereas, the other small singular value is a result of relative degree of one (the first Markov parameter is zero). Figure H.5

shows the desired butterfly shaped path, whereas Figure H.6 show the desired paths position along the X and Y axes (for more details see [90]). The duration of the trajectory is 1 second (i.e., M = 10000, based on 10 kHz sampling frequency).

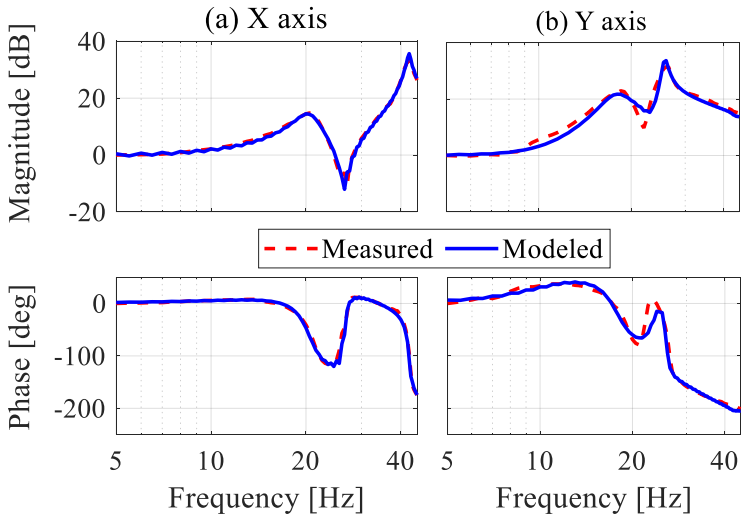

Figure H.3 Measured and modeled frequency response functions of the X and Y axes of the biaxial stage

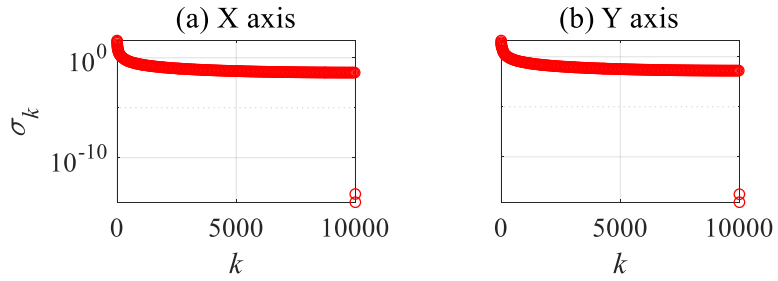

Figure H.4 Singular values of the LSRs of the X and Y axes dynamics

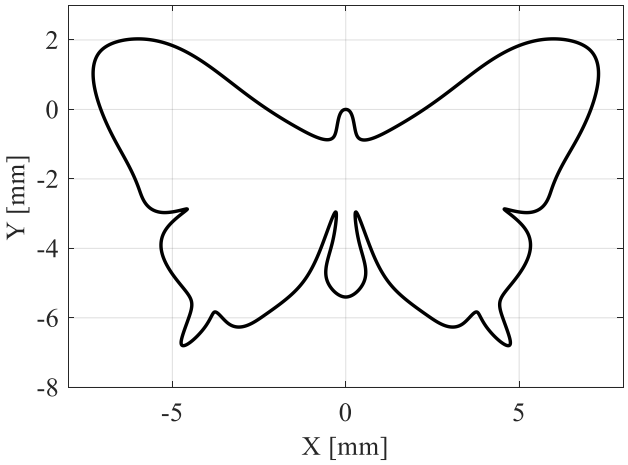

Figure H.5 Desired path

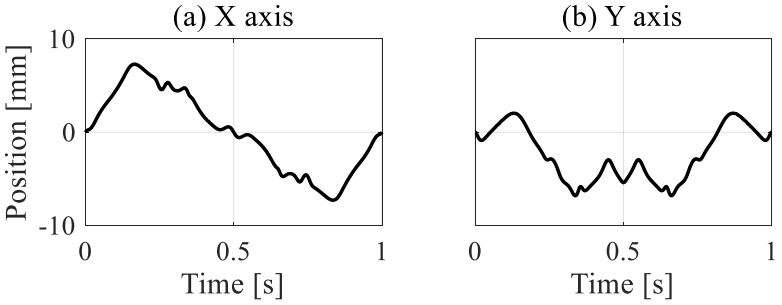

Figure H.6 Desired position trajectories along the X and Y axes

For experiments, the optimal basis functions proposed in Section 3.4 are compared with B-splines, because they are often the basis functions of choice for manufacturing and robotics applications [20,47,48,81,90]. Figure H.7 shows the control input (i.e., modified position commands) sent to the X and Y axes for the two sets of basis functions (for n = 600). Also, shown are the resultant tracking errors, which are based on position signals derived from measured acceleration signals using an observer. Note that the B-spline based control input show rapid growth in magnitude towards the end of the signal because of the small singular values of the LSR corresponding to the NMP zero and the relative degree. For safety reasons, a limit ± 10 mm is placed on the position commands for both axes, as shown in Figure H.7; the B-spline control input saturates at the limit. Notice that, before saturation, the control inputs for the proposed optimal basis functions and B-splines are quite similar which results in similar tracking errors. In the time

interval between 0 and 0.99 s, the RMS tracking errors for optimal basis functions and B-splines are 263.31 μm and 250.85 μm, respectively, for the X-axis and between 0 and 0.96 s, 171.29 μm and 186.12 μm, respectively, for the Y-axis. However, because of saturation, the B-spline based commands generate large tracking errors, as shown in Figure H.7. Consequently, the overall RMS tracking error for B-splines, along the X and Y axes, are respectively 3 and 19 times the RMS tracking error for the optimal basis functions (see Table H.1). Moreover, the optimal basis functions require 3% and 13% lower control effort than B-splines for X-axis and Y-axis, respectively. The proposed optimal basis functions track much better than B-splines and require less control effort.

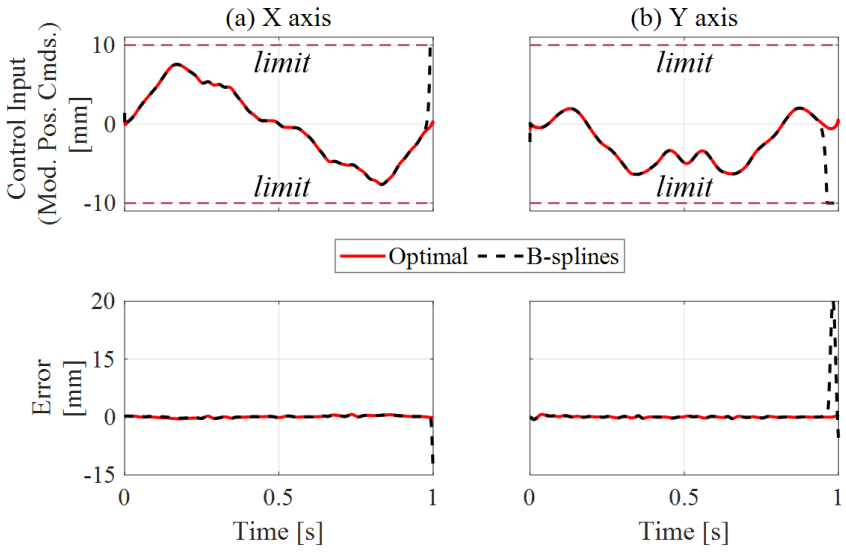

Figure H.7 X and Y control inputs (i.e., modified position command) signals and tracking errors for optimal basis functions and B-splines (M = 10000, n = 600)

Table H.1 Summary of tracking error and control effort for experiments

Basis Functions	X axis		Y axis	
	$\mathbf{e}_{RMS}/\mathbf{y}_{d,RMS}$	$\mathbf{u}_{RMS}/\mathbf{y}_{d,RMS}$	$\mathbf{e}_{RMS}/\mathbf{y}_{d,RMS}$	$\mathbf{u}_{RMS}/\mathbf{y}_{d,RMS}$
Optimal	0.06	1.05	0.05	0.98
B-splines	0.17	1.08	0.94	1.12

Appendix I

A Frequency Domain-based Optimization Approach for Nominal Model Selection for Robust Filtered Basis Functions Approach

This appendix presents a frequency domain-based approach for nominal model selection to improve the robustness of the FBF approach [70]. Also, presented are simulations and experiments on a desktop 3D printer, to demonstrate the effectiveness of the robust FBF approach as compared to the standard FBF approach (presented in Section 2.3).

I.1 Definition of Robust Nominal Model

The standard FBF controller discussed in Section 2.3 assumes that the (nominal) model, is a perfect representation of the actual plant. However, in practice, the nominal model is not an accurate representation of the actual plant, due to uncertainty. In this section, we propose a robust FBF approach that uses a robust nominal model to improve the robustness of the FBF approach. The robust nominal model accounts for known uncertainty in G, and retains the elegance of the least squares solution which facilitates limited preview filtered B-splines (LPFBS).

In the presence of uncertainty in G, the optimal tracking controller has been proposed in the literature [64] as the controller that minimizes the following cost function (at each frequency, ω) over the uncertainty

$$\begin{aligned} J_r &= \int_{\Delta} f(\Delta)\left|E_{ff}\right|^2 d\Delta \\ E_{ff} &= 1 - CG \end{aligned} \tag{I.1}$$

where $f(\Delta)$ is the distribution of the actual plant G w.r.t. the uncertainty Δ. Note that for simplicity of notation, the dependence of $f(\Delta)$ and E_{ff} on ω is not explicitly shown in Eq. (I.1) and in the

following equations. The optimal controller can be obtained by differentiating J_r w.r.t. C^* and equating the result to zero, where the superscript * denotes complex conjugate. The optimal controller is given by

$$C_{opt} = \frac{\int_{\Delta} f(\Delta) G^* d\Delta}{\int_{\Delta} f(\Delta) G G^* d\Delta} \tag{I.2}$$

The problem is that C_{opt} as defined in Eq. (I.2) cannot directly be used within the FBF framework shown in Figure 2.2; it is a stand-alone controller different from $\mathbf{C}_{FBF}$ in Eq. (2.11). However, notice that the standard FBF approach assumes that the nominal model matches the plant perfectly. Hence, $E_{ff} = 1 - CG_{nom}$ and the minimum E_{ff} can be realized using $C = G_{nom}^{-1}$. Therefore, to approximate $C = G_{nom}^{-1}$, the standard FBF approach uses $G_{nom} = C^{-1}$ to filter the basis functions. By analogy, in the presence of uncertainty in G, we want the FBF controller to approximate C_{opt}. Therefore, we propose the robust nominal model, G_r, as

$$G_r \triangleq C_{opt}^{-1} = \frac{\int_{\Delta} f(\Delta) G G^* d\Delta}{\int_{\Delta} f(\Delta) G^* d\Delta} \tag{I.3}$$

Accordingly, referring to Figure 2.2, the robust FBF approach filters the user-defined basis functions $\boldsymbol{\varphi}_i$ using G_r (instead of the nominal model used by the standard FBF approach), to obtain the filtered basis functions $\widetilde{\boldsymbol{\varphi}}_i$. The coefficients are then obtained using the least squares solution given by Eq. (2.10). Hence, the proposed robust FBF approach retains the elegance of the least squares solution, which facilitates LPFBS.

I.2 Incorporation of Dynamic Uncertainty with Kernel Distribution into Robust Nominal Model

The previous section did not consider the specifics of the uncertainty and its distribution. The work by Lunenburg [64] in defining C_{opt} in Eq. (I.2) considered only multiplicative uncertainty

with uniform distribution. This section presents the robust filter considering dynamic uncertainty with a kernel distribution.

In the presence of dynamic uncertainty, the actual plant can be expressed as

$$\begin{aligned} &G(\omega) = r(\omega) e^{j\theta(\omega)}; \\ &r(\omega) \in \left[r_{\min}(\omega), \quad r_{\max}(\omega) \right] \\ &\theta(\omega) \in \left[\theta_{\min}(\omega), \quad \theta_{\max}(\omega) \right] \end{aligned} \tag{I.4}$$

where j is the unit imaginary number, r is magnitude of the actual plant, θ is phase of the actual plant, ω is frequency in rad/s and the subscripts 'max' and 'min' denote upper and lower bounds. Figure I.1 illustrates G using the Bode plot and the complex plane.

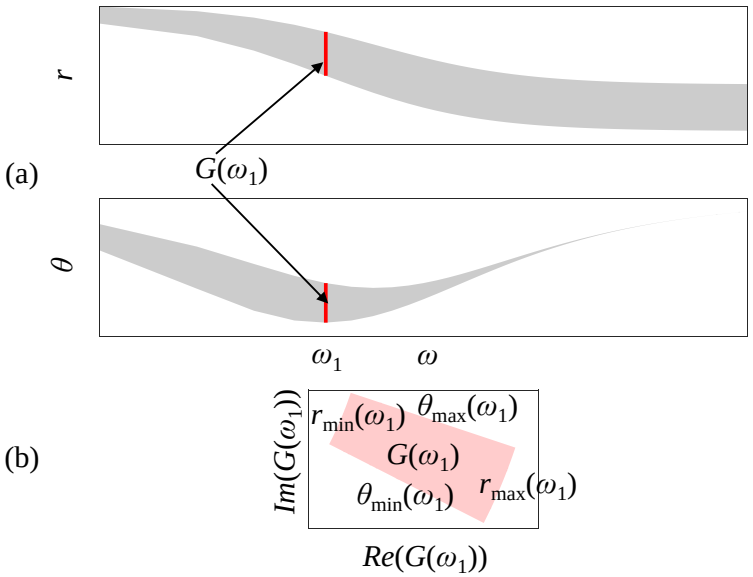

Figure I.1 Illustration of dynamic uncertainty using (a) Bode plot and (b) complex plane.

The distribution of uncertainty $f(\Delta) = f(r,\theta)$ can take different forms. Prior work [69] considered a uniform distribution of uncertainty, which is unlikely to hold in practice. Here, without loss of generality, a kernel distribution (with normal kernels) is proposed because of its versatility. The kernel distribution is defined as follows (for frequency ω)

$$
\begin{aligned}
f(r,\theta) &= f_1(r)\, f_2(\theta); \\
f_1(r) &= \frac{1}{l\sigma_r}\sum_{i=1}^{l} K\left(\frac{r-r_i}{\sigma_r}\right) = \frac{1}{\sqrt{2\pi}l\sigma_r^2}\sum_{i=1}^{l} e^{-\frac{(r-r_i)^2}{2\sigma_r^2}} \\
f_2(\theta) &= \frac{1}{l\sigma_\theta}\sum_{i=1}^{l} K\left(\frac{\theta-\theta_i}{\sigma_\theta}\right) = \frac{1}{\sqrt{2\pi}l\sigma_\theta^2}\sum_{i=1}^{l} e^{-\frac{(\theta-\theta_i)^2}{2\sigma_\theta^2}}
\end{aligned}
\tag{I.5}
$$

where the indices $i = 1, 2, \ldots, l$, denote frequency response functions (FRFs) sampled from G, corresponding to the different operating conditions; l is the total number of FRF samples; K is the normal kernel with mean values (r_i, θ_i) and standard deviations $(\sigma_r, \sigma_\theta)$. The mean values r_i and θ_i are the magnitude and phase of the i^{th} FRF at frequency ω, respectively. For a given frequency ω, the standard deviations σ_r and σ_θ are identical for all l kernels. Figure I.2 depicts an example of individual normal kernels and their summation. Substituting function $f(r,\theta)$ defined by Eq. (I.5) and uncertainty given by Eq. (I.4) in Eq. (I.3), the robust filter can be expressed as

$$
\begin{aligned}
G_r &= \frac{\left\{\sum_{i=1}^{l}\alpha_{ri}\right\}\left\{\sum_{i=1}^{l}\alpha_{\theta i}\right\}}{\left\{\sum_{i=1}^{l}\beta_{ri}\right\}\left\{\sum_{i=1}^{l}\beta_{\theta i}\right\}}; \\
\alpha_{ri} &\triangleq \int_{r_{\min}}^{r_{\max}} K\left(\frac{r-r_i}{\sigma_r}\right) r^3 dr, \quad \alpha_{\theta i} \triangleq \int_{\theta_{\min}}^{\theta_{\max}} K\left(\frac{\theta-\theta_i}{\sigma_\theta}\right) d\theta, \\
\beta_{ri} &\triangleq \int_{r_{\min}}^{r_{\max}} K\left(\frac{r-r_i}{\sigma_r}\right) r^2 dr, \quad \beta_{\theta i} \triangleq \int_{\theta_{\min}}^{\theta_{\max}} K\left(\frac{\theta-\theta_i}{\sigma_\theta}\right) e^{-j\theta} d\theta
\end{aligned}
\tag{I.6}
$$

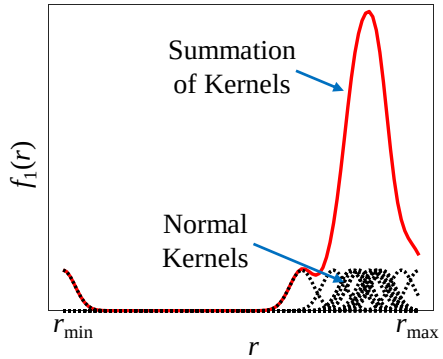

Figure I.2 Illustration of kernel distribution of the dynamic uncertainty.

Wu & Zou [63] designed an optimal controller in the presence of dynamic uncertainty (given by Eq. (I.4)) using worst-case optimization, but assumed a gain modulated inversion structure for their optimal controller. To improve the worst-case tracking error using FBF, the inverse of the optimal controller proposed by Wu & Zou [63] can be used as the filter G_r, similar to Eq. (I.3).

I.3 Setup for Simulation and Experiments

This section validates the robust FBF approach using simulations and experiments on a Lulzbot TAZ 6 desktop 3D printer, shown in Figure 3.4. For system identification and control, motion commands are sent to the printer's stepper motors at 1 kHz sampling rate using a real-time controller (dSPACE 1202) via stepper motor drivers (Pololu DRV8825).

The frequency response functions (FRFs) of the 3D printer are obtained by applying swept sine acceleration signals (with amplitudes ranging from 2 m/s^2 to 5 m/s^2 in increments of 0.2 m/s^2) to the printer's stepper motors (each having 10 μm stepping resolution) and measuring the relative acceleration of the build platform and print head using accelerometers (SparkFun ADXL335 triple-axis). The uncertainty region shown in Figure I.3 represents the variations in magnitude and phase of the measured FRFs as functions of input acceleration amplitude.

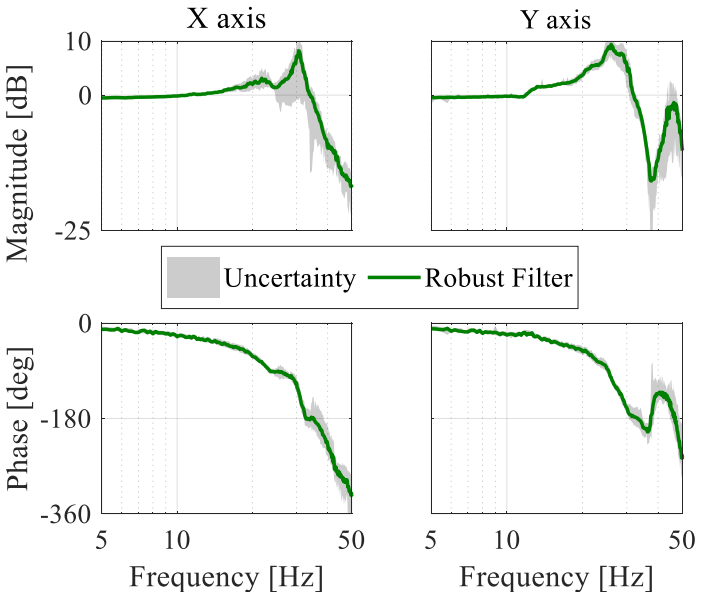

Figure I.3 Frequency response functions (FRFs) corresponding to dynamic uncertainty and robust filter (nominal model).

The standard deviations σ_r and σ_θ for the normal kernels are estimated optimally from FRF data using the *fitdist* function in MATLAB®. Using Eq. (I.6), the robust filters for the *x*- and *y*-axes are obtained and their FRFs are shown in Figure I.3. Figure I.4 shows the singular values of the lifted system representation (LSR) of the robust filters. Since the highest singular values do not deviate from the cluster of singular values, the robust filters are stable. However, the two smallest singular values for the *x* axis deviate from the cluster which implies that the robust filter for the *x* axis has a pair of complex NMP zeros (for details about LSR and its singular values, interested readers can see [73,103]).

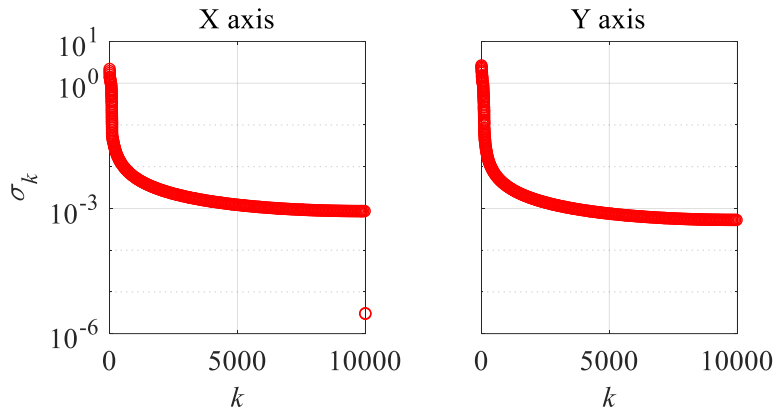

Figure I.4 Singular values of LSR of *x* and *y* axes robust nominal models showing NMP behavior in *x* axis.

I.4 Simulations

This section uses simulations to demonstrate the effectiveness of the robust approach presented in Section I.1 as compared to the standard approach presented in Section 2.3, using B-splines as basis functions. This section uses the B-splines [48] because they are commonly used to parameterize commands sent to manufacturing machines and robots [85]. The mathematical expressions for B-splines are given in Appendix F.

For comparison of robust FBF with standard FBF, a signal with frequency content uniformly distributed between 5 and 50 Hz, along the *x* axis, is used as the desired trajectory. The length of the desired trajectory is 1 second, resulting in 1001 discrete points (i.e., $M = 1000$) based on sampling time T_s = 1 millisecond. For each acceleration magnitude shown in Figure I.5, the basis functions are filtered with the corresponding FRF to generate a standard FBF controller for that particular FRF. The robust FBF and each case of the standard FBF approach is simulated for 10,000 realizations of G (generated using the kernel distribution specified by function $f(r,\theta)$), along the *x* axis. B-splines with parameters m = 5 and n = 200 are used as basis functions. The performance of the robust FBF relative to standard FBF approach is quantified by the following metric q

$$q = \frac{\text{mean}(e_{RMS,S}) - \text{mean}(e_{RMS,R})}{\text{mean}(e_{RMS,S})} \times 100 \tag{I.7}$$

where $e_{RMS,S}$ and $e_{RMS,R}$ denote the root mean square (RMS) errors corresponding to standard and robust FBF, respectively, for the 10,000 realizations of G. Figure I.5 plots q for each FRF acceleration magnitude. It is seen that robust FBF outperforms the standard FBF approach by factors ranging from 1% to 99%, depending on the FRF acceleration magnitude.

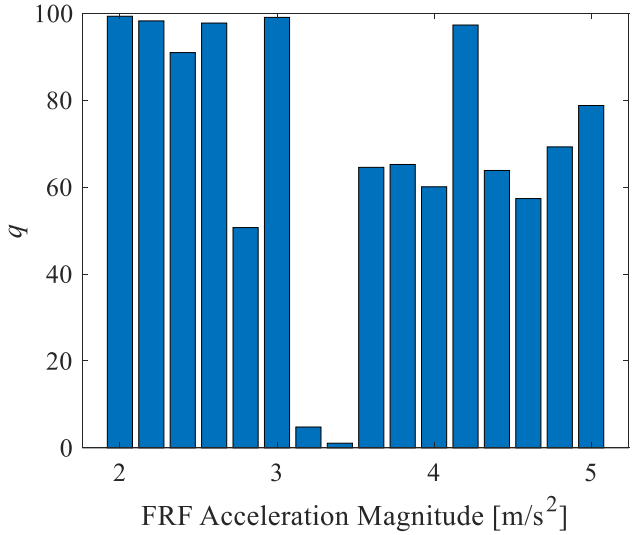

Figure I.5 Bar graph showing metric defined in Eq. (I.7) for different FRFs based on simulations of 10,000 realizations of the actual plant dynamics of the x axis using B-spline basis functions (n = 200, M = 1000).

I.5 Experiments

The model shown in Figure I.6 is printed using the 3D printer, shown in Figure 3.4, with a maximum speed of 130 mm/s and acceleration limits of 3 m/s^2, 4 m/s^2 and 5 m/s^2 imposed separately on the desired trajectory. To generate the axis-level commands, the controller reads a G-code file (generated using Cura^{TM} software package) and parses the G-code information into axis-level commands. The model is printed using robust FBF as well as standard FBFs (using FRFs corresponding to 3 m/s^2, 4 m/s^2 and 5 m/s^2). Since, the length of the desired trajectory is large, the parts are printed using the limited preview version of FBF using B-splines, i.e., LPFBS. The LPFBS parameters are n_{up} = 28, n_C = 56, L_C = 952, m = 5, L = 17 (for more details about the LPFBS approach see [20]). For each printed model, the thickness x of each of the 24 triangles is measured using Husky digital calipers (model# 1467H, 10 μm resolution) and compared to desired thickness

of the triangles x_{des} = 4.05 mm.

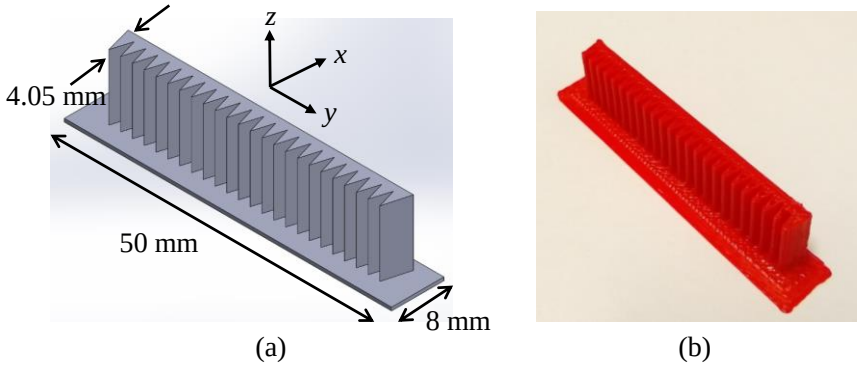

Figure I.6 (a) CAD model of the part and (b) sample of a printed part.

Figure I.7 shows a bee-swarm plot comparing the relative error ($\Delta x/x_{des}$, $\Delta x = |x_{des} - x|$) in the triangles for the robust and standard FBF (using FRFs 3 m/s^2, 4 m/s^2 and 5 m/s^2) cases. In an average sense, the robust FBF approach improves $\Delta x/x_{des}$ w.r.t. 3 m/s^2, 4 m/s^2 and 5m/s^2 standard FBFs by 7%, 2% and 12%, respectively. Using the worst-case scenario as a metric, the robust FBF approach improves $\Delta x/x_{des}$ by 4%, 10% and 16%, respectively, as compared to 3 m/s^2, 4m/s^2 and 5 m/s^2 standard FBFs.

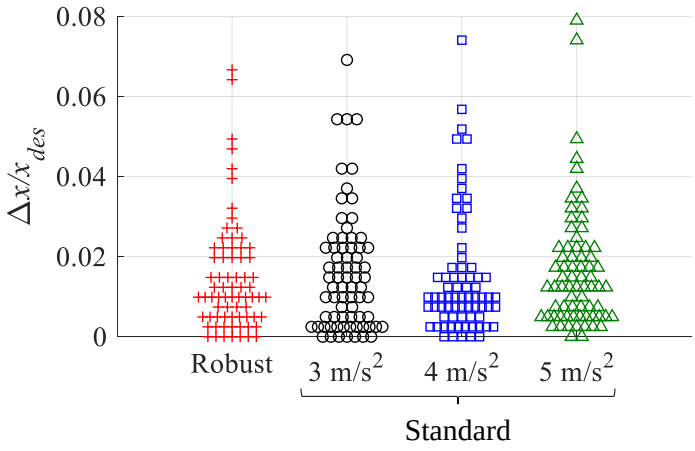

Figure I.7 Bee-swarm plot comparing the relative error in thickness of the total 72 triangles of 3 printed parts using robust FBF and three cases of standard FBF generated using the FRFs corresponding to the acceleration magnitudes shown in the figure.

I.6 Summary

This appendix has presented a robust filtered basis functions approach for feedforward tracking control of linear time invariant systems with known uncertainty. The standard filtered basis functions approach uses an arbitrarily selected nominal model of the plant for filtering basis functions. Conversely, the proposed robust FBF approach substitutes a robust nominal model in place of an arbitrary nominal model. As the robust nominal model, this paper proposes the inverse of an optimal controller obtained by minimizing a cost function over the range of known plant uncertainty. The robust and standard FBF approaches are compared in simulations and experiments using a commercial desktop 3D printer as an example. Dynamic uncertainty with a kernel distribution is used to model the uncertain 3D printer. The simulations and experiments demonstrate the effectiveness of the robust approach as compared to the standard method.

Ref. [70] also discusses stability issues associated with the robust filter and presents an approach for resolving them.

BIBLIOGRAPHY

[1] Altintas, Y., Verl, A., Brecher, C., Uriarte, L., and Pritschow, G., 2011, "Machine Tool Feed Drives," CIRP Ann. - Manuf. Technol., **60**(2), pp. 779–796.

[2] Potsaid, B., Wen, John Ting-Yung Unrath, M., Watt, D., and Alpay, M., 2007, "High Performance Motion Tracking Control for Electronic Manufacturing," J. Dyn. Syst. Meas. Control, **129**(6), pp. 767–776.

[3] Yao, B., and Xu, L., 2002, "Adaptive Robust Motion Control of Linear Motors for Precision Manufacturing," Mechatronics, **12**(4), pp. 595–616.

[4] Slotine, J.-J., and Sastry, S. S., 1983, "Tracking Control of Non-Linear Systems Using Sliding Surfaces, with Application to Robot Manipulators," Int. J. Control, **38**(2), pp. 465–492.

[5] Fukao, T., Nakagawa, H., and Adachi, N., 2000, "Adaptive Tracking Control of a Nonholonomic Mobile Robot," IEEE Trans. Robot. Autom., **16**(5), pp. 609–615.

[6] Qu, Z., and Dawson, D. M., 1995, *Robust Tracking Control of Robot Manipulators*, IEEE press.

[7] Setlur, P., Wagner, J. R., Dawson, D. M., and Braganza, D., 2006, "A Trajectory Tracking Steer-by-Wire Control System for Ground Vehicles," IEEE Trans. Veh. Technol., **55**(1), pp. 76–85.

[8] Aguiar, A. P., and Hespanha, J. P., 2007, "Trajectory-Tracking and Path-Following of Underactuated Autonomous Vehicles with Parametric Modeling Uncertainty," IEEE Trans. Automat. Contr., **52**(8), pp. 1362–1379.

[9] Kim, G.-W., and Wang, K., 2009, "Switching Sliding Mode Force Tracking Control of Piezoelectric-Hydraulic Pump-Based Friction Element Actuation Systems for Automotive Transmissions," Smart Mater. Struct., **18**(8), p. 085004.

[10] Jin, E., and Sun, Z., 2008, "Robust Controllers Design with Finite Time Convergence for Rigid Spacecraft Attitude Tracking Control," Aerosp. Sci. Technol., **12**(4), pp. 324–330.

[11] Liao, F., Wang, J. L., and Yang, G.-H., 2002, "Reliable Robust Flight Tracking Control: An LMI Approach," IEEE Trans. Control Syst. Technol., **10**(1), pp. 76–89.

[12] Koo, T. J., and Sastry, S., 1998, "Output Tracking Control Design of a Helicopter Model Based on Approximate Linearization," *Proceedings of the 37th IEEE Conference on Decision and Control*, pp. 3635--3640.

[13] Tomizuka, M., 1987, "Zero Phase Error Tracking Algorithm for Digital Control," J. Dyn. Syst. Meas. Control, **109**(1), pp. 65–68.

[14] Faanes, A., and Skogestad, S., 2004, "Feedforward Control under the Presence of Uncertainty," Eur. J. Control, **10**(1), pp. 30–46.

[15] Bruijnen, D., and van Dijk, N., 2012, "Combined Input Shaping and Feedforward Control for Flexible Motion Systems," *Proceedings of the 2012 American Control Conference*, pp. 2473–2478.

[16] Wohlers, T., Caffrey, T., Campbell, R. I., Diegel, O., and Kowen, J., 2018, *Wohlers Report 2018: 3D Printing and Additive Manufacturing State of the Industry; Annual Worldwide Progress Report*.

[17] Ronde, M., van den Bulk, J., van de Molengraft, R., and Steinbuch, M., 2013, "Feedforward for Flexible Systems with Time-Varying Performance Locations," *2013 American Control Conference*, pp. 6033–6038.

[18] Lunenburg, J., Bosgra, O., and Oomen, T., 2009, "Inversion-Based Feedforward Design for Beyond Rigid Body Systems : A Literature Survey," DCT Rep. 2009.105, Eindhoven Univ. Technol. Eindhoven, Netherlands.

[19] Miu, D. K., 2012, *Mechatronics: Electromechanics and Contromechanics*, Springer Science & Business Media.

[20] Duan, M., Yoon, D., and Okwudire, C. E., 2018, "A Limited-Preview Filtered B-Spline Approach to Tracking Control – with Application to Vibration-Induced Error Compensation

of a Commercial 3D Printer," Mechatronics, **56**, pp. 287--296.

[21] Astrom, K., and Wittenmark, B., 1984, *Computer Controlled Systems: Theory and Design*, Prentice Hall.

[22] Clayton, G. M., Tien, S., Leang, K. K., Zou, Q., and Devasia, S., 2009, "A Review of Feedforward Control Approaches in Nanopositioning for High-Speed SPM," J. Dyn. Syst. Meas. Control, **131**(6), p. 061101.

[23] van Zundert, J., and Oomen, T., 2018, "On Inversion-Based Approaches for Feedforward and ILC," Mechatronics, **50**, pp. 282–291.

[24] Rigney, B. P., Pao, L. Y., and Lawrence, D. A., 2009, "Nonminimum Phase Dynamic Inversion for Settle Time Applications," Control Syst. Technol. IEEE Trans., **17**(5), pp. 989–1005.

[25] Gross, E., Tomizuka, M., and Messner, W., 1994, "Cancellation of Discrete Time Unstable Zeros by Feedforward Control," J. Dyn. Syst. Meas. Control, **116**(1), pp. 33–38.

[26] Torfs, D., De Schutter, J., and Swevers, J., 1992, "Extended Bandwidth Zero Phase Error Tracking Control of Nonminimal Phase Systems," J. Dyn. Syst. Meas. Control, **114**(3), pp. 347–351.

[27] Yamada, M., Funahashi, Y., and Fujiwara, S., 1997, "Zero Phase Error Tracking System With Arbitrarily Specified Gain Characteristics," J. Dyn. Syst. Meas. Control, **119**(2), p. 260.

[28] Yamada, M., Funahashi, Y., and Riadh, Z., 1999, "Generalized Optimal Zero Phase Error Tracking Controller Design," J. Dyn. Syst. Meas. Control, **121**(2), p. 165.

[29] Butterworth, J. A., Pao, L. Y., and Abramovitch, D. Y., 2012, "Analysis and Comparison of Three Discrete-Time Feedforward Model-Inverse Control Techniques for Nonminimum-Phase Systems," Mechatronics, **22**(5), pp. 577–587.

[30] Wen, J. T., and Potsaid, B., 2004, "An Experimental Study of a High Performance Motion Control System," *American Control Conference, 2004. Proceedings of the 2004*, pp. 5158–5163.

[31] Fujimoto, H., Hori, Y., and Kawamura, A., 2001, "Perfect Tracking Control Based on Multirate Feedforward Control with Generalized Sampling Periods," IEEE Trans. Ind. Electron., **48**(3), pp. 636–644.

[32] Weck, Manfred and Ye, G., 1990, "Sharp Corner Tracking Using the IKF Control Strategy," CIRP Ann. Technol., **39**(1), pp. 437–441.

[33] Haack, B and Tomizuka, M., 1991, "The Effect of Adding Zeroes to Feedforward Controllers," J. Dyn. Syst. Meas. Control, **113**(1), pp. 6–10.

[34] Hunt, L., Meyer, G., and Su, R., 1996, "Noncausal Inverses for Linear Systems," Autom. Control. IEEE Trans., **41**(4), pp. 608–611.

[35] Devasia, S., Chen, D., and Paden, B., 1996, "Nonlinear Inversion-Based Output Tracking," Autom. Control. IEEE Trans., **41**(7), pp. 930–942.

[36] Marro, G., Prattichizzo, D., and Zattoni, E., 2002, "Convolution Profiles for Right Inversion of Multivariable Non-Minimum Phase Discrete-Time Systems," Automatica, **38**(10), pp. 1695–1703.

[37] Kwon, D.-S., and Book, W. J., 1994, "A Time-Domain Inverse Dynamic Tracking Control of a Single-Link Flexible Manipulator," J. Dyn. Syst. Meas. Control, **116**(2), p. 193.

[38] Trautt, T. A., and Bayo, E., 1997, "Inverse Dyamics of Non-Minimum Phase Systems with Non-Zero Initial Conditions," Dyn. Control, **7**(1), pp. 49–71.

[39] Zou, Q., and Devasia, S., 1999, "Preview-Based Stable-Inversion for Output Tracking of Linear Systems," J. Dyn. Syst. Meas. Control, **121**(4), pp. 625–630.

[40] Marconi, L., Marro, G., and Melchiorri, C., 2001, "A Solution Technique for Almost Perfect Tracking of Non-Minimum-Phase, Discrete-Time Linear Systems," Int. J. Control, **74**(5), pp. 496–506.

[41] Jetto, L., Orsini, V., and Romagnoli, R., 2014, "Accurate Output Tracking for Nonminimum Phase Nonhyperbolic and Near Nonhyperbolic Systems," Eur. J. Control, **20**(6), pp. 292–300.

[42] Devasia, S., 1997, "Output Tracking with Nonhyperbolic and Near Nonhyperbolic Internal

Dynamics: Helicopter Hover Control," J. Guid. Control. Dyn., **20**(3), pp. 573–580.

[43] Devasia, S., 2011, "Nonlinear Minimum-Time Control with Pre-and Post-Actuation," Automatica, **47**(7), pp. 1379–1387.

[44] Butterworth, J. A., Pao, L. Y., and Abramovitch, D. Y., 2008, "The Effect of Nonminimum-Phase Zero Locations on the Performance of Feedforward Model-Inverse Control Techniques in Discrete-Time Systems," *American Control Conference, 2008*, IEEE, pp. 2696–2702.

[45] Piazzi, A., and Visioli, A., 2005, "Using Stable Input-Output Inversion for Minimum-Time Feedforward Constrained Regulation of Scalar Systems," Automatica, **41**(2), pp. 305–313.

[46] Jetto, L., Orsini, V., and Romagnoli, R., 2015, "Spline Based Pseudo-Inversion of Sampled Data Non-Minimum Phase Systems for an Almost Exact Output Tracking," Asian J. Control, **17**(5), pp. 1866–1879.

[47] Wang, H., Kim, K., and Zou, Q., 2013, "B-Spline-Decomposition-Based Output Tracking With Preview for Nonminimum-Phase Linear Systems," Automatica, **49**(5), pp. 1295–1303.

[48] Duan, M., Ramani, K. S., and Okwudire, C. E., 2015, "Tracking Control of Non-Minimum Phase Systems Using Filtered Basis Functions: A NURBS-Based Approach," *ASME 2015 Dynamic Systems and Control Conference*, American Society of Mechanical Engineers, p. V001T03A006--V001T03A006.

[49] Frueh, J. A., and Phan, M. Q., 2000, "Linear Quadratic Optimal Learning Control (LQL)," Int. J. Control, **73**(10), pp. 832–839.

[50] Romagnoli, R., and Garone, E., 2019, "A General Framework for Approximated Model Stable Inversion," Automatica, **101**, pp. 182–189.

[51] Kasemsinsup, Y., Romagnoli, R., Heertjes, M., Weiland, S., and Butler, H., 2017, "Reference-Tracking Feedforward Control Design for Linear Dynamical Systems through Signal Decomposition," *American Control Conference (ACC), 2017*, pp. 2387--2392.

[52] Zhao, Y., and Jayasuriya, S., 1995, "Feedforward Controllers and Tracking Accuracy in the

Presence of Plant Uncertainties," J. Dyn. Syst. Meas. Control, **117**(4), pp. 490–495.

[53] Pao, L. Y., Butterworth, J. A., and Abramovitch, D. Y., 2007, "Combined Feedforward/Feedback Control of Atomic Force Microscopes," *2007 American Control Conference*, pp. 3509--3515.

[54] Aphale, S. S., Devasia, S., and Moheimani, S. R., 2008, "High-Bandwidth Control of a Piezoelectric Nanopositioning Stage in the Presence of Plant Uncertainties," Nanotechnology, **19**(12), p. 125503.

[55] Wu, Y., and Zou, Q., 2009, "An Iterative-Based Feedforward-Feedback Control Approach to High-Speed Atomic Force Microscope Imaging," J. Dyn. Syst. Meas. Control, **131**(6), p. 061105.

[56] de Rozario, R., Fleming, A. J., and Oomen, T., 2016, "Iterative Control for Periodic Tasks with Robustness Considerations, Applied to a Nanopositioning Stage," IFAC-PapersOnLine, **49**(21), pp. 623–628.

[57] Yoon, D., Ge, X., and Okwudire, C. E., 2019, "Optimal Inversion-Based Iterative Learning Control for Overactuated Systems," IEEE Trans. Control Syst. Technol.

[58] Tsao, T.-C., and Tomizuka, M., 1987, "Adaptive Zero Phase Error Tracking Algorithm for Digital Control," J. Dyn. Syst. Meas. Control, **109**(4), pp. 349–354.

[59] Adam, E. J., and Marchetti, J. L., 2004, "Designing and Tuning Robust Feedforward Controllers," Comput. Chem. Eng., **28**(9), pp. 1899–1911.

[60] Vilanova, R., Arrieta, O., Ibeas, A., Balaguer, P., and Pedret, C., 2008, "Disturbance Compensation on Uncertain Systems: Feedforward Control Design for Stable Systems," IFAC Proc. Vol., **41**(2), pp. 11310--11315.

[61] Schitter, G., and Stemmer, A., 2004, "Identification and Open-Loop Tracking Control of a Piezoelectric Tube Scanner for High-Speed Scanning-Probe Microscopy," IEEE Trans. Control Syst. Technol., **12**(3), pp. 449–454.

[62] Devasia, S., 2002, "Should Model-Based Inverse Inputs Be Used as Feedforward under Plant Uncertainty?," Autom. Control. IEEE Trans., **47**(11), pp. 1865–1871.

[63] Wu, Y., and Zou, Q., 2009, "Robust Inversion-Based 2-DOF Control Design for Output Tracking : Piezoelectric-Actuator Example," IEEE Trans. Control Syst. Technol., **17**(5), pp. 1069–1082.

[64] Lunenburg, J. J. M., 2010, "Inversion-Based MIMO Feedforward Design Beyond Rigid Body Systems," Eindhoven Univ. Technol. Tech. Rep.

[65] Bristow, D. A., Tharayil, M., and Alleyne, A. G., 2006, "A Survey of Iterative Learning Control," IEEE Control Syst. Mag., **26**(3), pp. 96–114.

[66] Astrom, K. J., and Wittenmark, B., 1995, *Adaptive Control*, Addison-Wesley.

[67] Ioannou, P. A., and Sun, J., 2012, *Robust Adaptive Control*, Courier Corporation.

[68] Ramani, K. S., and Okwudire, C. E., 2016, "Regularized Filtered Basis Functions Approach for Accurate Tracking of Discrete-Time Linear Time Invariant Systems with Bounded Random Uncertainties," *ASME 2016 Dynamic Systems and Control Conference, American Society of Mechanical Engineers*.

[69] Ramani, K. S., and Okwudire, C. E., 2018, "Robust Filtered Basis Functions Approach for Feedforward Tracking Control," *ASME 2018 Dynamic Systems and Control Conference*.

[70] Ramani, K. S., Edoimioya, N., and Okwudire, C. E., "A Robust Filtered Basis Functions Approach for Feedforward Tracking Control - with Application to a Desktop 3D Printer," Submitt. to IEEE/ASME Trans. Mechatronics.

[71] Ramani, K. S., Duan, M., Okwudire, C. E., and Ulsoy, A. G., 2017, "Tracking Control of Linear Time-Invariant Nonminimum Phase Systems Using Filtered Basis Functions," J. Dyn. Syst. Meas. Control, **139**(1), p. 011001.

[72] Ramani, K. S., Duan, M., Okwudire, C. E., and Ulsoy, A. G., 2018, "A Lifted Domain-Based Metric for Performance Evaluation of LTI and LTV Discrete-Time Tracking Controllers," *2018 International Symposium on Flexible Automation*.

[73] Ramani, K. S., Duan, M., Okwudire, C. E., and Ulsoy, A. G., 2019, "Optimal Selection of Basis Functions for Minimum-Effort Tracking Control of Nonminimum Phase Systems Using Filtered Basis Functions," J. Dyn. Syst. Meas. Control, **141**(11).

[74] Ramani, K. S., and Okwudire, C. E., "Optimal Selection of Basis Functions for Robust Tracking Control of Linear Systems Using Filtered Basis Functions," *Submitted to American Control Conference (ACC) 2020*.

[75] Ramani, K. S., and Okwudire, C. E., "Optimal Selection of Basis Functions and Nominal Model for Robust Tracking Control of Linear Systems Using Filtered Basis Functions," To be Submitt. to IEEE Trans. Control Syst. Technol.

[76] Strang, G., 1993, "The Fundamental Theorem of Linear Algebra," Am. Math. Mon., **100**(9), pp. 848–855.

[77] Bay, J. S., 1999, *Fundamentals of Linear State Space Systems*, McGraw-Hill Science, Engineering & Mathematics.

[78] Barton, K. L., Bristow, D. A., and Alleyne, A. G., 2010, "A Numerical Method for Determining Monotonicity and Convergence Rate in Iterative Learning Control," Int. J. Control, **83**(2), pp. 219–226.

[79] Butterworth, J. A., Pao, L. Y., and Abramovitch, D. Y., 2012, "Analysis and Comparison of Three Discrete-Time Feedforward Model-Inverse Control Techniques for Nonminimum-Phase Systems," Mechatronics, **22**(5), pp. 577–587.

[80] Ye, Y., and Wang, D., 2005, "DCT Basis Function Learning Control," Mechatronics, IEEE/ASME Trans., **10**(4), pp. 449–454.

[81] Piegl, L., and Tiller, W., 1997, *The NURBS Book*, New York: Springer.

[82] Ahmed, N., Natarajan, T., and Rao, K. R., 1974, "Discrete Cosine Transform," Comput. IEEE Trans., **100**(1), pp. 90–93.

[83] Rao, K. R., and Yip, P., 2014, *Discrete Cosine Transform: Algorithms, Advantages, Applications*, Academic press.

[84] Jain, A. K., 1989, *Fundamentals of Digital Image Processing*, Englewood Cliffs, NJ: Prentice Hall,.

[85] Piegl, L., 1991, "On NURBS: A Survey," IEEE Comput. Graph. Appl., **11**(1), pp. 55–71.

[86] Phan, M., and Frueh, J., 1996, "Learning Control for Trajectory Tracking Using Basis

Functions," *Decision and Control, 1996., Proceedings of the 35th IEEE Conference On*, pp. 2490–2492.

[87] Yoon, D., and Okwudire, C. E., 2016, "Active Assist Device for Simultaneous Reduction of Heat and Vibration in Precision Scanning Stages," Precis. Eng., **46**, pp. 193–205.

[88] Laub, A. J., 2005, *Matrix Analysis for Scientists and Engineers*, Siam.

[89] Ronde, M., van de Molengraft, R., and Steinbuch, M., 2012, "Model-Based Feedforward for Inferential Motion Systems, with Application to a Prototype Lightweight Motion System," *American Control Conference (ACC), 2012*, pp. 5324–5329.

[90] Okwudire, C., Ramani, K., and Duan, M., 2016, "A Trajectory Optimization Method for Improved Tracking of Motion Commands Using CNC Machines That Experience Unwanted Vibration," CIRP Ann. - Manuf. Technol., **65**(1), pp. 373–376.

[91] Bell, C., 2015, *3D Printing with Delta Printers*, Apress.

[92] De Luca, A., and Siciliano, B., 1993, "Inversion-Based Nonlinear Control of Robot Arms with Flexible Links," J. Guid. Control. Dyn., **16**(6), pp. 1169--1176.

[93] Hauser, J., Sastry, S., and Meyer, G., 1992, "Nonlinear Control Design for Slightly Non-Minimum Phase Systems: Application to V/STOL Aircraft," Automatica, **28**(4), pp. 665–679.

[94] Zou, Q., and Devasia, S., 2007, "Precision Preview-Based Stable-Inversion for Nonlinear Nonminimum-Phase Systems: The VTOL Example," Automatica, **43**(1), pp. 117–127.

[95] Richalet, J., and O'Donovan, D., 2009, *Predictive Functional Control: Principles and Industrial Applications*, Springer Science & Business Media.

[96] Oppenheim, A. V, Schafer, R. W., and Buck, J. R., 1989, *Discrete-Time Signal Processing*, Prentice-hall Englewood Cliffs.

[97] Riley, K. F., Hobson, M. P., and Bence, S. J., 2006, *Mathematical Methods for Physics and Engineering: A Comprehensive Guide*, Cambridge university press.

[98] Bernstein, D. S., 2009, *Matrix Mathematics: Theory, Facts, and Formulas*, Princeton University Press.

[99] Eckart, C., and Young, G., 1936, “The Approximation of One Matrix by Another of Lower Rank,” Psychometrika, **1**(3), pp. 211–218.

[100] Mirsky, L., 1960, “Symmetric Gauge Functions and Unitarily Invariant Norms,” Q. J. Math., **11**, pp. 50–59.

[101] Markovsky, I., 2008, “Structured Low-Rank Approximation and Its Applications,” Automatica, **44**(4), pp. 891–909.

[102] Altintas, Y., and Okwudire, C. E., 2009, “Dynamic Stiffness Enhancement of Direct-Driven Machine Tools Using Sliding Mode Control with Disturbance Recovery,” CIRP Ann. - Manuf. Technol., **58**(1), pp. 335–338.

[103] Dijkstra, B. G., 2004, “Iterative Learning Control With Applications to a Wafer Stage,” Doctoral Thesis, Delft University of Technology, Netherlands.